FORT NELSON CAP ROCK PETROGRAPHIC ANALYSIS – JULY 2011

Prepared for:

Dr. Ernie Perkins
Alberta Innovates Technology Futures

Prepared by:

Jordan M. Bremer
Corey D. Lindeman
Jonathan L. LaBonte
Benjamin W. Huffman
Alexander Azenkeng
Blaise A.F. Mibeck
Steven A. Smith
James A. Sorensen
Charles D. Gorecki
Edward N. Steadman
John A. Harju

Energy & Environmental Research Center
University of North Dakota
15 North 23rd Street, Stop 9018
Grand Forks, ND, 58202-9018

August 2011

DOE DISCLAIMER

This report was prepared as an account of work sponsored by an agency of the United States Government. Neither the United States Government, nor any agency thereof, nor any of their employees, makes any warranty, express or implied, or assumes any legal liability or responsibility for the accuracy, completeness, or usefulness of any information, apparatus, product, or process disclosed, or represents that its use would not infringe privately owned rights. Reference herein to any specific commercial product, process, or service by trade name, trademark, manufacturer, or otherwise does not necessarily constitute or imply its endorsement, recommendation, or favoring by the United States Government or any agency thereof. The views and opinions of authors expressed herein do not necessarily state or reflect those of the United States Government or any agency thereof.

NDIC DISCLAIMER

This report was prepared by the Energy & Environmental Research Center (EERC) pursuant to an agreement partially funded by the Industrial Commission of North Dakota, and neither the EERC nor any of its subcontractors nor the North Dakota Industrial Commission nor any person acting on behalf of either:

(A) Makes any warranty or representation, express or implied, with respect to the accuracy, completeness, or usefulness of the information contained in this report or that the use of any information, apparatus, method, or process disclosed in this report may not infringe privately owned rights; or

(B) Assumes any liabilities with respect to the use of, or for damages resulting from the use of, any information, apparatus, method, or process disclosed in this report.

Reference herein to any specific commercial product, process, or service by trade name, trademark, manufacturer, or otherwise does not necessarily constitute or imply its endorsement, recommendation, or favoring by the North Dakota Industrial Commission. The views and opinions of authors expressed herein do not necessarily state or reflect those of the North Dakota Industrial Commission

EERC DISCLAIMER

LEGAL NOTICE This research report was prepared by the Energy & Environmental Research Center (EERC), an agency of the University of North Dakota, as an account of work sponsored by the U.S. Department of Energy. Because of the research nature of the work performed, neither the EERC nor any of its employees makes any warranty, express or implied, or assumes any legal liability or responsibility for the accuracy, completeness, or usefulness of any information, apparatus, product, or process disclosed or represents that its use would not infringe privately owned rights. Reference herein to any specific commercial product, process, or service by trade name, trademark, manufacturer, or otherwise does not necessarily constitute or imply its endorsement or recommendation by the EERC.

TABLE OF CONTENTS

LIST OF FIGURES ii

LIST OF TABLES iv

EXECUTIVE SUMMARY v

INTRODUCTION 1

SUMMARY OF TESTING 4

ANALYTICAL RESULTS 7
- Bulk Mineralogy by XRD 7
  - Key Observations 9
- Trace Element Analysis by XRF 10
  - Key Observations 11
- Petrographic Analysis 12
  - Key Observations 15
- QEMSEM Analysis 16
  - Key Observations 18
- SEM Reporting 19
  - Key Observations 22
- CHN/S Analysis 23
  - Key Observations 23
- Surface Area 24
  - Key Observations 26
- Skeletal Density 26
  - Key Observations 26
- ICP–MS 28
  - Key Observations 29

SUMMARY 31

REFERENCES 32

BULK MINERALOGY XRD SCANS ..... Appendix A

PETROGRAPHIC THIN SECTIONS ..... Appendix B

SCANNING ELECTRON MICROSCOPY ..... Appendix C

SEM–EDS DATA ..... Appendix D

LIST OF FIGURES

1 Stratigraphic and hydrostratigraphic delineation and nomenclature as well as general lithology for the northern part of the Alberta Basin, including northeastern British Columbia 2

2 Stratigraphic architecture of the Middle Devonian formations in the Fort Nelson area, northeastern British Columbia 3

3 Gamma and lithology logs from Well C-061-E, with marked sample locations from the Fort Simpson and Muskwa Formations 3

4 Illustration depicting the depositional history of the Keg River, Slave Point, and Fort Simpson Formations in the Fort Nelson area 5

5 Photographs of Fort Nelson cap rock samples as received 6

6 Flow chart showing defined clay assemblages identified through oriented glycolation methods. 8

7 XRD patterns for Fort Nelson cap rock samples with annotated peaks for prevalent minerals detected through analysis 10

8 Photomicrograph of TH-1, plane-polarized light, 100× magnification 13

9 Photomicrograph of T-1, plane-polarized light, 100× magnification 13

10 Photomicrograph of T-3, reflected light, 40× magnification 14

11 QEMSEM image of the TH-1 interval 17

12 QEMSEM image of the T-1 interval 17

13 QEMSEM image of the T-3 interval 18

14 Fracture-mounted photomicrograph of Sample TH-1 at 5000× magnification 20

15 Electron backscatter micrograph of polished section of Interval T-1 taken at 750× magnification 20

16 Electron backscatter micrograph of T-3 taken at 750× magnification 21

17 Results of sulfur analysis derived through XRF and CHN/S and calculated from pyrite contents derived from QEMSEM and XRD data 24

Continued . . .

LIST OF FIGURES (continued)

18 Comparison of results of surface area testing for Fort Nelson cap rock samples 25

19 Skeletal density testing of whole (blue) and pulverized (red) test samples 27

20 Results of trace element analysis comparing Samples TH-1, T-1, and T-3 with Glass Mountain rhyolite (RGM-1)..... 29

21 Results of trace element analysis for Samples TH-1, T-1, and T-3 for elements not reported in RGM-1 sample literature 30

LIST OF TABLES

1 Depth and Identification Information for Fort Nelson Cap Rock Samples 4

2 Relative Weight Percentages of Identified Mineral Phases in Each Sample 9

3 Quantitative Common Oxide Weight Percentages for Fort Nelson Samples 11

4 Semiquantitative Report of Detectable Phases in Sample T-3 12

5 Mineralogical Estimates Derived Through Thin-Section Analysis 15

6 Rock Fabric Descriptions Related to Grain, Pore, and Clay Characteristics, Based on Thin-Section Analysis 15

7 Quantitative Mineral Assemblages Present in QEMSEM Samples 17

8 Elemental Compositions at Probed EDS Locations for Figure 15, Sample T-1 21

9 Mineralogical Interpretation of Probed EDS Locations for Figure 15, Sample T-1 21

10 Elemental Compositions at Probed EDS Locations for Figure 16, Sample T-3 22

11 Mineralogical Interpretation of Probed EDS Locations for Figure 16, Sample T-3 22

12 Results of CHN/S Analysis 23

13 Results and Calculations from Surface Area Measurements for Fort Nelson (C-61-E/94-J-10) C1-49528 25

14 Measurements and Calculations Performed for Skeletal Density Values 27

15 Trace Elements Measured During ICP–MS Analysis Against RGM-1 Standard 28

16 Trace Elements Measured During ICP–MS Analysis that Had No Values Reported for Standard RGM-1 28

17 Concentrations of ICP–MS Measured Trace Elements for Metals with RGM-1 Standard 30

18 Concentrations of ICP-MS Measured Trace Elements for Metals Without RGM-1 Standard 30

EXECUTIVE SUMMARY

Petrographic assessment was performed on primary cap rock samples from the Fort Nelson area provided by Dr. Ernie Perkins of Alberta Innovates Technology Futures. The cap rock samples represent three intervals from Well C-61-E/94-J-10, corresponding to depths of 2030.4, 2042.11, and 2045.75 meters. The samples are dark gray to black pyritic, dolomitic shales that increase in hardness and degree of cementation with depth.

It is expected that the rock sequence in the area represents a brief regression from the productive carbonate reef-building time, leading to fluid enrichment and dolomitization. This was followed by a large-scale transgression that blankets the rocks under the thick Fort Simpson Shale. The rocks collected for analysis represent shale samples from above the reef complex that have received differential cementation because of hypersaline water (Meijer Drees, 2008).

A broad geochemical understanding of these samples is required to predict the cap rock integrity and reservoir security of large-scale acid gas injection. To collect geochemical and pertinent rock properties for the cap rock samples, the Energy & Environmental Research Center (EERC) submitted samples collaboratively between its Applied Geology, Analytical Research, and Natural Materials Research Laboratories, each with their own focus and expertise. In all, the following tests and measurements were performed:

- X-ray diffraction (XRD) for bulk mineralogy
- X-ray fluorescence (XRF) for trace element analysis
- Petrographic analysis via thin section for mineralogy and rock fabric descriptions
- QEMSEM (quantitative elemental mapping using scanning electron microscopy) for mineralogical mapping
- SEM with energy-dispersive spectroscopy for mineralogical identification and rock fabric descriptions
- Total carbon, hydrogen, and sulfur measurements for elemental composition information
- Surface area to determine reactive surface

- Skeletal density to support mineralogy and examination of total vs. effective porosity and degree of cementation

- Inductively coupled plasma–mass spectrometry (ICP–MS) to examine trace element abundance

Results from the various tests are shown to correlate well with one another, forming defensible conclusions regarding bulk and trace mineralogy and measured rock properties through several different methods and observations as follows:

- The cap rock intervals tested were found to be composed of a tight, dense collection of typically stable minerals.

- Bulk sample mineralogy, collected by XRD, QEMSEM, and thin-section analysis, is presented in Tables ES-1–ES-3. Mineralogy is supported by SEM images, XRF, and skeletal density measurements.

- Common trace elements and their relative percentages were collected by XRF and ICP–MS. These data are partially supported by SEM and CHN/S. Results for five trace metals from XRF (plus additional metals from Sample T-3) and the top 10 most abundant trace elements detected in ICP–MS for each sample are presented in Tables ES-4–ES-6.

- Rock property measurements and specifically measured elements including total porosity, effective porosity, skeletal density, total sulfur, total carbon, total hydrogen, and surface area are presented in Table ES-7.

While the testing and analysis were performed for the purpose of geochemical characterization, results may also be of additional use in petrophysical modeling, monitoring, verification, and accounting practices and other scientific and engineering aspects of the project.

Table ES-1. Mineralogy Report Summary for Sample TH-1, 2030.4 meters

	Common Mineral Phases							
Method	Illite	Kaolinite	Quartz	Carbonate	Pyrite	Feldspars	Apatite	Unit
XRD	47.0	ND[1]	41.6	1.8	7.0	0.8	ND	wt%
QEMSEM	74.9	6.65	6.21	1.38	8.14	0.53	0.08	% area
Thin Section	75		ND	15	10	ND	ND	% area

[1] Not detected.

Table ES-2. Mineralogy Report Summary for Sample T-1, 2042.11 meters

	Common Mineral Phases							
Method	Illite	Kaolinite	Quartz	Carbonate	Pyrite	Feldspars	Apatite	Unit
XRD	46.2	ND	40.9	2.7	6.5	2.5	ND	wt%
QEMSEM	75.83	6.37	6.59	2.50	3.71	0.99	0.05	% area
Thin Section	75		Trace	15	10	ND	ND	% area

Table ES-3. Mineralogy Report Summary for Sample T-3, 2045.75 meters

	Common Mineral Phases							
Method	Illite	Kaolinite	Quartz	Carbonate	Pyrite	Feldspars	Apatite	Unit
XRD	21.6	ND	31.0	41.1	3.5	0.6	ND	wt%
QEMSEM	16.11	3.96	12.91	46.65	4.04	3.90	0.08	% area
Thin Section	15		5	65	5	ND	ND	% area

Table ES-4. Trace Element Report Summary for Sample TH-1, 2030.4 meters

Method	Trace Elements										Unit
	K	Ti	Ba	Sr	Mn						
XRF	3.744	0.396	0.134	0.017	0.007						wt%
	Ti	Mn	Cr	V	Ni	Th	Ce	Cu	Gd	Y	
ICP–MS	1886	657	52.7	47.6	39.1	24.4	23.4	22.8	22.3	17.2	µg/g

Table ES-5. Trace Element Report Summary for Sample T-1, 2042.11 meters

Method	Trace Elements										Unit
	K	Mn	Ti	Ba	Sr						
XRF	3.943	1.780	0.640	0.140	0.008						wt%
	Ti	V	Ni	Cr	Mn	Zn	Ce	Cu	Th	La	
ICP–MS	3661	197.6	117.9	92.6	85.9	70.7	57.9	57.8	39.7	30.7	µg/g

Table ES-6. Trace Element Report Summary for Sample T-3, 2045.75 meters

Method	Trace Elements										Unit
	K	Cr	Ti	Mn	Ba	Y	Sr	V	Ni	Cu	
XRF	2.142	0.658	0.261	0.083	0.080	0.051	0.020	0.012	0.007	0.004	wt%
	Ti	Zn	V	Mn	Ni	Cr	Cu	Ce	Th	Pb	
ICP–MS	3473	266.7	202.0	167.0	101.8	92.1	76.8	46.9	42.0	31.1	µg/g

Table ES-7. Rock Property Report for Fort Nelson Cap Rock Samples

Sample	Skeletal Density, g/cm^3	Total Sulfur, wt%	Total Carbon, wt%	Total Hydrogen, wt%	Surface Area, m^2/g
TH-1	2.73	3.14	1.67	0.27	14.66
T-1	2.82	3.60	27.6	0.28	20.16
T-3	2.82	2.07	8.28	0.07	14.82

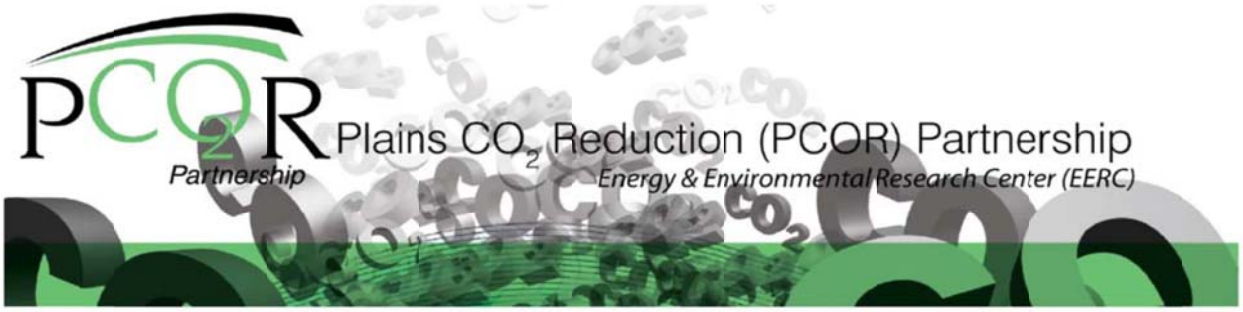

INTRODUCTION

The Energy & Environmental Research Center (EERC), through the Plains CO_2 Reduction (PCOR) Partnership, is working with Spectra Energy Transmission (SET) to investigate the feasibility of a carbon capture and storage (CCS) project to mitigate carbon dioxide (CO_2) emissions produced by SET's Fort Nelson Gas Plant (FNGP). The gas stream produced by the FNGP will include up to 5% sulfur dioxide (SO_2) and a small amount of methane (CH_4) and, as such, is referred to as a "sour" CO_2 stream. The sour CO_2 gas stream will be injected into a deep saline carbonate formation.

Over the past 50 years, exploration activities for mineral and energy resources in the area have yielded a significant amount of information about the geology of northeastern British Columbia and northwestern Alberta. The sedimentary succession in the Fort Nelson area consists, in ascending order from the Precambrian crystalline basement to the surface, of Middle and Upper Devonian carbonates, evaporates, and shales; Mississippian carbonates; and Lower Cretaceous shales overlain by Quaternary glacial drift and unconsolidated sediments (Figures 1–3).

With respect to formations that will prevent upward migration of the injected sour CO_2, shales of the overlying Middle Devonian Fort Simpson Group will provide the primary seal with respect to preventing leakage to the surface. The Mississippian-age Banff Formation, a carbonate formation that directly overlies the Devonian section in the northern portion of the Western Canadian Sedimentary Basin, is considered regionally to be an aquitard, thereby providing an additional seal between the target injection zones and the surface. Finally, the shales of the Cretaceous-age lower Fort St. John Group provide yet another layer of protection from leakage to the surface.

To gain a thorough understanding of the sealing capabilities of the Fort Simpson and Muskwa Shales, three samples were taken from cap rock intervals of the C-61-E test well core in January 2011 and delivered to the EERC shortly thereafter. Sample intervals were chosen by Dr. Ernie Perkins at a meeting of the geological team for the Fort Nelson project and are thought to represent a transition zone from the carbonate-rich reservoir into organic-rich shales with decreasing carbonate content. Table 1 shows the sample depths with their unique identification numbers as assigned by the EERC. The interval tags TH-1, T-1, and T-3 are used throughout this document to reference the samples.

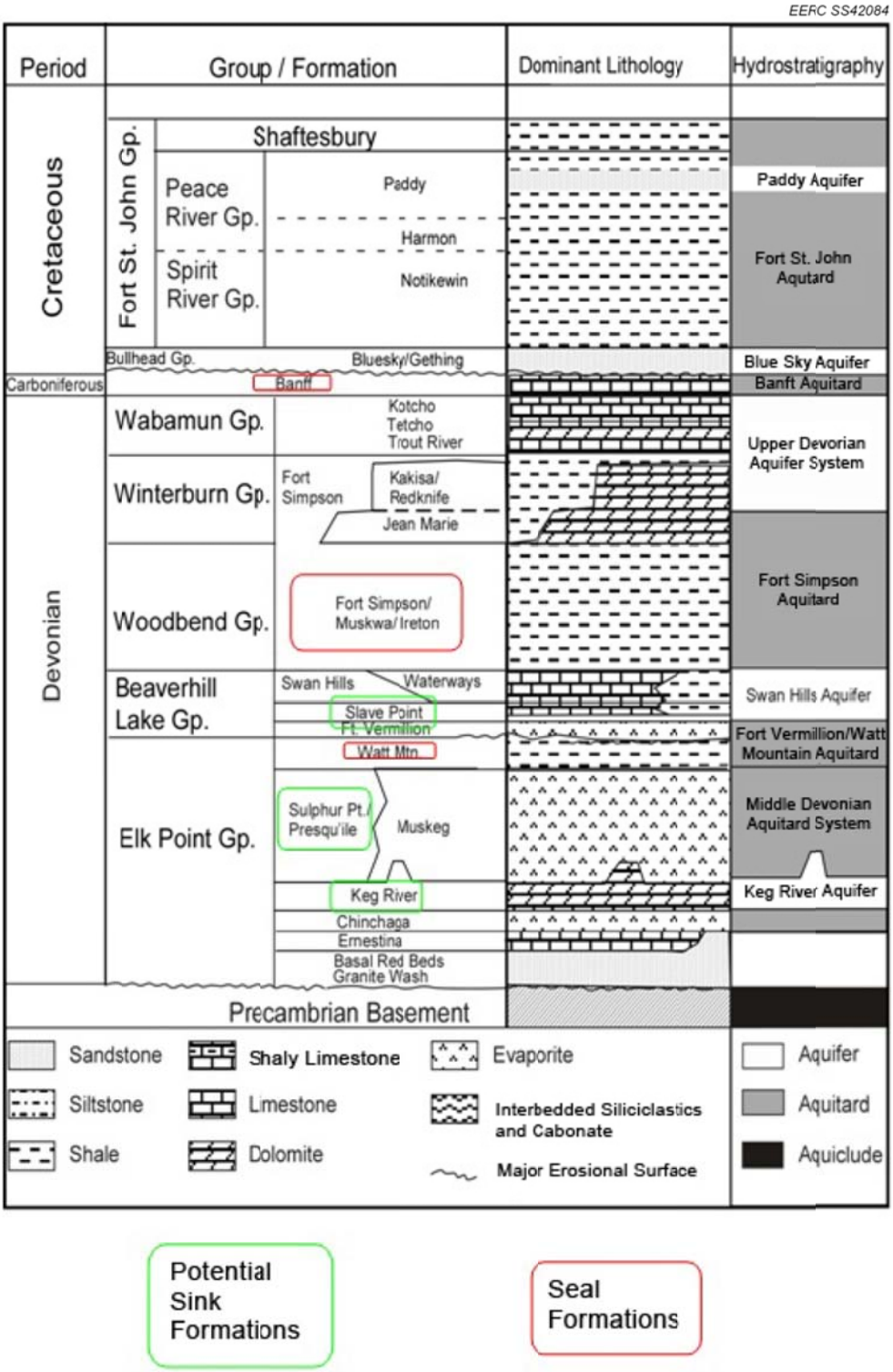

Figure 1. Stratigraphic and hydrostratigraphic delineation and nomenclature as well as general lithology for the northern part of the Alberta Basin, including northeastern British Columbia (from Gorecki and others, 2010).

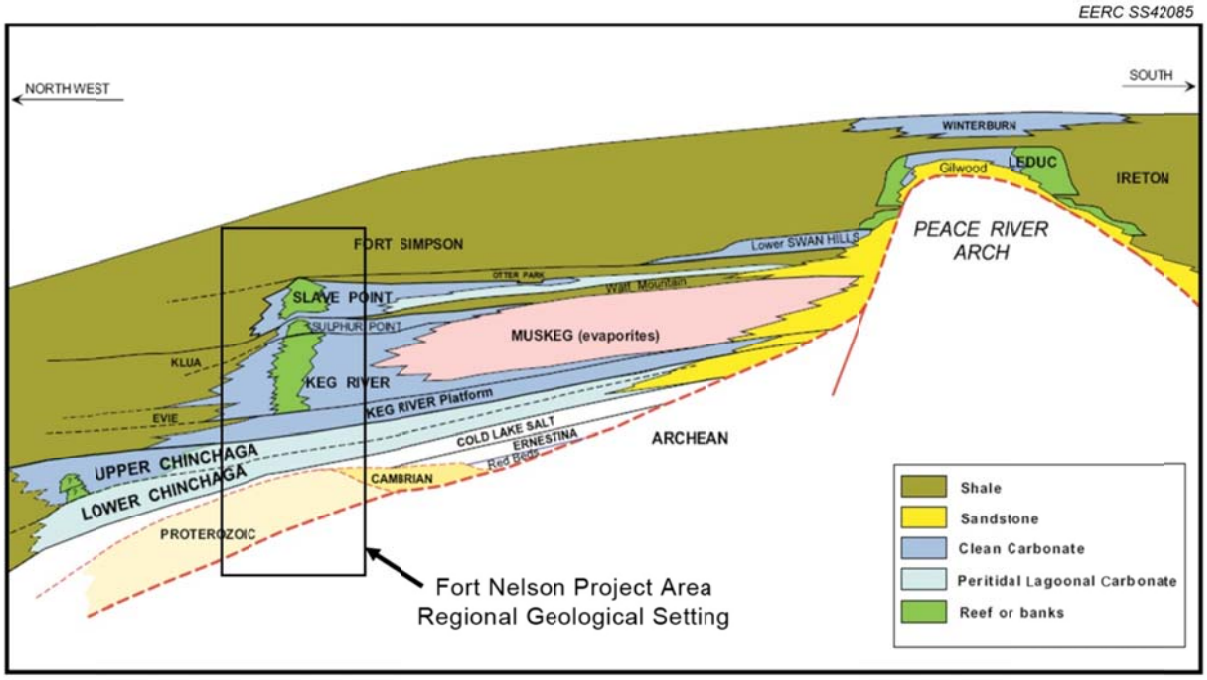

Figure 2. Stratigraphic architecture of the Middle Devonian formations in the Fort Nelson area, northeastern British Columbia (from Gorecki and others, 2010).

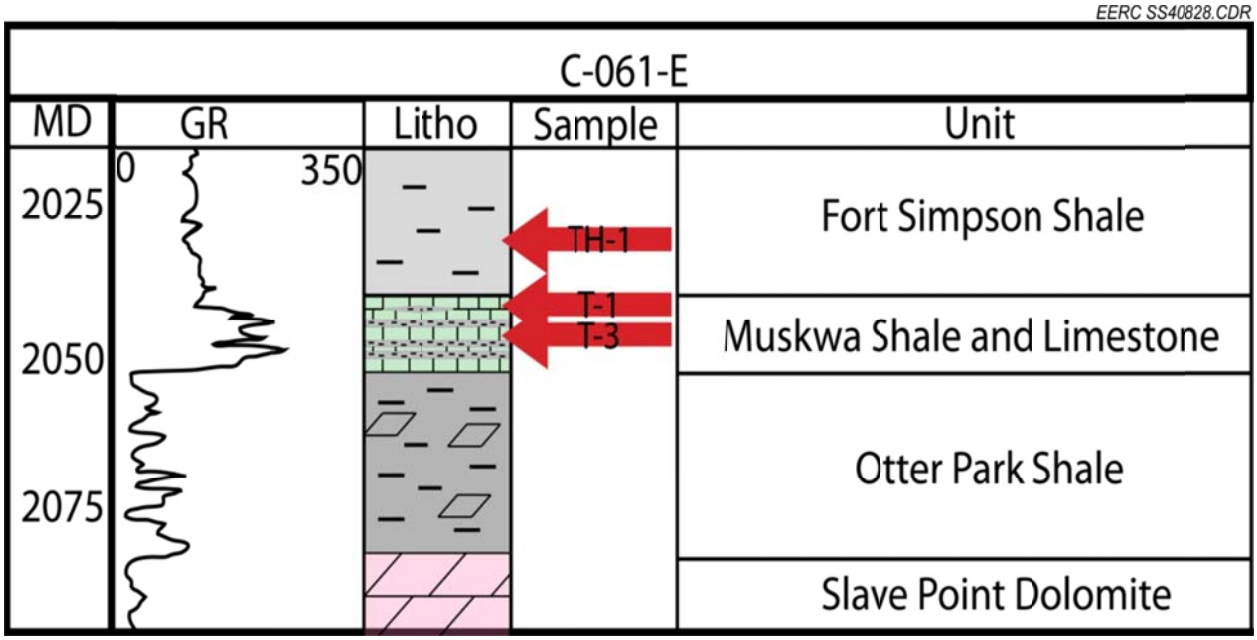

Figure 3. Gamma and lithology logs from Well C-061-E, with marked sample locations from the Fort Simpson and Muskwa Formations.

Table 1. Depth and Identification Information for Fort Nelson Cap Rock Samples

Depth, meters	Formation	Sample Designation	NMARL[1] No.	AGL[2] No.
2030.04	Fort Simpson	TH-1	10-0209	1663-019-02
2042.11	Muskwa	T-1	10-0208	1663-019-01
2045.75	Muskwa	T-3	11-0210	1663-019-03

[1] Natural Materials Analytical Research Laboratory.
[2] Applied Geology Laboratory.

It is expected that rocks in the area represent a typical shallow marine shelf setting that experienced a short-term marine regression, resulting in nearshore deposition of Muskeg salts in a restricted setting, followed by a larger-scale transgressive event. The deeper water was sufficient to bury the system in shale and organic material, which was preserved by anoxic conditions (Figure 4). High-salinity fluids were later expelled from the carbonate reefs during early-period compaction (and possibly later during hydrocarbon generation), leading to secondary mineralization surrounding the reservoir.

In order to facilitate a geochemical evaluation to be performed by Dr. Perkins, testing of these cap rock samples was performed at the EERC. Laboratory activities focused on quantification of mineral phases and elemental compositions, sample morphology and diagenesis, and rock properties.

This data set will be used to fully characterize cap rocks, with the goal of understanding potential rock–injected fluid reactions that may arise because of a variety of gas compositions that may exist over the lifetime of the Fort Nelson CCS project.

SUMMARY OF TESTING

Testing was conducted to collect a suite of mineralogic and lithologic data from the core samples provided (Figure 5). The testing was designed to minimize sample handling and, at the same time, produce the range of desired test methods. The analyses performed involved a suite of techniques that each provide their own unique view of the sample and output data.

- **Bulk mineralogy:** X-ray diffraction (XRD) techniques were employed on powdered specimens using a Bruker D8 Advance apparatus to attain bulk mineralogy.

- **Trace element detection:** X-ray fluorescence (XRF) techniques were employed on sintered, powdered specimens. Elemental signatures were collected and analyzed as weight percentages of oxide phases (if applicable) or anionic species.

- **Petrographic analysis**: Samples were mounted, cut, and polished to ~30 micrometers in thickness using water as the cutting fluid. Sections were analyzed and photographed using a petrographic microscope.

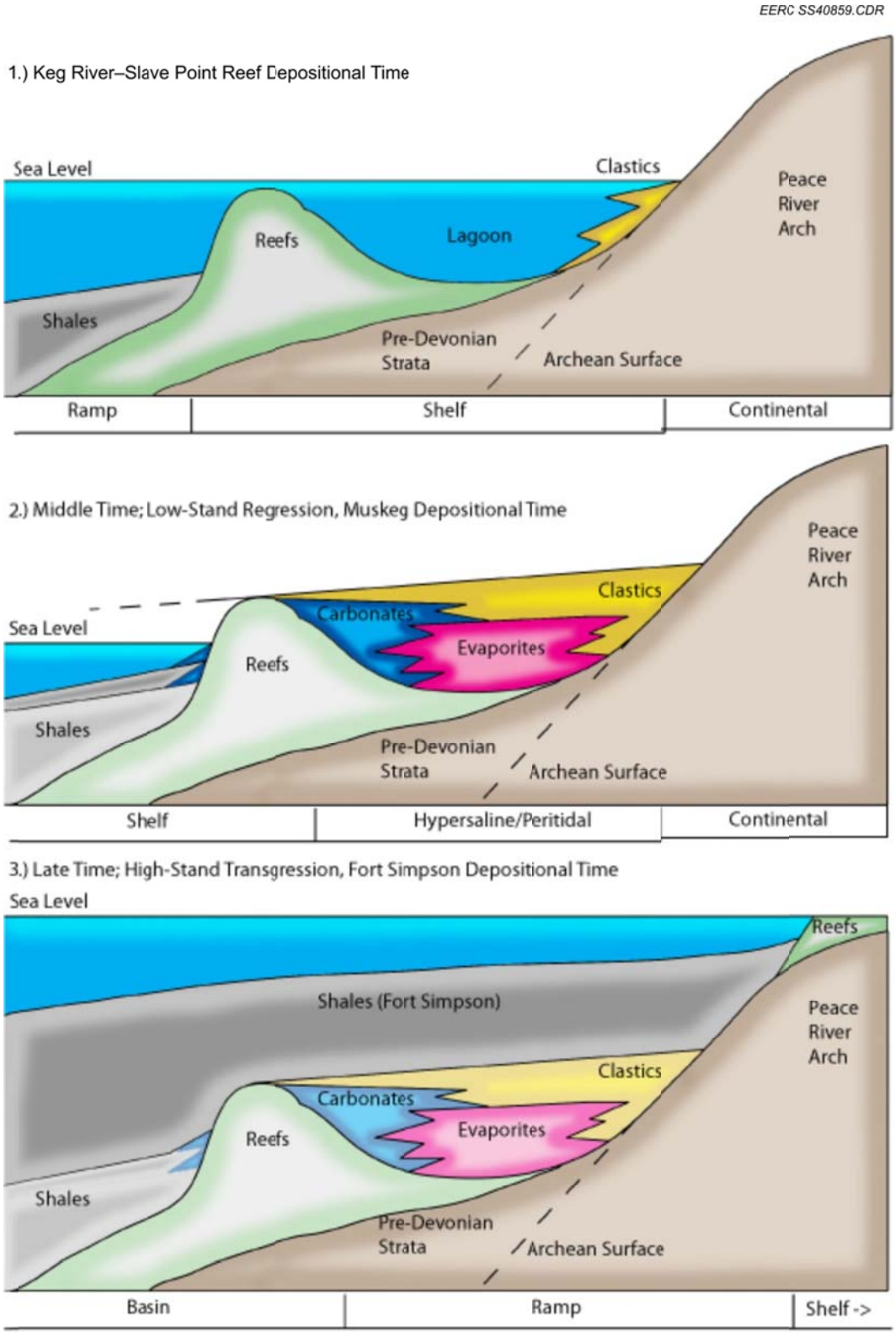

Figure 4. Illustration depicting the depositional history of the Keg River, Slave Point, and Fort Simpson Formations in the Fort Nelson area.

Figure 5. Photographs of Fort Nelson cap rock samples as received. These samples represent three cap rock intervals present in the Fort Nelson area.

- **QEMSEM** (quantitative elemental mapping using scanning electron microscopy): QEMSEM was used to collect backscatter electron and energy-dispersive spectroscopy (EDS) data two-dimensionally across a sample surface. This technique provides information pertaining to grain shape, mineralogy, location, and situation in the sample.

- **SEM**: High-resolution backscatter electron images were collected using a scanning electron microscope. EDS was also employed to examine specific points for elemental attributes, which aids in mineralogical identification.

- **CHN/S**: A carbon–hydrogen–nitrogen/sulfur (CHN/S) analyzer was used to determine the elemental prevalence of carbon, hydrogen, and sulfur within the sample.

- **Surface area**: A surface area analyzer was employed to measure a pulverized sample's surface area using gas adsorption.

- **Skeletal density**: Also known as grain density, skeletal density was measured using a helium pycnometer. The device measures the reduction of gas volume in the sample chamber caused by the presence of the rock sample.

- **ICP–MS/AES (**inductively coupled plasma–mass spectroscopy/atomic emission spectroscopy)**:** Elemental concentrations were measured for 32 trace metals, including rare earth, transition, lanthanides, and actinides.

ANALYTICAL RESULTS

Bulk Mineralogy by XRD

XRD was used to detect and identify crystalline phases of the shale samples provided for this evaluation.

For phase identification and Rietveld quantitative phase analysis (QPA), samples are prepared by reducing the specimen in a percussion mill followed by grinding into a powder using a micronizing mill. The sample is then dried and prepared as a randomly oriented powdered XRD sample. Crystalline phases are first identified using an automated search. After this, a Rietveld analysis is performed using whole-pattern general least-squares refinement to quantify mineral constituents.

For clay analysis, a decantation method first separates clay from silt. An oriented aggregate sample is made from the clay fraction to force platelike particles to lie flat, allowing the incident and diffracted beams to strongly interact with the [0 0 n] planes within the clay phases. XRD analysis of these low-angle reflections allows the direct observation of the spacing between these planes. The degree to which changes in spacing occur after the sample absorbs ethylene glycol is used to determine whether the clay has a smectite component. For a high concentration of clay sample, it is also possible to identify mixed-layer clays and to determine the ratio between illite group and smectite group layers by following procedures similar to U.S. Geological Survey (USGS) methodology (Środań, 1980; U.S. Geological Survey, 2001). The glycolation methodology flow chart that defines end member products is presented in Figure 6.

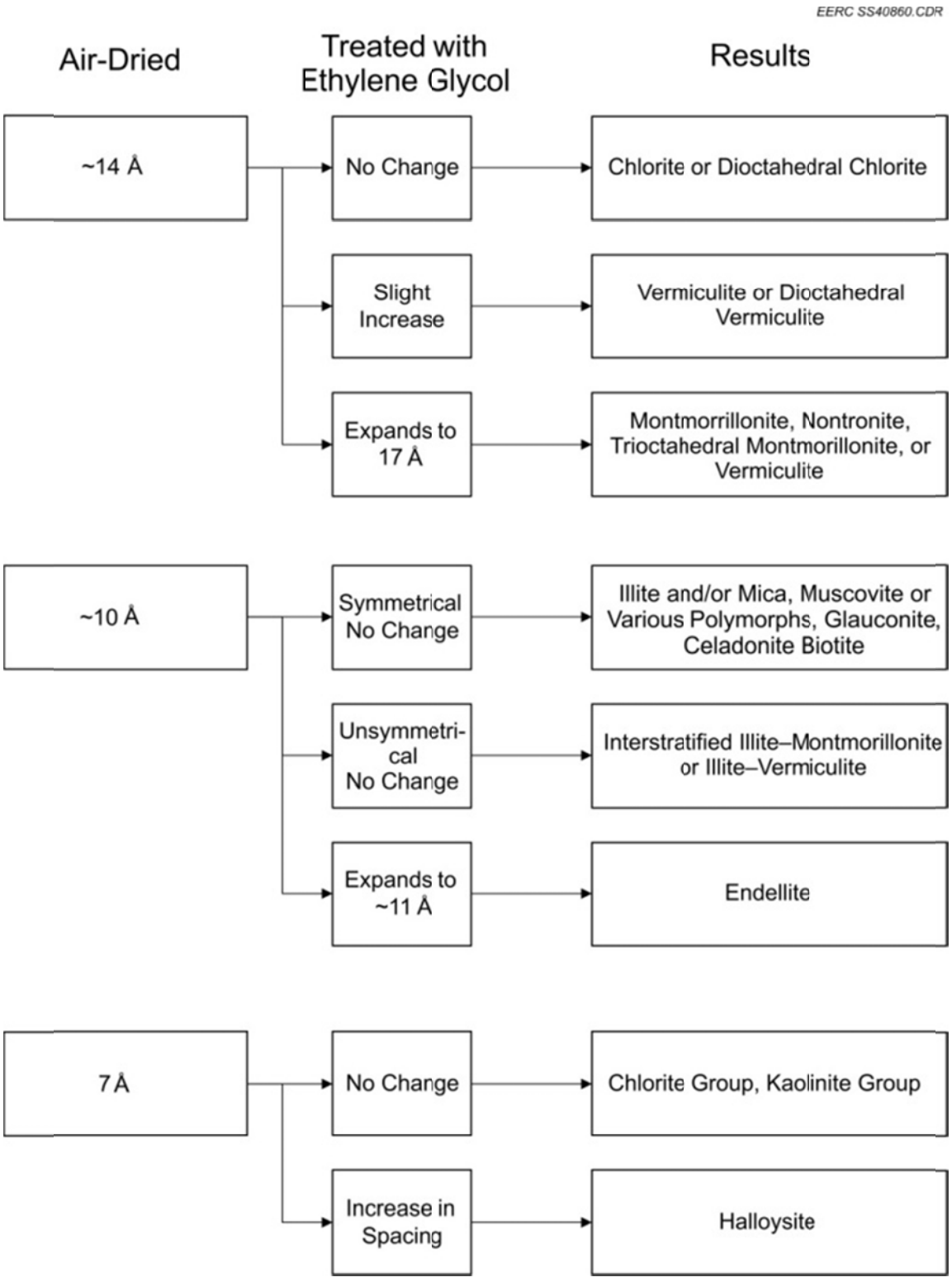

Figure 6. Flow chart showing defined clay assemblages identified through oriented glycolation methods.

For QPA, the Rietveld method is used to reduce the difference between a calculated diffraction pattern and the experimental data. Effects that normally detract from the quality of information from semiquantitative XRD, such as preferred orientation, instrument aberrations, and peak overlap can be accounted for using this method. Quartz was measured in higher quantities than were found through other methods (SEM, QEMSEM, XRF, and thin-section analysis). XRD is selective in measuring only phases that are crystalline. Chemical phases without long-range structure or comprising particles below several nanometers in size will appear amorphous and not yield a significant diffraction pattern. These phenomena are expected to affect clay detection and result in underestimation.

Key Observations

Relative weight percentages and XRD spectra were determined for prominent minerals in each sample and are reported in Table 2 and Figure 7. Quartz and clay were found to be the most common phases in these samples, followed by dolomite and ankerite, which were only prevalent in Sample T-3. Pyrite was a common accessory mineral in all three intervals, but was least common in Sample T-3. The remainder of detected phases represents a combination of clastic and chemical species.

- Nonswelling illite clay is thought to be the dominant clay type in the examined samples.
- Concentrations of swelling clays were found to be below detectable limits.
- Additional spectral images including glycolation scans are presented in Appendix A.

Table 2. Relative Weight Percentages of Identified Mineral Phases in Each Sample

	TH-1, 11-0209	T-1, 11-0208	T-3, 11-0210
Illite	47.0	46.2	21.6
Pyrite	7.0	6.5	3.5
Quartz	41.6	40.9	31.0
Sanidine $Na_{0.56}$	2.0	2.5	0.6
Anhydrite	0.0	0.0	0.0
Ankerite $Fe_{0.55}$	0.8	2.0	16.1
Dolomite	1.0	0.7	25.0
Ankerite $Fe_{0.7}$	0.0	0.0	1.9
Dolomite Disordered	0.0	0.0	0.0
Muscovite-2M1	0.4	0.5	0.2
Kaolinite (BISH)	0.0	0.0	0.0
Siderite	0.3	0.7	0.0
Goodness of Fit	1.67	1.77	1.47
R_{exp}	9.66	9.53	9.30

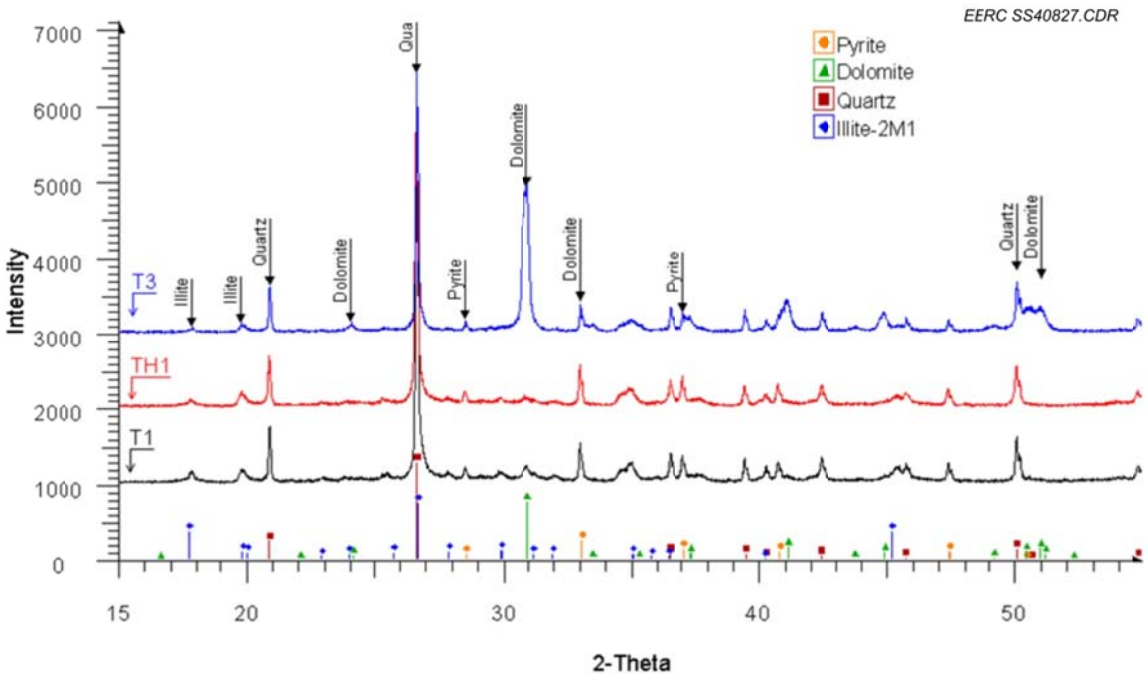

Figure 7. XRD patterns for Fort Nelson cap rock samples with annotated peaks for prevalent minerals detected through analysis.

- Other than quartz/clay portions, prevalence of other detected minerals is highly agreeable to results derived from QEMSEM/thin-section analysis.

- XRD results are thought to overestimate quartz and underestimate clay.

- Quartz was measured in higher quantities than were found through other methods (SEM, QEMSEM, XRF, and thin-section analysis) and is thought to be a product of oriented-aggregate sample preparation. This method of sample preparation settles the powdered sample onto a filter paper where less buoyant materials (pyrite, quartz, etc.) will be deposited before suspended clays, possibly causing preferential sampling of quartz present in the sample.

- Additional clay may have been lost in the amorphous background because of the small crystallite size.

Trace Element Analysis by XRF

XRF is a technique that provides the bulk elemental composition of samples. The device allows semiquantitative determinations to be made for elements with atomic numbers of 6 through 92 (carbon through uranium), with accuracies that can be attained to the ppm level (typical reporting to 0.1 wt%). Although XRF by itself cannot distinguish elemental arrangements, it excels at detecting products of trace minerals, elemental replacement, and small concentrations of elements.

Samples TH-1 and T-1 were processed through a typical routine that quantitatively analyzes 14 elements (reported as oxide weight percentages). Sample T-3 had a significant amount of material that was not included in ordinary analysis, and an additional 12 elements were semiquantitatively collected.

Only two elements were subject to shared analysis between XRF and ICP–MS, these being titanium and manganese. Titanium concentrations were found to be in agreement, with titanium decreasing with depth. Manganese concentrations are in disagreement between the two devices, with XRF reporting high manganese in Sample T-1, while ICP–MS methods detected this interval to have the lowest of the three samples. The cause of this disagreement is unknown. Additional semiquantitative analysis of T-3 overlapped nine elements with ICP–MS testing. Results appear to be in agreement for arsenic, zinc, copper, nickel, manganese, vanadium, and titanium. Discrepancies are apparent between the two device's measurements of chromium and yttrium. It is difficult to diagnose the cause of this difference, although it is expected that small sample size and low concentrations of these elements may have eluded XRF analysis.

Key Observations

Results of XRD testing are presented in Tables 3 and 4. The following observations were noted while analyzing results of XRF testing on Fort Nelson cap rock samples:

- Samples TH-1 and T-1 had low volumes (less than 2%) of unknown phases.
- Because of a high amount of unknown phases (9.5%) in Sample T-3, additional processing resulted in semiquantitative relative weight percentages of each phase present. Carbon was found to be a significant phase in this sample.
- Elemental signatures were highly similar between Samples TH-1 and T-1. A notable difference was observed, however, in manganese content.
- Significantly higher calcium and magnesium levels were detected in Sample T-3, indicating a higher concentration of dolomite. The previously noted significant carbon phase in this sample also supports this finding.
- A variety of trace metals are apparent in the samples, suggesting continental influx and/or hydraulic enrichment.

Table 3. Quantitative Common Oxide Weight Percentages for Fort Nelson Samples

	SiO_2	Al_2O_3	Fe_2O_3	TiO_2	P_2O_5	CaO	MgO	Na_2O	K_2O	SO_3	BaO	SrO	MnO	Cl	Total
TH-1	64.80	19.01	5.05	0.66	0.07	0.43	1.47	0.29	4.51	1.88	0.15	0.02	0.01	0.03	98.37
T-1	62.46	18.86	5.40	0.64	0.10	1.13	1.81	0.28	4.75	2.49	0.14	0.01	1.78	0.03	99.88
T-3	47.38	8.61	3.50	0.40	0.07	18.21	7.48	0.10	2.58	2.17	0.08	0.02	0.11	0.03	90.73

Table 4. Semiquantitative Report of Detectable Phases in Sample T-3

No.	Component	Result, wt%	Detection Limit, wt%
1	CO_2	17.0000	0.10406
2	F	0.1810	0.07410
3	Na_2O	0.1320	0.01012
4	MgO	8.0900	0.00990
5	Al_2O_3	8.9200	0.00685
6	SiO_2	37.2000	0.00882
7	P_2O_5	0.0874	0.00144
8	SO_3	3.3400	0.00290
9	Cl	0.0202	0.00243
10	K_2O	2.3900	0.00241
11	CaO	17.1000	0.00474
12	TiO_2	0.4350	0.00724
13	V_2O_5	0.0213	0.00689
14	Cr_2O_3	0.0137	0.00393
15	MnO	0.1070	0.02249
16	Fe_2O_3	3.1400	0.00332
17	NiO	0.0085	0.00175
18	CuO	0.0052	0.00146
19	ZnO	0.0030	0.00123
20	As_2O_3	0.0023	0.00119
21	Rb_2O	0.0079	0.00078
22	SrO	0.0164	0.00080
23	Y_2O_3	0.0064	0.00413
24	ZrO_2	0.0140	0.00084
25	BaO	0.0961	0.01857
26	C	1.6900	–

Petrographic Analysis

Optical petrography is a geologic technique that utilizes thin (approximately 30 micrometers thick) polished sections of rock to differentiate mineralogy and fabric within the sample. This type of analysis is often able to identify common mineral assemblages and estimate their prevalence as well as identify any microscopic structures or fractures present in the sample. Pore sizes may be measured and defined, and diagenetic events (including pore creation) may be inferred.

Thin sections of Samples TH-1, T-1, and T-3 were created using a standard thin-section mill to cut and grind the epoxy-mounted rock specimens. Samples were analyzed with a petrographic microscope utilizing plane-polarized, cross-polarized, and reflected light. Photomicrographs of the finished thin sections and complete descriptions are provided in Appendix B. Annotated photomicrographs showing representative areas of each interval are shown in Figures 8–10.

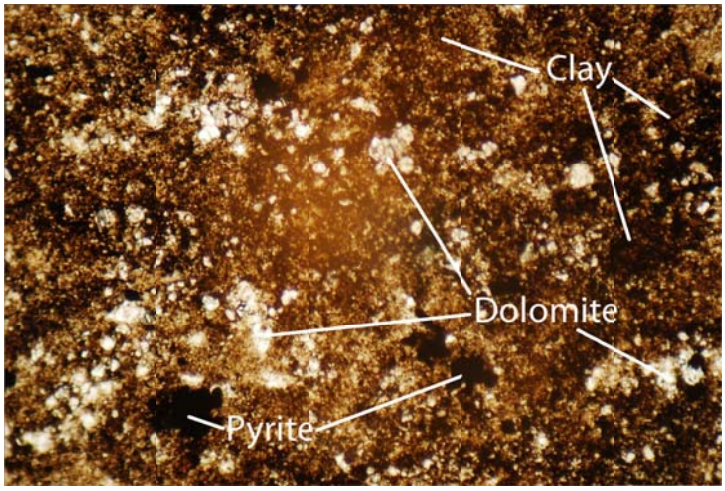

Figure 8. Photomicrograph of TH-1, plane-polarized light, 100× magnification.

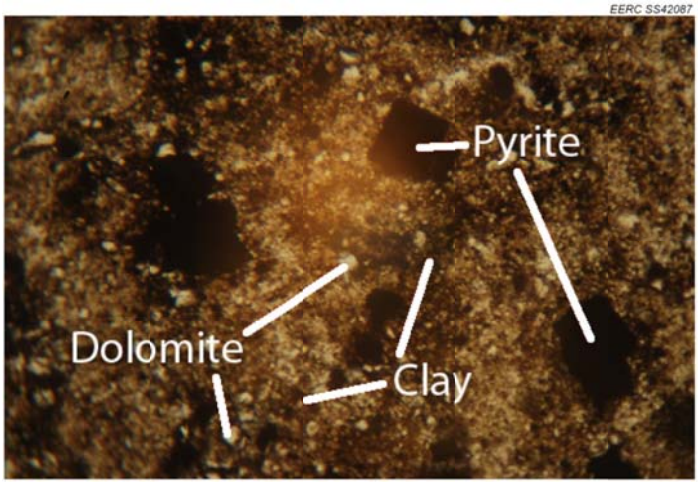

Figure 9. Photomicrograph of T-1, plane-polarized light, 100× magnification.

No dyes were used for thin-section production, which may be applied for various purposes such as carbonate typing or simplified porosity identification. As such, all carbonates were identified as dolomite based on observable rhombahedral shape. This was validated as dolomite in subsequent analyses of these samples. No point counts were performed on thin sections, as QEMSEM and scanning electron microscope data provide higher accuracy and precision in their measurements.

No porosity was observed during thin-section analysis, which is in disagreement with porosity measurements obtained during skeletal density measurements. This impasse is the result of the very fine microporosity in the samples, which, even at high magnification, does not become apparent in a ~30-µm-thick thin section. This observation is supported by high-magnification scanning electron microscope images showing fine pore structure of the rock samples.

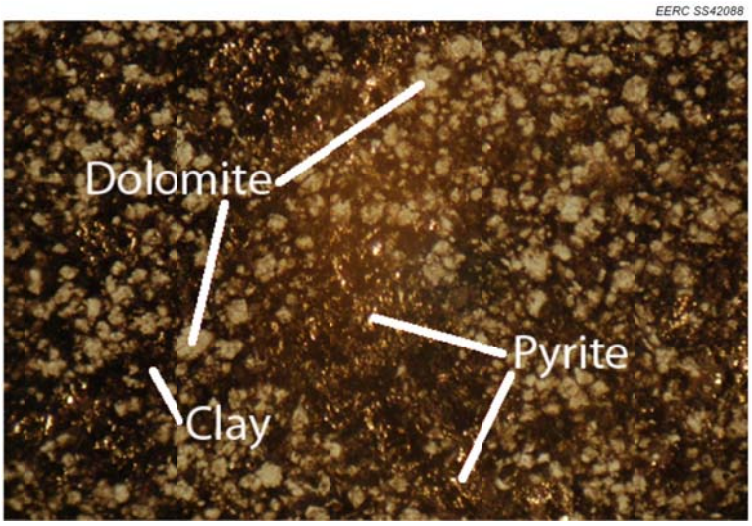

Figure 10. Photomicrograph of T-3, reflected light, 40× magnification.

Sample TH-1 lithologically comprises consolidated shale/mudstone. Thin sections are approximately 75% clay and 10% pyrite, with 15% fine-grained sparry carbonate. Grains are very fine-textured with the exception of interclasts, and the sample contains no visible porosity. Carbonate interclast growth is diagenetic. No microstructures were observed, and the sample is fairly homogeneous. Rare dolomite-cemented microfractures were observed. Dolomite clasts are euhedral to subhedral, and pyrite is subhedral to anhydral. Both mineralization varieties are of variable size. The sample likely contains low levels of organic material. Rock material was interpreted to have been originally deposited in a deep restricted marine setting followed by hypersaline influx postdepositionally.

Sample T-1 is a slightly mineralized, consolidated shale/mudstone. The section is approximately 75% clay, 15% sparry dolomite interclasts, and 10% pyrite, with trace quartz (silt) grains. The sample is very fine-grained, with the exception of the euhedral/subhedral dolomite and subhedral–anhedral pyrite clasts, which are secondary formations. The sample contained no visible porosity. No microstructures were observed, and the sample is fairly homogeneous, with the exception of scattered/loosely bedded pyrite growths. The sample likely contains low levels of organic material. The sample is thought to have been originally deposited in an anoxic, deep, restricted marine environment, followed by hypersaline influx postdepositionally.

The T-3 interval comprised argillaceous sparry dolomite. The section is approximately 70% coarse dolomite grains with significant clay (20%) and traces of silt (5%) and pyrite (5%). The sample is fairly homogeneous, with no preferential bedding or microstructure and no visible porosity. Dolomite clasts appear euhedral to anhedral and are of similar size. Pyrite varies in size and is anhedral to subhedral, with rare euhedral crystals. This rock has been highly impacted by diagenetic activity. T-3's carbonate fabric is classified as a sparite/dismicrite according to the Folk classification system and a packstone by the Dunham system. The interpreted depositional environment for this interval is restricted marine, followed by diagenetic hypersaline influx.

Key Observations

All three specimens represent various tight cap rock units from the Fort Nelson area. The first two intervals were very similar, containing high percentages of clay, with variable pyrite, silt and fine-grained carbonate, while the third interval contained a much higher degree of sparry carbonate growth (Tables 5 and 6). No microstructure was visible in any of the sections. These results confirm 1) the Fort Simpson Shale will provide a significant barrier to flow and 2) the Muskwa Formation warrants additional study to determine the flow characteristics and potential for reactivity between injected CO_2 and carbonates contained within the shale matrix. Other observations included the following:

- Samples TH-1 and T-1 were observed to be remarkably similar, with only minor differences noted in pyrite crystalline behavior and size. Sample T-3 was different in that scattered carbonate growth was much more common throughout the sample.

- No porosity was observed in any of the sections.

- Observations are consistent with the geological interpretation of an offshore restricted marine environment that has received postdepositional dolomitization seen to increase with depth, likely because of enriched water exiting the underlying Slave Point carbonates.

- Pyrite growth is more apparent in the clay-rich TH-1 and T-1, likely caused postdepositionally by enriched water moving through the reducing organic shales.

- Results of optical mineralogy analysis are in agreement for major phases observed in QEMSEM and SEM data. Results are in agreement with XRD-derived bulk mineralogy in non-clay/quartz phases.

Table 5. Mineralogical Estimates Derived Through Thin-Section Analysis

Sample	Clay/Silt, %	Carbonate, %	Pyrite, %	Quartz
TH-1	75	15	10	–
T-1	75	15	10	Trace
T-3	20	70	5	5%

Table 6. Rock Fabric Descriptions Related to Grain, Pore, and Clay Characteristics, Based on Thin-Section Analysis

Sample	Grain Size	Texture	Porosity Est.	Uniformity
TH-1	Very Fine	Anhedral–subhedral	None observed	Well, except for pyrite
T-1	Very Fine	Anhedral–subhedral	None observed	Well, except for pyrite
T-3	Fine	Anhedral–euhedral	None observed	Well, except for pyrite

QEMSEM Analysis

QEMSEM is a specialized scanning electron microscope technique that allows for acquisition of high-resolution backscatter and EDS scans of a polished sample surface. Data are collected and processed through software that allows the user to define modeled mineralogic phases based on collected elemental and back-scatter signatures. The device is used in the mining industry to characterize the size, shape, and concentration of product in ore; however, the two-dimensional mapping capability has found new uses in geochemistry, kinetics, and characterization.

Rough samples were prepared by suspension in epoxy, which was allowed to harden prior to slabbing a fresh face using a diamond-impregnated steel saw, with IsoCut® fluid as the cutting medium. Samples were polished using a progressively fining diamond–alcohol suspension fluid. The samples were coated with a thin layer of gold to prevent electron charging in the microscope. Scans collecting electron backscatter and EDS were performed at 15 μm resolution across the entire polished surface.

Mineral assemblages were decoded from elemental signatures and were quantified across the sample surface, as shown in Table 7. Color-coded photomicrographs of each QEMSEM sample representing the detected mineral contents are shown in Figures 11–13. Epoxy surrounding the samples has been removed from quantification, while epoxy surrounded by the sample was retained. Removed epoxy quantifications include the separation feature in Sample T-1.

Porosity was not observed in any of the samples except for microfractures. This is in disagreement with SEM and skeletal density measurements and is the result of porosity being of finer size than the 15-μm scan resolution. Because of the small pore size and relatively high scan resolution, the device is able to detect enough of the polished rock surface to register it as rock, rather than inference caused by the pores.

Sample TH-1 is primarily illite clay (76%), with silt-sized quartz grains (7%) and minor kaolinite (6%) scattered throughout the muddy fabric. Pyrite (4%) and dolomite (2%) are prevalent thoughout the sample as small inclusions that are primarily subhedral, with rare euhedral crystals. Thin bedding is observable in QEMSEM imagery as laminations of quartz and porous bedding planes, concentrated in the upper half of the sample. Trace apatite, barite, and sphalerite were also detected.

Sample T-1 comprises primarily illite clay (75%), with silt-sized quartz grains (6%) and minor kaolinite (7%) to form the muddy rock fabric. Pyrite (8%) is concentrated across the sample in a band; however, a small amount is dispersed through the sample as small crystals. The size and concentration of dolomite is reduced from the lower intervals, only present as 1% of this sample. Trace amounts of apatite and barite were also detected. Microfractures across the sample are not laminar, possibly indicative of cross-bedding, although quartz bedding is not observable in this sample.

Table 7. Quantitative Mineral Assemblages Present in QEMSEM Samples

Interval	Illite	Kaolinite	Quartz	Dolomite	Pyrite	Other	Unidentified
TH-1	76	6	7	2	4	2	3
T-1	75	7	6	1	8	1	2
3	16	4	13	46	4	10	7

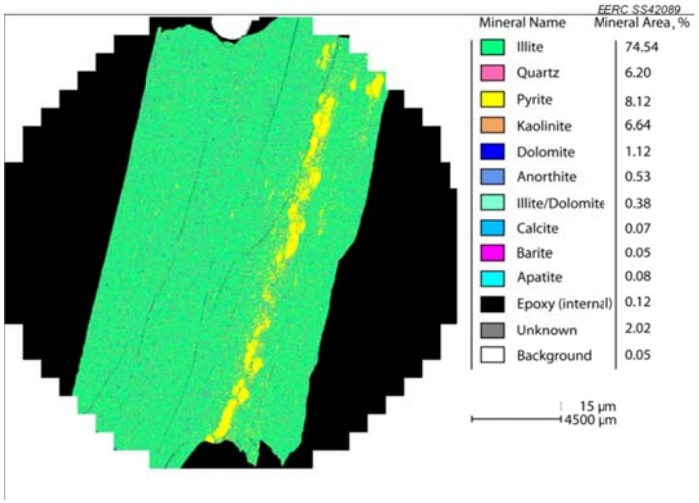

Figure 11. QEMSEM image of the TH-1 interval. Groundmass consisting of illite clay (green) with quartz (pink) and dolomite (blue) should be noted. A dominating band of pyrite (yellow) cuts across the sample. The sample contains several microfractures (black – epoxy) which possibly indicate fine-scale cross-bedding.

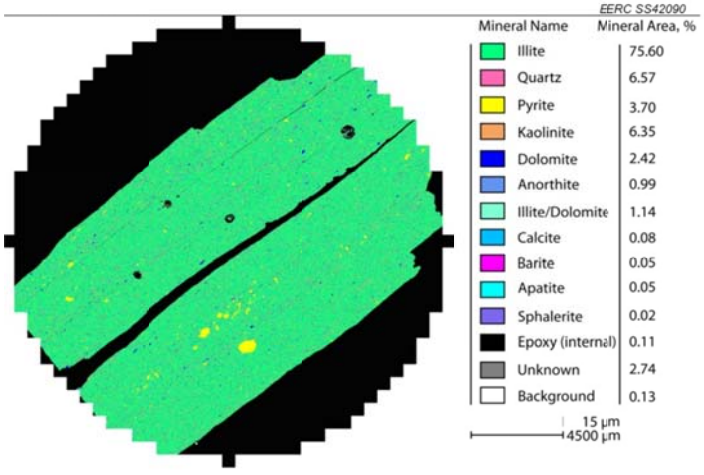

Figure 12. QEMSEM image of the T-1 interval. Groundmass consisting of illite clay (green) containing quartz (pink) and dolomite (blue) should be noted. The sample contains inclusions of pyrite (yellow). Microfractures (black – epoxy) may indicate laminar bedding plains across the sample.

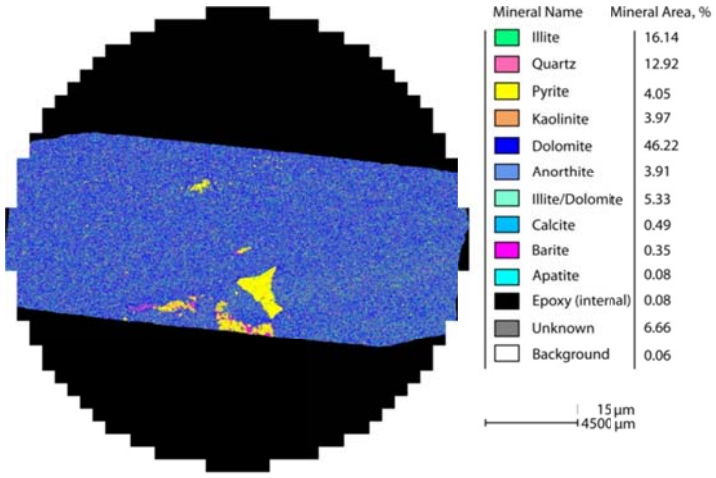

Figure 13. QEMSEM image of the T-3 interval. This sample contains significant dolomite (blue) with mixed argillaceous material. Pyrite (yellow) and barite (magenta) are possibly replacing fossiliferous material in the middle of the sample or filling irregular vuggy porosity. No microfractures or observable bedding are present in the sample.

Sample T-3 is observably different than the other two examples, comprising primarily dolomite (46%), with a high percentages of argillaceous, dispersed illite (16%), silt-sized quartz (13%), and kaolinite (4%). Large and small inclusions of pyrite (4%) appear to be replacing possibly fossiliferous material in conjunction with associated barite and apatite (trace). This sample contains a significant portion of unidentified material (7%). No microfractures or observable bedding are present across the sample.

Key Observations

The following observations were made during QEMSEM analysis of the Fort Nelson cap rock samples:

- No porosity (other than microfractures) was found in any of the samples.
- Illite clay (potassium-rich) was the prevalent groundmass of Samples TH-1 and T-1.
- Dolomite was the most common mineral in Sample T-3, but the rock mass remains highly argillaceous.
- Sample TH-1 appears to have thin laminar bedding. The bedding in T-1 appears to be less linear, possibly indicating fine-scale cross-bedding.
- Sample T-3 has the highest concentration of "uncommon" phases, such as barite and apatite, as well as the most unidentified phases.

- QEMSEM results are consistent with mineralogical estimations made through thin-section analysis and are supported by SEM data. XRD is in reasonable agreement for non-clay/quartz phases.

SEM Reporting

Scanning electron microscopes are used extensively to capture detailed images at high magnification. Rather than using transmitted or reflected light, as in typical optical microscopy, scanning electron microscopes use an electron beam that bombards the surface of the sample, resulting in several sensory phenomena, foremost being backscatter electrons. By scanning the beam across a surface, high-resolution images may be captured that correlate to the density of the viewed object.

An additional phenomenon arises when electrons are absorbed by struck atoms, which releases a characteristic x-ray unique to the atom's atomic number. By collecting and analyzing the x-ray wavelengths, atomic signatures can be collected through a process known as EDS.

SEM was performed on both polished and fractured sample fragments. Prior to scanning, a thin coat of carbon or gold was applied to the sample to prevent electrical charging of the surface. Backscatter electron-based images were captured at high magnification of the surface in conjunction with EDS measurements. Descriptions of key observations are presented in this portion of the document, with additional high-magnification backscatter electron images, EDS point count data, and additional descriptions presented in Appendix C.

For Sample TH-1, the sample fabric contains high concentrations of microporous silt and potassium-rich clay. Rare fossil and chemically deposited material comprising apatite is present in the sample as well as scattered accumulations of subhedral, radial (variable marcasite), and framboidal pyrite. Dolomite recrystallized zones appear to contain significant portions of iron, possibly indicative of ankerite alteration. Rare accumulations of titanium were also observed in the sample (Figure 14).

For sample T-1, potassium- and magnesium-rich clay constitutes a majority of the sample fabric, with trace amounts of iron and titanium present. Pyrite and, possibly, marcasite accumulations are obvious as bright zones in any frame of the sample and consist of framboidal, radial, occasionally globby, and subhedral cubic forms. Dolomite recrystallization in the sample is zonal and appears to favor more porous areas with higher concentrations of quartz than the typical clay-rich accumulation. Rare porous fossiliferous material was observed comprising apatite (Figure 15, Tables 8 and 9).

Sample T-3 comprised primarily microporous dolomite and argillaceous dolomite, with accumulations of pyrite and a significant portion of barite. Pyrite exists as both subhedral-to-anhedral fine-grained inclusions to large recrystallized zones, showing both cubic and radial forms. Rarely, pyrite accumulations were observed to contain inclusions of barite (Figure 16, Tables 10 and 11).

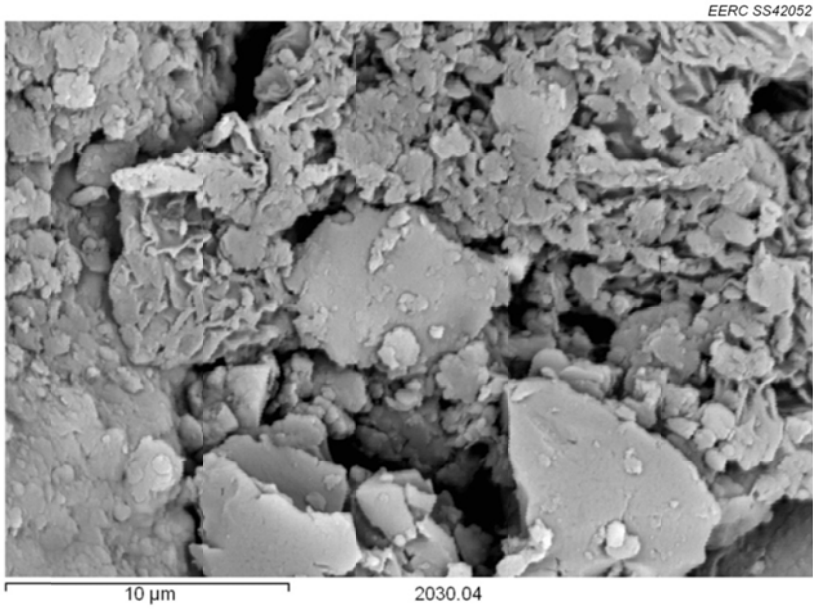

Figure 14. Fracture-mounted photomicrograph of Sample TH-1 at 5000× magnification. This sample shows microporous, disoriented clay particles.

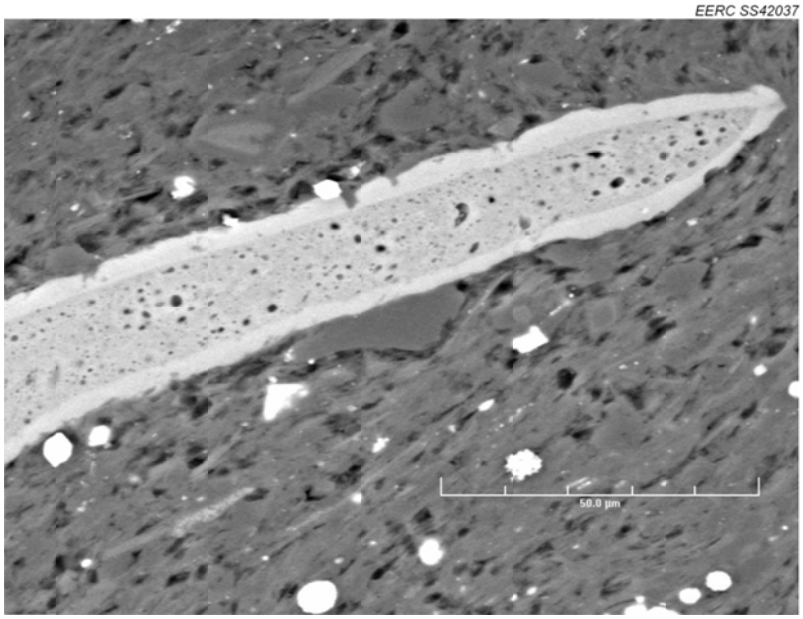

Figure 15. Electron backscatter micrograph of polished section of Interval T-1 taken at 750× magnification. This image depicts fossiliferious material comprising porous apatite (center) surrounded by a microporous silty shale groundmass. Fine-grained pyrite/marcasite is present throughout the sample as bright accumulations.

Table 8. Elemental Compositions at Probed EDS Locations for Figure 15, Sample T-1, as relative percentage

Tag	Na	Mg	Al	Si	P	S	Cl	K	Ca	Ti	Fe	Ba
1	0.00	18.69	0.74	2.74	0.20	0.08	0.00	0.39	58.14	0.00	19.02	0.00
2	0.00	0.58	10.15	76.85	0.00	0.50	0.00	9.74	0.88	0.09	1.20	0.00
3	0.00	0.04	5.12	86.45	0.24	0.00	0.00	6.29	1.06	0.00	0.59	0.20
4	0.00	0.00	0.10	0.92	32.81	0.00	0.00	0.12	66.01	0.00	0.03	0.00
5	0.00	0.00	0.18	1.19	32.04	0.00	0.00	0.14	66.45	0.00	0.00	0.00
6	0.09	0.00	0.05	0.52	32.61	0.00	0.00	0.12	66.54	0.00	0.07	0.00
7	0.00	0.00	0.00	0.44	32.80	0.00	0.10	0.06	66.60	0.00	0.00	0.00
8	0.00	0.00	0.63	95.95	0.39	0.00	0.00	2.70	0.21	0.00	0.11	0.00
9	0.00	0.00	4.52	88.54	0.00	0.00	0.00	5.39	0.00	0.81	0.74	0.00
10	0.00	0.00	4.71	88.32	0.00	0.00	0.00	5.99	0.00	0.33	0.65	0.00

Table 9. Mineralogical Interpretation of Probed EDS Locations for Figure 15, Sample T-1

Tag	Mineralogical Interpretation	Tag	Mineralogical Interpretation
1	Ankerite	6	Apatite
2	Illite	7	Apatite
3	Illite	8	Illite
4	Apatite	9	Illite
5	Apatite	10	Illite

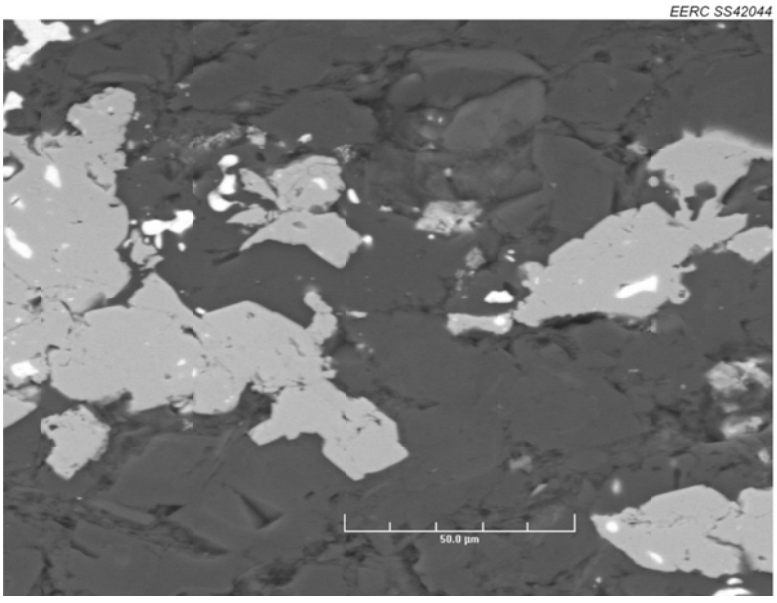

Figure 16. Electron backscatter micrograph of T-3 taken at 750× magnification. This image shows argillaceous dolomite (dark, rough surface), with secondary accumulations of subhedral to anhedral pyrite (gray) containing bright white inclusions of barite.

Table 10. Elemental Compositions at Probed EDS Locations for Figure 16, Sample T-3, as relative percentage

Tag	Na	Mg	Al	Si	P	S	Cl	K	Ca	Ti	Fe	Ba
1	0.00	25.08	0.32	1.65	0.29	0.41	0.00	0.14	70.47	0.00	1.65	0.00
2	0.00	27.27	0.00	0.58	0.50	0.12	0.00	0.00	70.43	0.00	1.09	0.00
3	0.00	30.16	0.13	0.29	0.41	0.15	0.00	0.00	67.63	0.00	1.22	0.00
4	0.00	0.00	0.00	0.30	0.24	54.14	0.10	0.00	0.05	1.48	43.69	0.00
5	0.00	0.00	0.00	8.89	0.05	16.91	0.00	0.00	0.03	9.17	1.11	63.85
6	0.00	0.00	0.00	0.03	0.33	53.97	0.22	0.00	0.08	1.55	43.80	0.00
7	0.01	0.00	0.00	0.04	0.10	30.05	0.00	0.00	0.00	6.89	14.83	48.08
8	0.00	0.00	0.00	0.59	0.00	28.67	0.00	0.00	0.00	7.46	12.22	51.06
9	0.00	25.68	0.87	3.01	0.68	0.31	0.09	0.42	67.94	0.00	1.00	0.00
10	0.00	27.13	0.21	0.62	0.48	0.12	0.00	0.00	69.61	0.00	1.83	0.00

Table 11. Mineralogical Interpretation of Probed EDS Locations for Figure 16, Sample T-3

Tag	Mineralogical Interpretation	Tag	Mineralogical Interpretation
1	Dolomite	6	Pyrite
2	Dolomite	7	Barite
3	Dolomite	8	Barite
4	Pyrite	9	Dolomite
5	Barite	10	Dolomite

Key Observations

The following observations were made while analyzing Fort Nelson cap rock samples under SEM:

- SEM data were found to be integral to describing the fine-scale microporosity in the samples. Porosity observed through SEM techniques explains measurements of surface area and skeletal density testing that were not found from thin-section or QEMSEM methods.

- SEM data found barite within pyrite masses, which is also seen with QEMSEM.

- Fracture-mounted images show chaotic clay bedding and three-dimensional images of crystallography and complex structures.

- Iron sulfide is seen in framboidal, cubic, and radial (marcasite) forms. Framboidal pyrite structures are often biogenically controlled (Kamamura, 2002).

CHN/S Analysis

CHN analyzers specialize in providing quantification of carbon, hydrogen, and nitrogen which are present in the sample. The device measures both elemental and ionic content, meaning that carbon is detected both as elemental carbon and the carbon portion of carbonate, if present. An additional module provides independent sulfur measurement capabilities to determine the total sulfur content of the sample.

In this study, total carbon, hydrogen, and sulfur were measured in each specimen (Table 12). Nitrogen was not measured and is expected to be a minor phase outside of detectable limits, as nitrogen does not incorporate into common rock-building minerals; instead, it is typically found in unaltered organic compounds, which are not present in these samples.

Carbon, hydrogen, and sulfur are common in rock-forming minerals, being present in carbonate, sulfate, sulfite, and sulfide salts as well as metal hydroxides. Aside from minerals and preserved organic material, hydrocarbons and hydrocarbon residues are known to accumulate CHN/S material.

Sulfur contents derived through this method were approximately four times higher than were observed through XRF testing. Calculations based on pyrite (FeS_2) content, which was the only major sulfur-containing mineral detected, yielded results approximately half of CHN/S analysis for QEMSEM values. Pyrite contents from XRD data calculated values approximately equal to CHN/S results for Samples T-1 and T-3 and showed greater sulfur concentration in Sample TH-1 than CHN/S. Sulfur content data remain inconclusive, as no clear trends or agreement in data could be attained. Sulfur in the cap rock system should be considered heterogeneous on a fine scale (observed in thin section, QEMSEM, and SEM), and may exist in the range of 0.5% to 3.7%. A plot of sulfur content data is presented in Figure 17.

Key Observations

Results from testing show that samples have variable contents of carbon, hydrogen, and sulfur, specifically:

- Carbon was significantly higher in Sample T-1 than in the other samples.
- Sample T-3 had significantly more carbon than TH-1. The high content of T-3 is in part due to the high carbonate content of the sample.

Table 12. Results of CHN/S Analysis

Sample	% Carbon	% Hydrogen	% Sulfur
TH-1	1.67	0.27	3.14
T-1	27.6	0.28	3.60
T-3	8.28	0.07	2.07

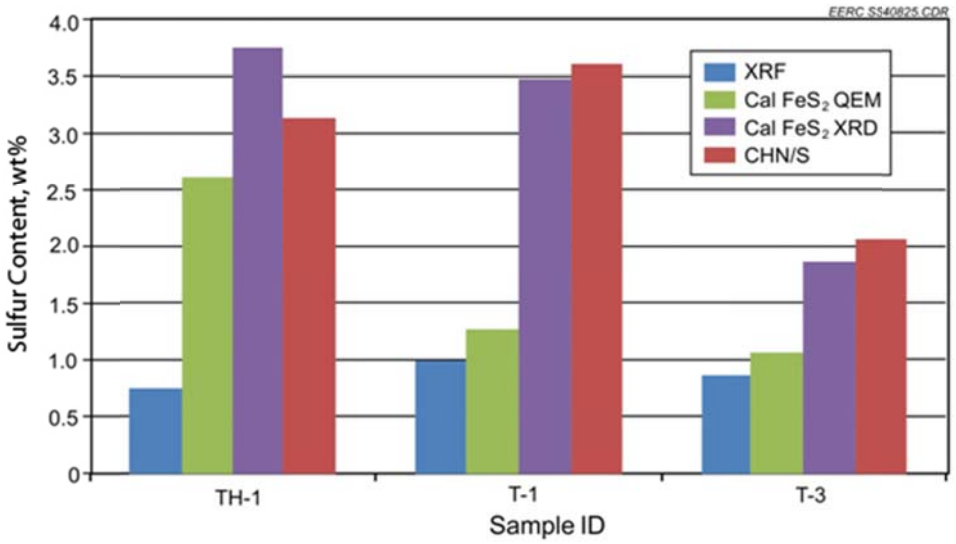

Figure 17. Results of sulfur analysis derived through XRF and CHN/S and calculated from pyrite contents derived from QEMSEM and XRD data.

- Hydrogen content was nearly equivalent in Samples TH-1 and T-1 but decreased sharply in Sample T-3.

- Sulfur increases slightly from Sample TH-1 to Sample T-1. Sample T-3 has the lowest concentration of sulfur. Sulfur content is thought to be a product of pyrite/marcasite content.

- Despite sample proximity and similarities in appearance, carbon, hydrogen, and sulfur contents show that heterogeneity still exists in the system.

- Sulfur contents found through total sulfur testing were higher than XRF measurements and from calculated pyrite concentrations derived through QEMSEM. Sulfur contents from XRD pyrite concentrations were close to CHN/S values; however, higher values for sulfur were observed in Sample TH-1.

Surface Area

A surface area analyzer was used in this study to measure total surface area of a sample in an effort to better understand reactive area and surface area-related attributes. The surface area of granulated and powdered solids or porous materials is measured by determining the quantity of gas that adsorbs as a single layer of molecules on the sample and is reported in square meters of coverage corrected to 1 gram of sample. These data have use in kinetics, as high surface areas can experience much faster and more dramatic reactions than tight crystalline materials.

Surface area correlates strongly to particle size and shape where small platelike clay particles tend to have higher surface area than more three-dimensional silt or dolomite portions. Carbon within a sample can be present in structures with a variety of surface areas and may

highly impact measurements. Surface area is used directly in chemical kinetics and may also be used to describe more abstract properties such as degree of cementation. Surface area measurements are reported in Figure 18 and Table 13.

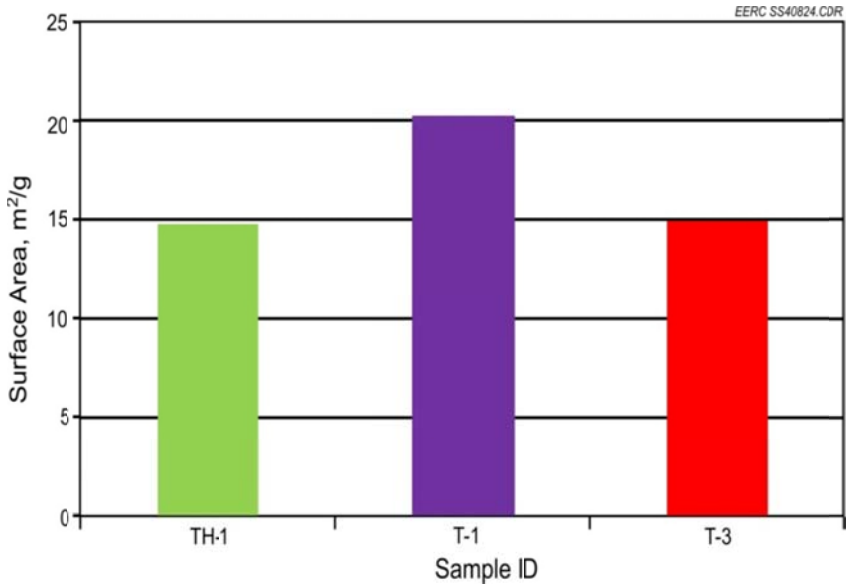

Figure 18. Comparison of results of surface area testing for Fort Nelson cap rock samples.

Table 13. Results and Calculations from Surface Area Measurements for Fort Nelson (C-61-E/94-J-10) C1-49528

Pulverized TH1 Depth 2030.04 m					
Sample	Monsorb Reading, m^2	Avg. Reading, m^2	Sample Weights	grams	Surface Area, m^2/g
1	10.82	10.82	Sx + tare:	11.4496	14.66
2	10.82		Tare:	10.7115	
3	10.81		Sx:	0.7381	
Pulverized T1 Depth 2042.11 m					
Sample	Monsorb Reading, m^2	Avg. Reading, m^2	Sample Weights	grams	Surface Area, m^2/g
1	12.28	12.28	Sx + tare:	11.6438	20.16
2	12.27		Tare:	11.0346	
3	12.28		Sx:	0.6092	
Pulverized T3 Depth 2045.75 m					
Sample	Monsorb Reading, m^2	Avg. Reading, m^2	Sample Weights	grams	Surface Area, m^2/g
1	9.73	9.73	Sx + tare:	11.3491	14.82
2	9.73		Tare:	10.6927	
3	9.74		Sx:	0.6564	

Key Observations

Results indicate the following:

- With respect to surface area, Sample T-1 has significantly more than Samples TH-1 and T-3. This is likely because of a significant amount of preserved porosity, including fossil fragments.

- Samples TH-1 and T-3 reported similar values, with slightly more surface area being observed in Sample T-3. This is unexpected because mineralogy differs greatly between the two samples. The discrepancy may be because of clay particle size differences in the samples.

- Results are in agreement with skeletal density measurements that show similar trends; in particular, the similarity of total density of Samples TH-1 and T-3 and the lower total density that indicates higher porosity in Sample T-1.

Skeletal Density

Densities of whole and crushed samples were determined using a helium pycnometer. This multivolume pycnometer determines the skeletal density by measuring the reduction of gas volume in the sample chamber caused by the presence of the research sample. Skeletal density correlates strongly with mineralogy and can help define pore volume within the sample. Through repeated testing of a crushed sample, an understanding can be gained regarding the isolation or connection relationship in the pore structure, as disaggregated samples provide access approaching the entire porous network.

The resulting density measurements (Table 14) have strong ties to mineralogy. Quartz, for example, has a known density of 2.62 g/cm³, whereas metal salts such as pyrite can have densities over 5.0 g/cm³ (Ralph and Chau, 2011). Observed densities of 2.7 to 2.8 suggest concentrations of clay (density ~2.75 g/cm³) and dolomite (density ~2.84 g/cm³) in these samples. Measured skeletal densities agree well with mineralogical contents determined by XRD, SEM, QEMSEM, and optical petrography.

Differences in density between whole and crushed specimens were performed to show the influence of pore space in the sample (Figure 19). Whole samples shelter ineffective porosity from the measurement and, overall, lead to showing lower density (i.e., higher volume with the same weight). Crushing a sample effectively removes any pore space that would have been present in the sample and shows the maximum attainable density of the material.

Key Observations

- Sample TH-1 shows very little difference between whole vs. crushed results. This sample is thought to have the most consistent fabric, despite heterogeneous pyrite.

- Sample T-3 has a much higher degree of ineffective porosity, likely because of the highly cemented fabric.

Table 14. Measurements and Calculations Performed for Skeletal Density Values

	TH-1 Crushed	TH-1 Whole	T-1 Crushed	T-1 Whole	T-3 Crushed	T-3 Whole
Mass, g	1.5719	4.8518	1.5387	5.0706	1.5387	4.227
Grain Volume, cm^3	0.5748	1.7766	0.5466	1.9174	0.5466	1.5496
Grain Density, g/cm^3	2.73469	2.730947	2.815038	2.644519	2.815038	2.727801
+Uncertainty	2.71784	2.715906	2.797458	2.628168	2.797458	2.722028
–Uncertainty	2.751751	2.746155	2.832841	2.661074	2.832841	2.733598

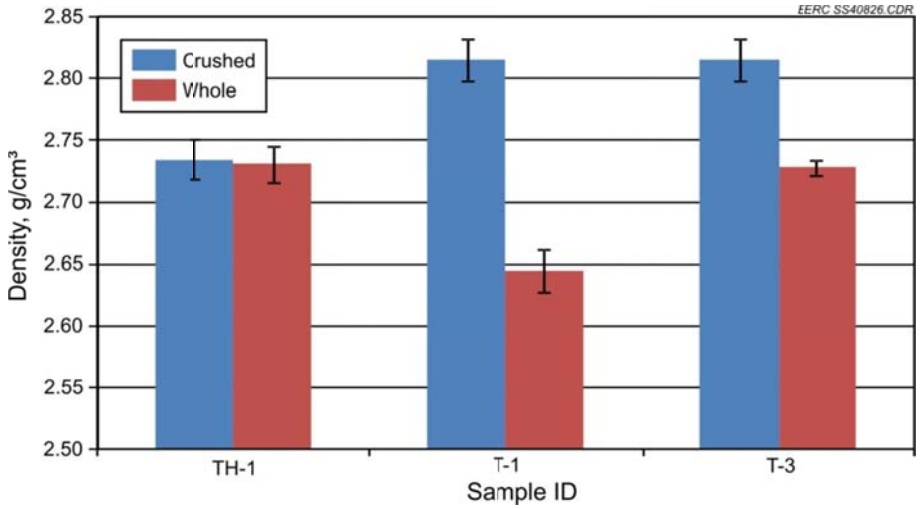

Figure 19. Skeletal density testing of whole (blue) and pulverized (red) test samples.

- Sample T-1 has a large difference in density found between whole and crushed tests. This is thought to be a result of disconnected porosity that formed as a result of pyrite and dolomite cementation.

- Samples T-1 and T-3 have very similar densities from crushed samples of approximately 2.81. This value is consistent with mineralogy high in illite and dolomite, measured through the various methods employed. Dense pyrite is also a significant factor in these samples.

- Sample TH-1 has a significantly lower density ~2.73. This is because of lower concentrations of pyrite and dolomite in the sample and remains consistent with measured mineralogy.

- Mineralogy-based density calculations using measured concentrations of mineral assemblages and estimated densities are shown to slightly overestimate skeletal density for these samples. This may be because of small overestimations of heavy, high-

visibility minerals or an underestimation of lighter phases present in clays, metals, and/or carbonates.

ICP–MS

MS is a type of destructive analysis that detects ionic energy at very high resolution. This type of analysis often is able to analyze trace constituents down to 1 part per trillion. For this analysis, rock samples were completely dissolved through mixed-acid digestion and run through the ICP–MS unit. The ICP ionized the liquefied stream, and ionic energy measurements were collected for 38 elements representing rare-earth, transition, lanthanide, and actinide groups. Thirty-one of these elements were compared with reported data for simultaneously processed RGM-1 standard reference material (Table 15). The remaining seven were not reported for RGM-1 standard reference material, so the standard error in detection for these phases is unknown. Semiquantitative analysis was still possible, however, and is reported in Table 16.

Clay-rich intervals of the Fort Simpson and Muskwa Shales showed higher trace element concentrations than the heavily dolomitized sections of the Muskwa Formation. Manganese is an exception to this, as it is a common replacement element in dolomites. Specifically, the shale samples had higher concentrations in 23 out of 27 elements, suggesting that clays have trapped significantly higher amounts of trace elements than the carbonate-rich units. The trace metal content of clay samples is thought to be the result of a combination of classic sedimentary accumulation from continental sources or of enriched water traveling through reducing organic carbon-rich units.

Trace element contents found through this method present a broad spectrum view of geochemical contents of the Fort Nelson cap rock samples. Some trace elements were detected in quantities sufficient to serve as natural tracers. This use is highly dependent on formation fluid sample quality and will require additional fluid analysis in both reservoir and monitoring lithologies.

Table 15. Trace Elements Measured During ICP–MS Analysis Against RGM-1 Standard

Yttrium	Lead	Copper	Lanthanum	Vanadium
Chromium	Antimony	Cerium	Cobalt	Beryllium
Neodymium	Manganese	Titanium	Scandium	Dysprosium
Gadolinium	Samarium	Ytterbium	Arsenic	Europium
Zinc	Thorium	Nickel	Lutetium	

Table 16. Trace Elements Measured During ICP–MS Analysis that Had No Values Reported for Standard RGM-1

Selenium	Promethium	Cadmium	Terbium
Holmium	Erbium	Thulium	

Key Observations

Results of ICP–MS testing are shown in Figures 20 and 21 and Tables 17 and 18. Specific observations while analyzing ICP–MS data include the following:

- 28 of the 31 measured elements were detected on the 0.5–1200-µg/g scale within all samples. Promethium, thulium, and holmium were not detected in at least one of the samples (less than 0.5 µg/g).

- Comparatively, TH-1 had the highest concentrations of 12 elements, followed closely by T-1, which had high concentrations of 11 elements. Sample T-3 only had higher concentrations of four elements (Gd, Mn, Dy, and Y).

- Only two elements had shared analysis with XRF testing, titanium and manganese. Titanium results appear to agree between the two methods; however, discrepancies exist in the manganese measurements.

- Sample T-3 received additional XRF testing, which covered nine of the same elements: arsenic, zinc, copper, nickel, manganese, vanadium, titanium, yttrium, and chromium. These were found to be in agreement, with the exception of yttrium and chromium, which is thought to be an error in XRF analysis because of small sample size and low elemental concentration.

- Metals, including toxic species (lead, cadmium, arsenic, etc.), are present within cap rock intervals. Geochemical modeling should be performed to assess and ensure that mobilization of metallic species does not have potential impact on water resources.

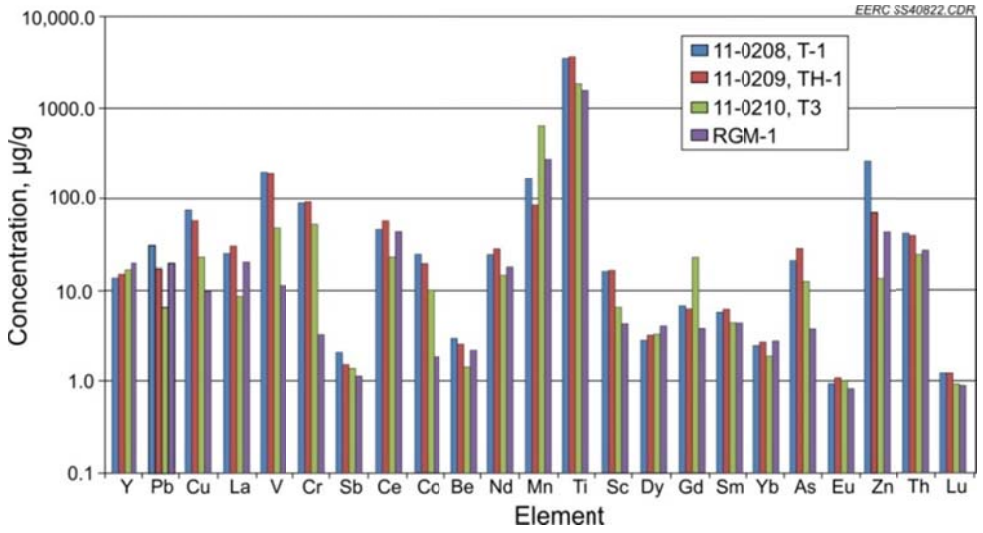

Figure 20. Results of trace element analysis comparing Samples TH-1, T-1, and T-3 with Glass Mountain rhyolite (RGM-1).

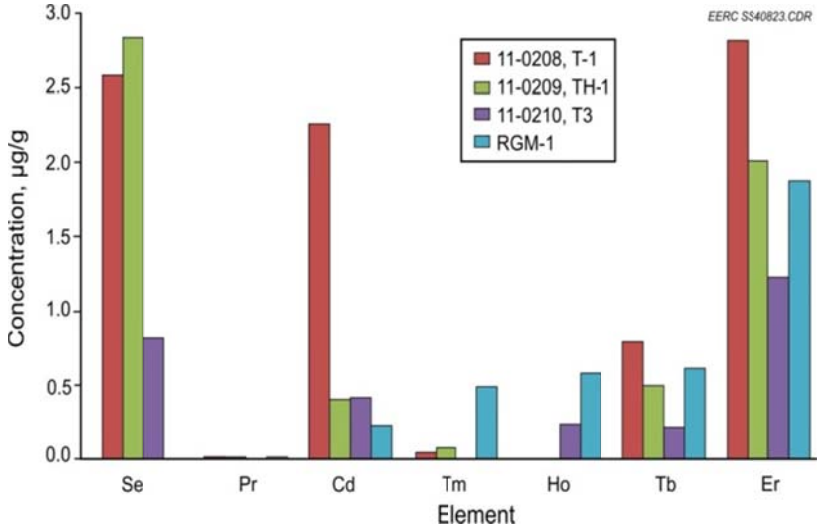

Figure 21. Results of trace element analysis for Samples TH-1, T-1, and T-3 for elements not reported in RGM-1 sample literature.

Table 17. Concentrations of ICP–MS Measured Trace Elements for Metals with RGM-1 Standard, µg/g

Sample	Y	Pb	Cu	La	V	Cr	Sb	Ce
TH-1	15.089	17.456	57.761	30.671	197.633	92.604	1.524	57.949
T-1	13.541	31.058	76.789	24.920	201.983	92.068	2.067	46.950
T-3	17.221	6.683	22.779	8.683	47.609	52.740	1.406	23.392

	Co	Be	Nd	Mn	Ti	Sc	Dy	Gd
TH-1	19.231	2.584	28.412	85.888	3660.750	16.489	3.156	6.223
T-1	24.400	3.022	24.655	167.044	3473.088	15.779	2.814	6.862
T-3	10.010	1.458	14.490	656.949	1886.297	6.449	3.279	22.255

	Sm	Yb	As	Eu	Zn	Th	Lu	Ni
TH-1	6.262	2.692	28.600	1.105	70.750	39.714	1.237	117.949
T-1	5.817	2.502	20.774	0.925	266.667	41.992	1.251	101.794
T-3	4.497	1.874	12.527	1.009	13.528	24.354	0.946	39.125

Table 18. Concentrations of ICP–MS Measured Trace Elements for Metals Without RGM-1 Standard, µg/g

Sample	Se	Pr	Cd	Tm	Ho	Tb	Er
TH-1	2.840	0.0119	0.400	0.076	ND	0.497	2.022
T-1	2.587	0.004	2.257	0.043	ND	0.788	2.842
T-3	0.816	ND	0.412	ND	0.229	0.218	1.236

SUMMARY

Petrographic assessment was performed on primary cap rock samples from the Fort Nelson demonstration project reservoir. Three samples from Well C-61-E/94-J-10 representing the Fort Simpson Shale and Muskwa Formation were characterized, with emphasis on geochemical stability, mineralogy, and rock properties pertinent to geochemical assessment. Ten separate analyses were conducted in order to collect properties, provide supporting data, correlate findings, and provide illustrations and explanations of results. Specifically, testing included the following:

- XRD for bulk mineralogy
- XRF for trace element analysis
- Petrographic analysis via thin section for mineralogy and rock fabric descriptions
- QEMSEM for mineralogical mapping
- SEM with EDS for mineralogical identification and rock fabric descriptions
- CHN/S measurements for elemental composition information
- Surface area to determine reactive surface
- Skeletal density to support mineralogy and examination of total vs. effective porosity and degree of cementation
- ICP–MS to examine trace element abundance

Paleoenvironmental interpretation based on rock mineralogy and fabric suggests that Keg River, Sulphur Point, and Slave Point reef complexes were deposited along a shallow shelf extending onto the flooded continental shelf. Brief marine regressions caused the back-reef environment to fill with siliclastic carbonate debris and evaporite deposits (Meijer Drees, 2008). Continental influx persistently provided clastic sediments to the system, which accelerated following a large-scale marine transgression that covered the area, resulting in the deposition of organic-rich marine shales including the Fort Simpson.

Illite group clay-rich cap rock samples contain inclusions of secondary dolomite and pyrite which are thought to be the result of enriched water moving through the system during lithification and/or hydrocarbon maturation. In some cases, these inclusions now outnumber the volume of autochthonous rock. Small portions of barite, calcite, silt-sized quartz, fossiliferous apatite, and lithic fragments were also detected through analysis. Sample porosity was difficult to visualize and practically inexistent on a macro/meso scale. SEM techniques proved invaluable to observing the porous structure of these rocks.

Selected intervals are consistent with published formation descriptions in the Fort Simpson and Muskwa Formations, although dolomitized portions of the Otter Park Formation underlying the Muskwa are expected to have formation characteristics similar to Sample T-3. The cap rock intervals were shown to contain tight, partially mineralized collections of stable minerals with low porosity and small pore throat diameter. No leakage pathways were observed in the submitted samples, and all three are expected to provide significant resistance to vertical migration of injected nonmiscible fluids. Geochemical and mechanical modeling and simulation are required to validate and confirm cap rock–fluid interactivity with injected fluids under reservoir conditions.

REFERENCES

Gorecki, C.D., Sorensen, J.A., Klapperich, R.J., Holubnyak, Y.I., Hamling, J.A., Bremer, J.M., Smith, S.A., Steadman, E.N. and Harju, J.A., 2010, Fort Nelson test site – site characterization, modeling, and monitoring plan: Plains CO_2 Reduction (PCOR) Partnership Phase III, Task 9, Deliverable D52, for U.S. Department of Energy National Energy Technology Laboratory Cooperative Agreement No. DE-FC26-05NT42592, EERC Publication 2011-EERC-08-06, Grand Forks, North Dakota, Energy & Environmental Research Center, September.

Kamamura, K., 2002, Growth process of framboidal pyrite in deep-sea sediments, sediments, clastic: processes, petrology and provenance [abs.]: Geological Society of America Paper No. 89-6.

Meijer Drees, N.C., 2008, Devonian Elk Point Group of the Western Canada Sedimentary Basin Geological Atlas of the Western Canada Sedimentary Basin, Chapter 10, Alberta Geological Survey.

Ralph, J., and Chau, I., 2011, Mineralogy Database: www.mindat (accessed July 2011).

Środań, J., 1980, Precise identification of illite/smectite interstratifications by x-ray powder diffraction: Clay and Clay Minerals, v. 28, no. 6, p. 401–411.

U.S. Geological Survey, 2001, A laboratory manual for x-ray powder diffraction: U.S. Geological Survey Open-File Report 01–041 http://pubs.usgs.gov/of/2001/of01-041/ htmldocs/methods.htm (accessed August 2011).

APPENDIX A

BULK MINERALOGY XRD SCANS

Table A-1. Relative Weight Percentages of Identified Mineral Phases in Each Sample Determined by X-Ray Diffraction

	TH-1, 11-0209	T-1, 11-0208	T-3, 11-0210
Illite	47.0	46.2	21.6
Quartz	41.6	40.9	31.0
Dolomite	1.0	0.7	25.0
Pyrite	7.0	6.5	3.5
Ankerite	0.8	2.0	18.0
Sanidine $Na_{0.56}$	2.0	2.5	0.6
Muscovite 2M1	0.4	0.5	0.2
Siderite	0.3	0.7	0.0
Kaolinite (BISH)	0.0	0.0	0.0
Anhydrite	0.0	0.0	0.0
Goodness of Fit	1.67	1.77	1.47
Rexp	9.66	9.53	9.30

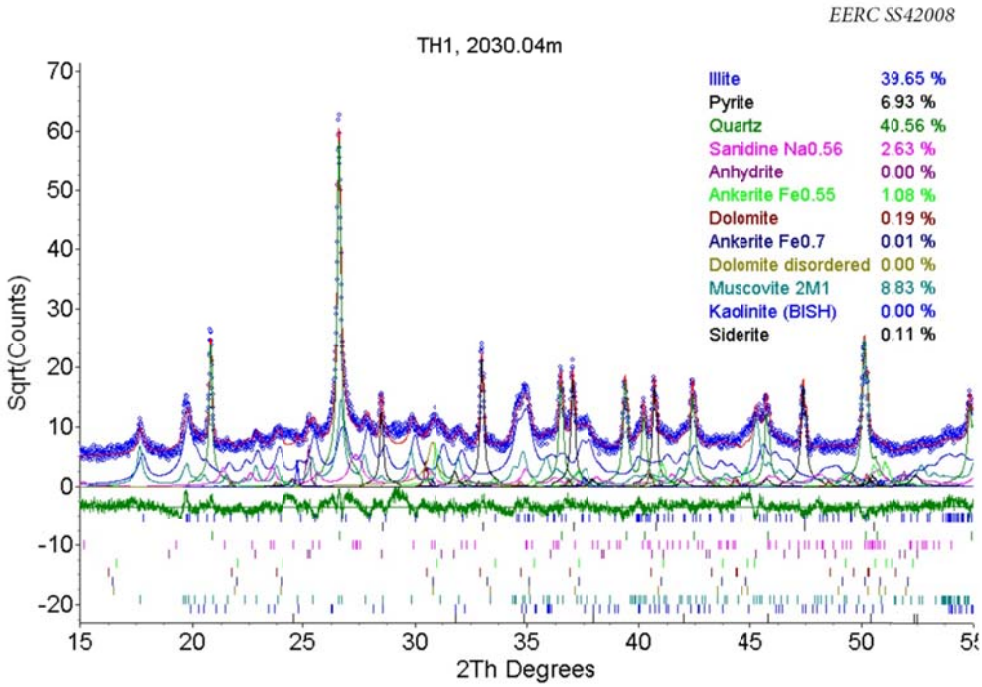

Figure A-1. Spectrographic scan and mineralogical phase identification of Sample TH-1 through Rietvelt refinement. The measured and modeled curves are displayed as well as model constituents and their individual peak spacing. This sample reported high contents of illite and quartz, with minor pyrite.

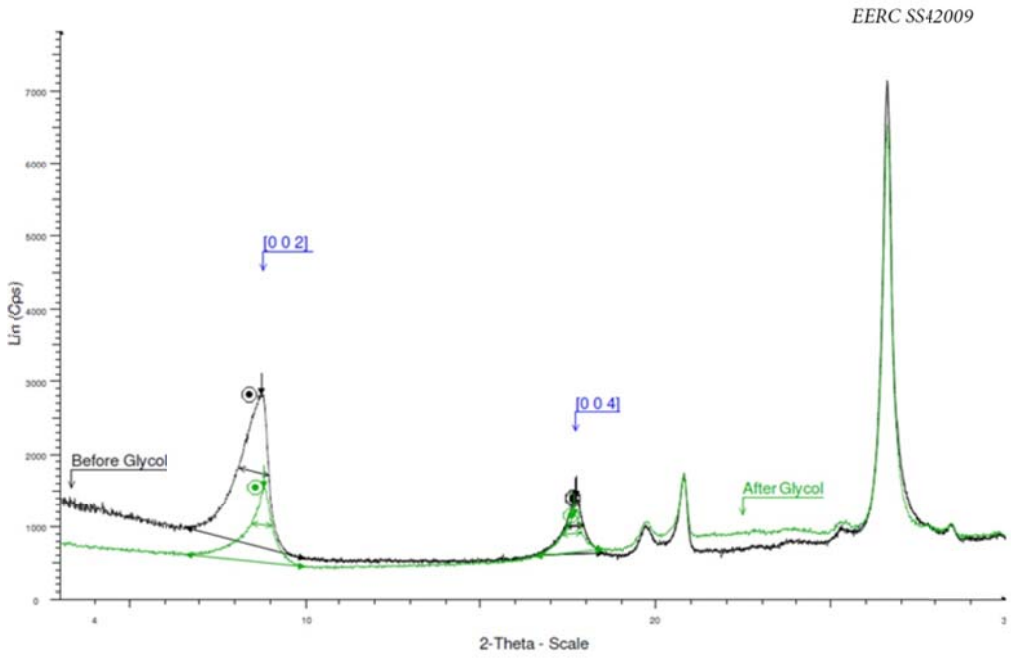

Figure A-2. Prior- and post-glycolation scans of Sample TH-1 showing low-angle peak behavior and swelling reaction due to glycol exposure.

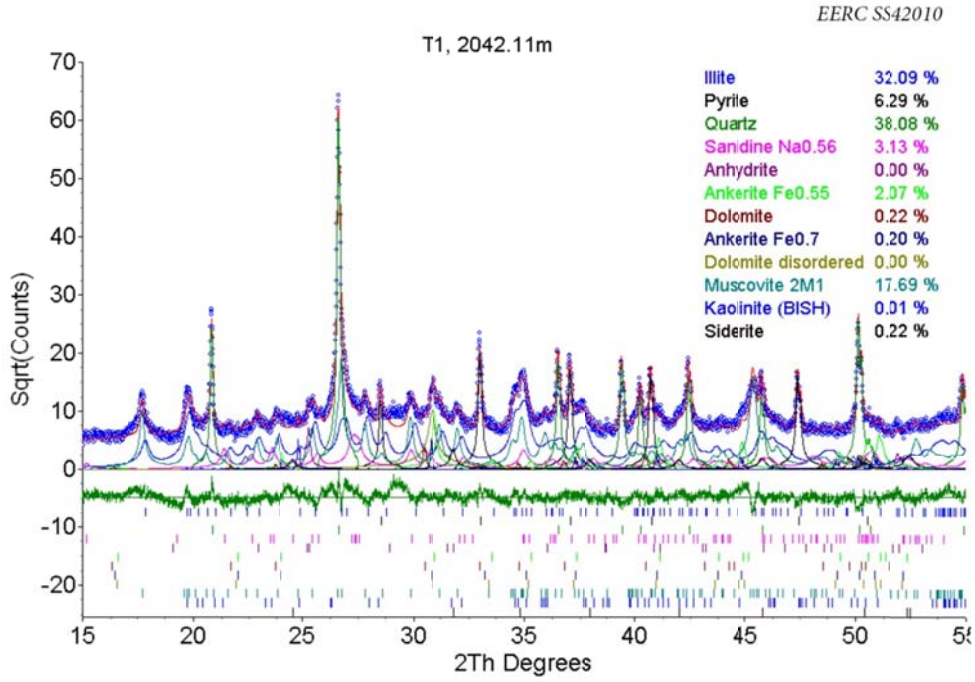

Figure A-3. Spectrographic scan and mineralogical phase identification of Sample T-1 through Rietvelt refinement. The measured and modeled curves are displayed as well as model constituents and their individual peak spacing. This sample reported high contents of illite and quartz, with minor pyrite.

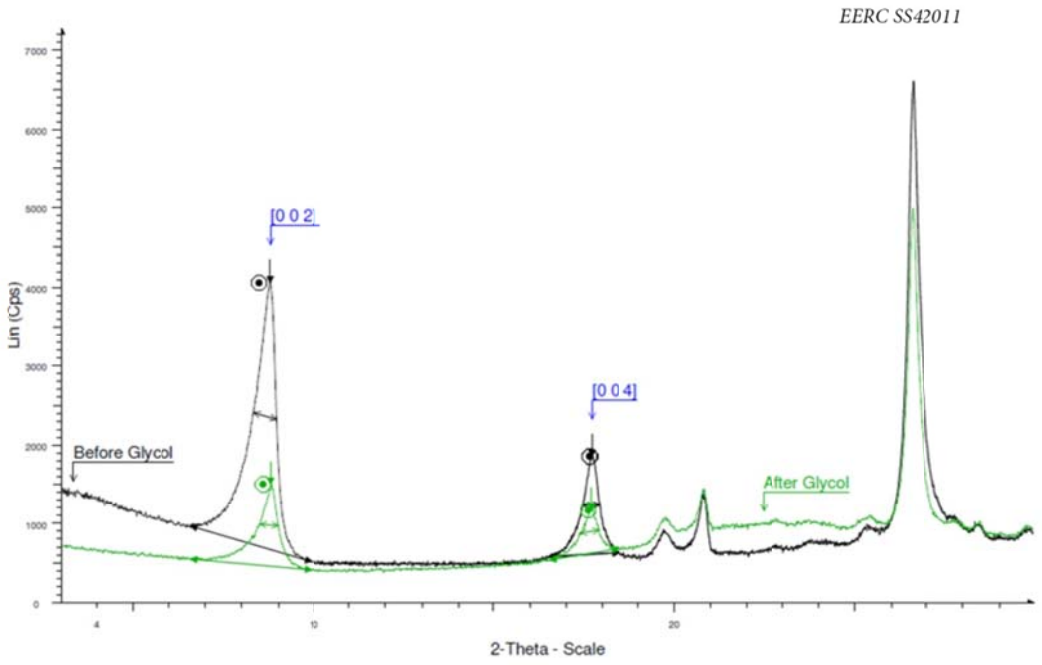

Figure A-4. Prior- and post-glycolation scans of Sample T-1 showing low-angle peak behavior and swelling reaction due to glycol exposure.

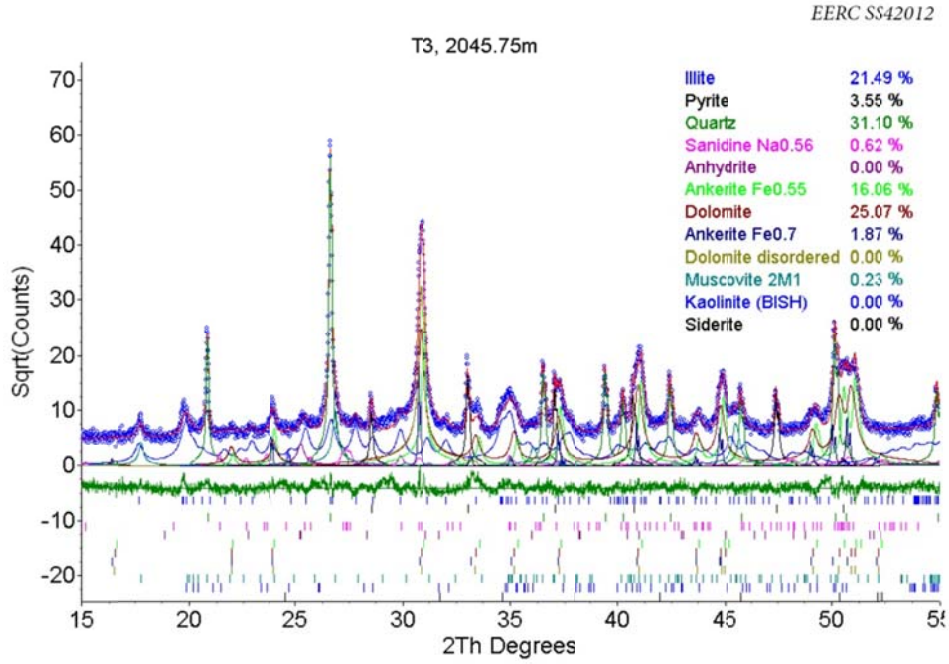

Figure A-5. Spectrographic scan and mineralogical phase identification of Sample T-3 through Rietvelt refinement. The measured and modeled curves are displayed as well as model constituents and their individual peak spacing. This sample reported significant portions of illite, quartz, dolomite, and ankerite, with minor pyrite.

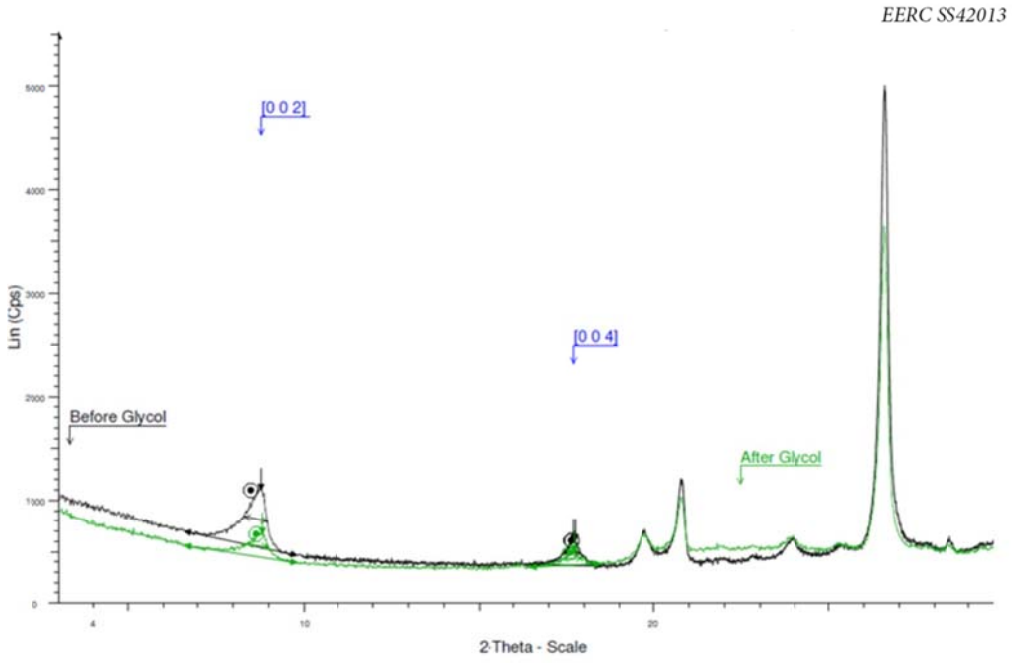

Figure A-6. Prior- and post-glycolation scans of Sample TH-3 showing low-angle peak behavior and swelling reaction due to glycol exposure.

APPENDIX B

PETROGRAPHIC THIN SECTIONS

Table B-1. Sample TH-1, 2030.04 meters

Assemblage	Percentage	Comments
Clay/Silt	75	No observable porosity
Carbonate	15	Subhedral to euhedral
Pyrite	10	Subhedral/anhedral

Sample TH-1 is very fine-grained, poorly sorted, well-consolidated shale that is dark charcoal gray to black. Thin-section analysis estimated that the rock is composed primarily of clay (75%) spread throughout the sample, with scattered accumulations of dolomite (15%) and pyrite (10%). No apparent porosity or fossil assemblages were encountered during analysis (Figures B-1 and B-2).

Table B-2. Sample T-1, 2042.11 meters

Assemblage	Percentage	Comments
Clay/Silt	75	No observable porosity
Carbonate	15	Subhedral
Pyrite	10	Subhedral to euhedral

Sample T-1 is a very fine-grained, poorly sorted, well-consolidated shale that is dark charcoal gray to black. A thin-section sample produced from the interval showed high concentrations of clay (75%) spread throughout the sample, with scattered subhedral dolomite (15%) and subhedral to euhedral pyrite (10%). No porosity or fossil assemblages were observed in this sample, which, other than the increased crystal structure in pyrite, appears identical to the TH-1 interval (Figures 3 and 4).

Table B-3. Sample T-3, 2045.75 meters

Assemblage	Percentage	Comments
Clay/Silt	25	No observable porosity
Carbonate	70	Subhedral
Pyrite	5	Anhedral

The T-3 interval is a very fine-grained, poorly sorted, well-consolidated and cemented shale that is black in color. The rock contains digenetic subhedral dolomite (70%), which has become the dominant phase in the sample. A significant percentage of clay (25%) is present in the sample, with approximately 5% pyrite. No porosity or fossil assemblages were observed in this sample (Figures 5-7). Despite high carbonate content, the sample appears very similar to the previous intervals in hand specimen.

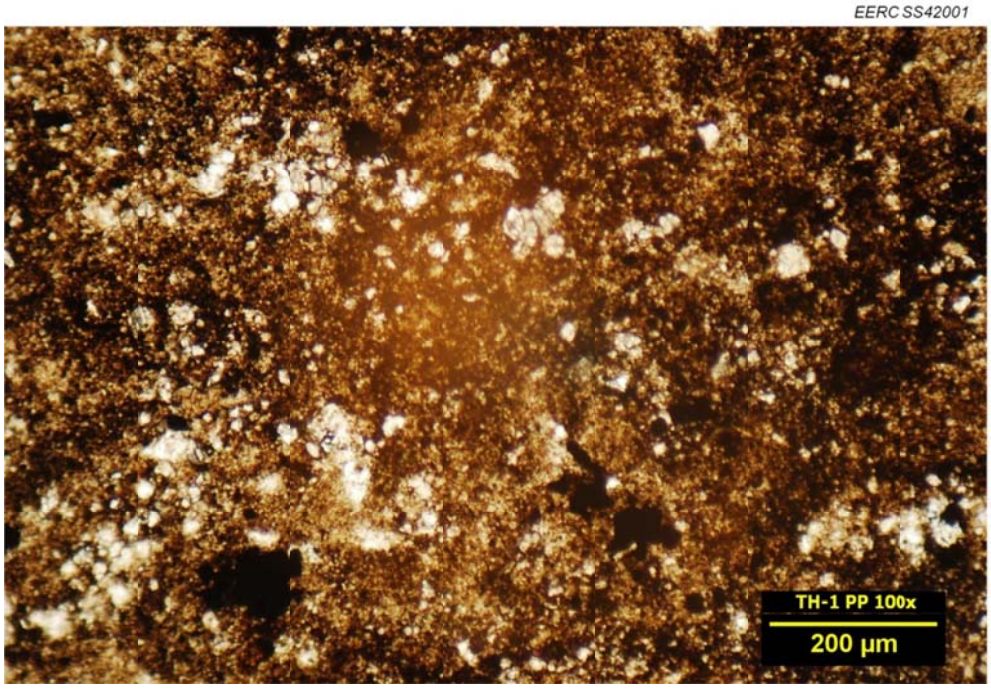

Figure B-1. Photomicrograph of TH-1, plane-polarized light, 100× magnification.

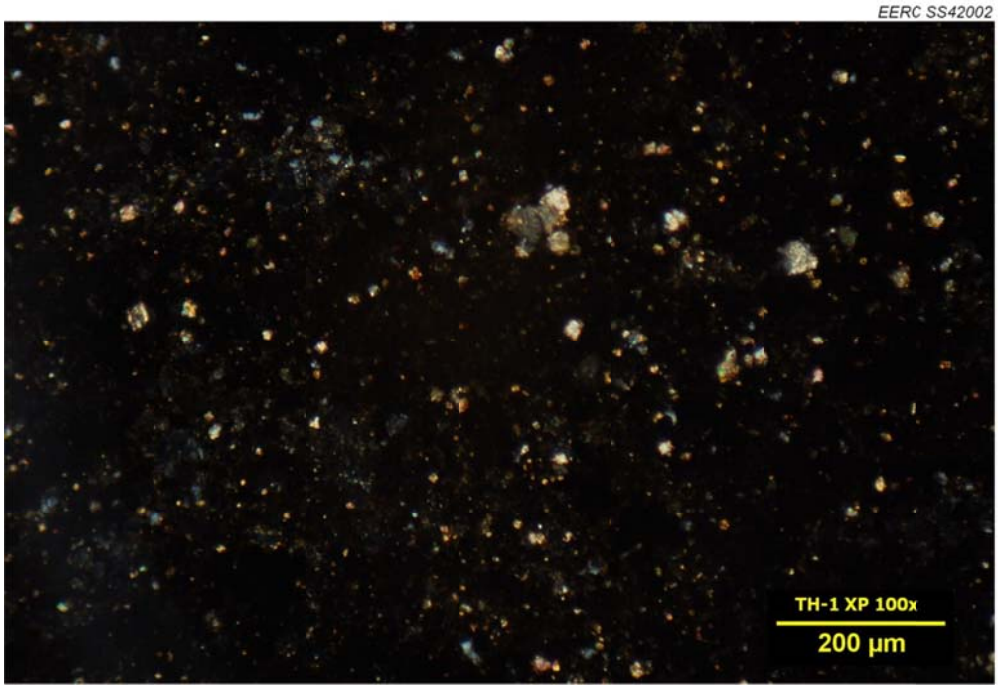

Figure B-2. Photomicrograph of TH-1, cross-polarized light, 100× magnification.

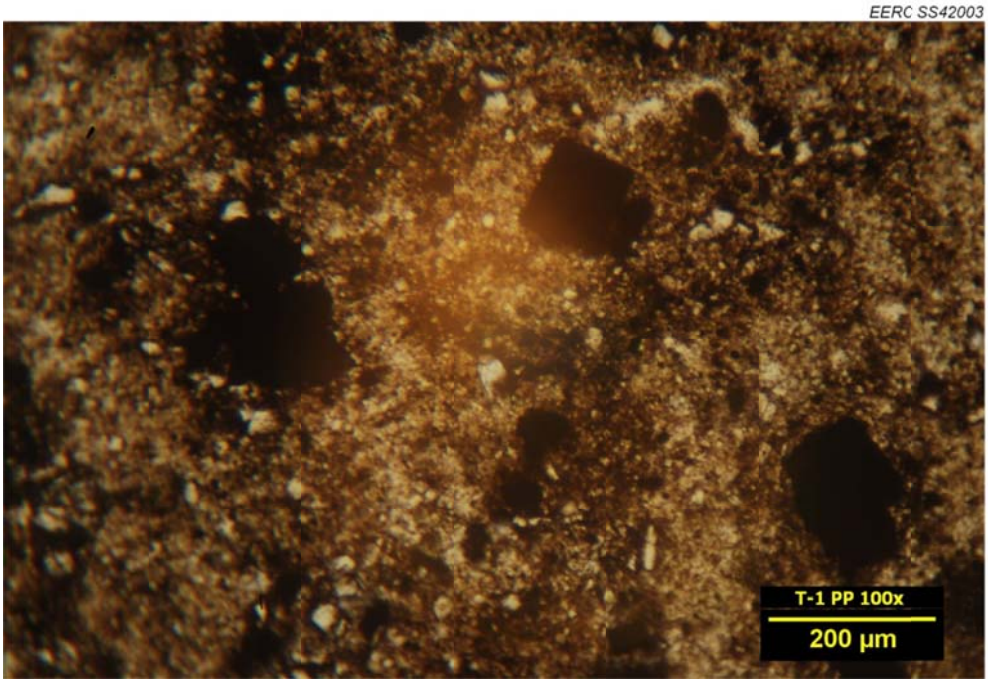

Figure B-3. Photomicrograph of T-1, plane-polarized light, 100× magnification.

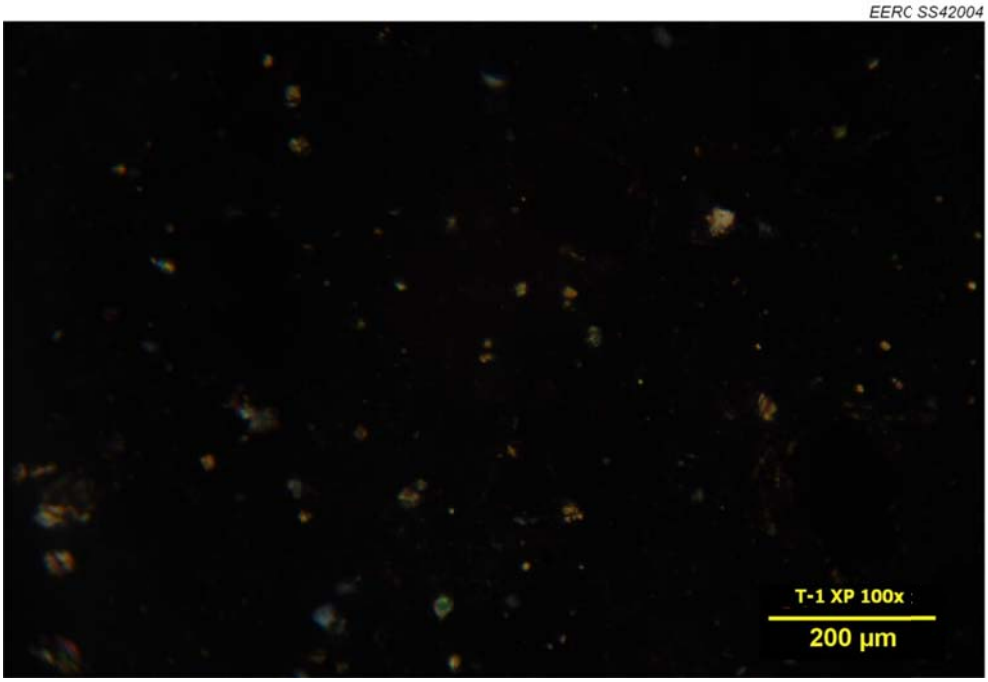

Figure B-4. Photomicrograph of T-1, cross-polarized light, 100× magnification.

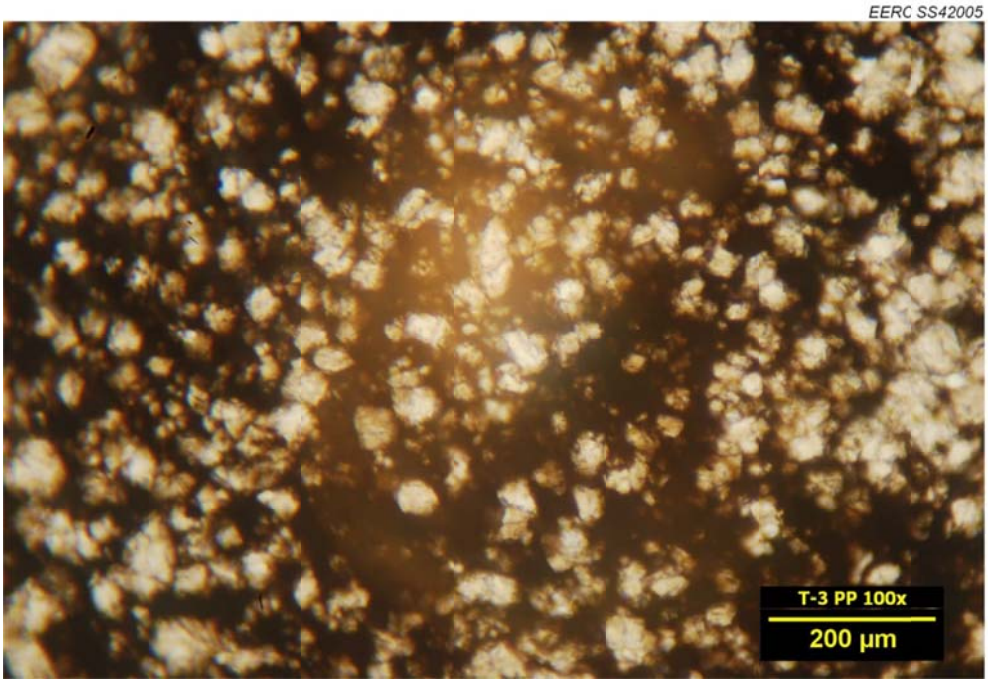

Figure B-5. Photomicrograph of T-3, plane-polarized light, 100× magnification.

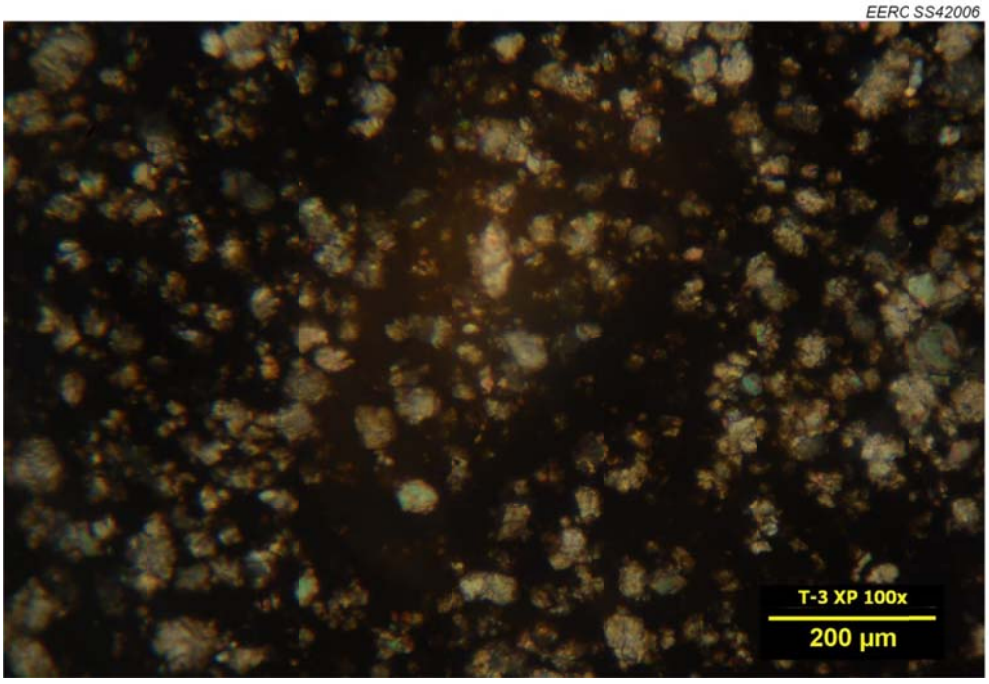

Figure B-6. Photomicrograph of T-3, cross-polarized light, 100× magnification.

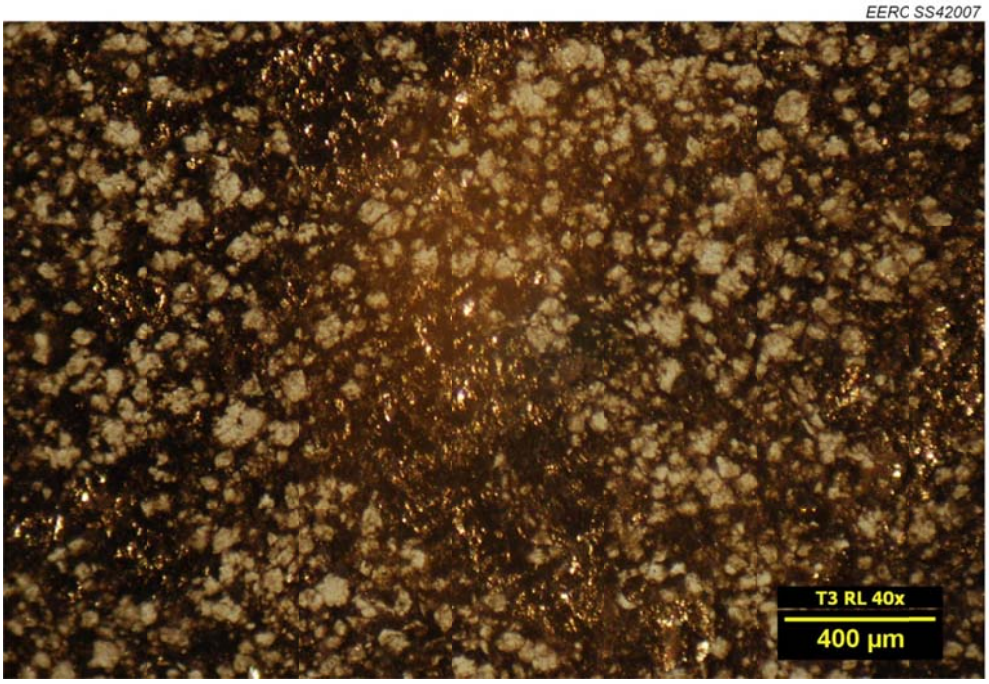

Figure B-7. Photomicrograph of T-3, reflected light, 40× magnification. Gold-colored reflective areas are high in pyrite, darker areas are primarily clay, and light areas are carbonates.

APPENDIX C

SCANNING ELECTRON MICROSCOPY (SEM)

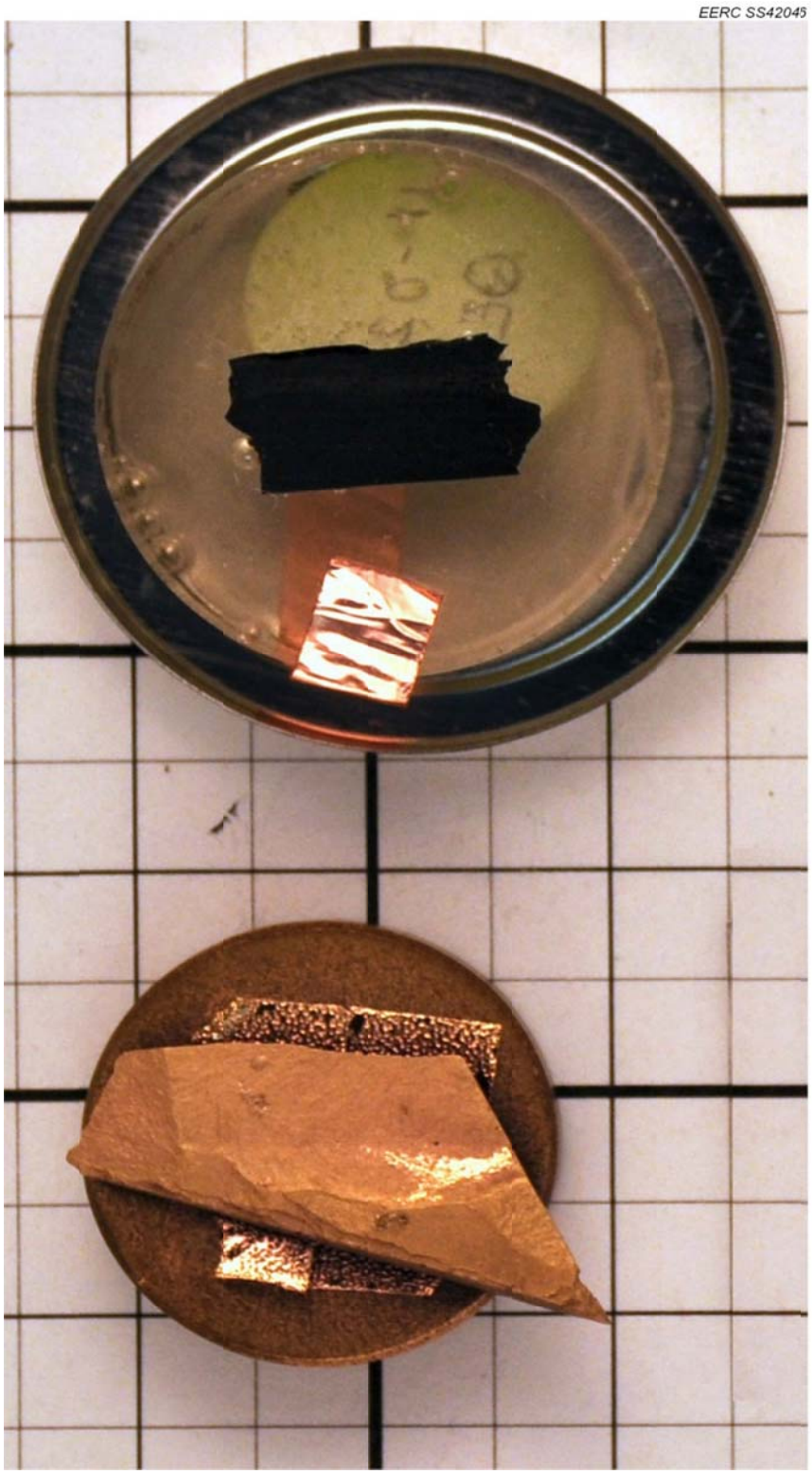

Figure C-1. Photograph of the TH-1 interval specimens after experiment. The polished epoxy-mounted sample (above) was used for SEM–EDS and QEMSEM, and fractured, gold-dusted SEM sample (below) was used for SEM imagery.

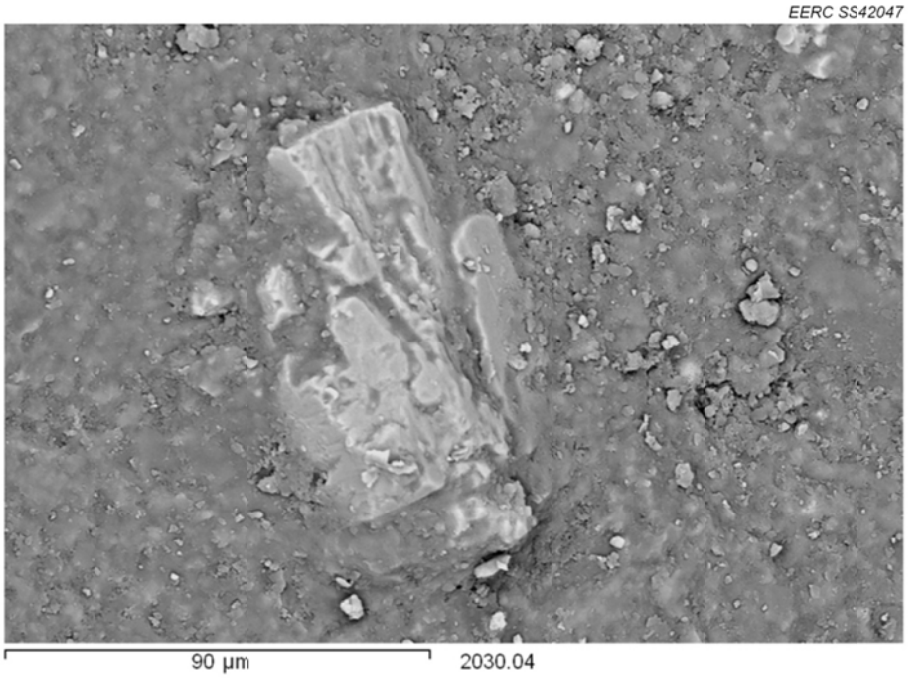

Figure C-2. SEM photomicrograph of TH-1, fractured, 750× magnification, showing pyrite growing out of the primarily illite matrix.

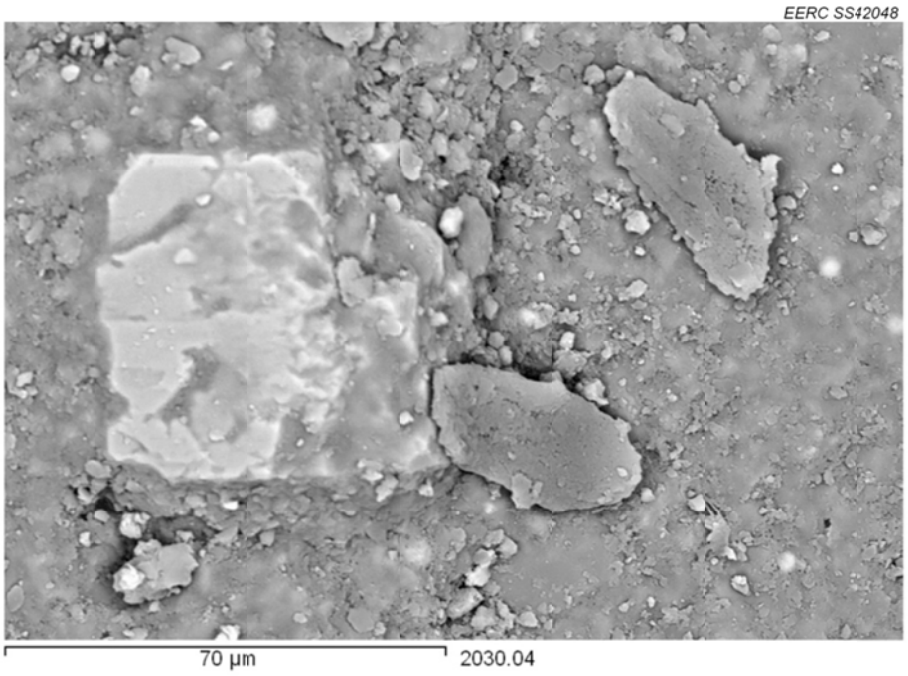

Figure C-3. SEM photomicrograph of TH-1, fractured, 1000× magnification, showing pyrite growing out of an illite matrix.

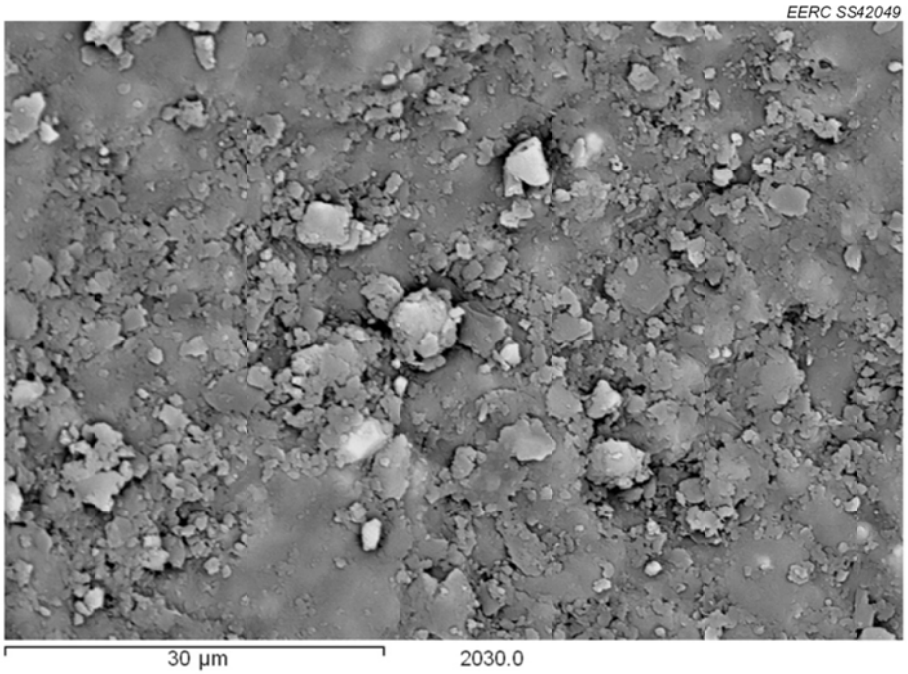

Figure C-4. SEM photomicrograph of TH-1, fractured, 2000× magnification, showing primarily illite clay.

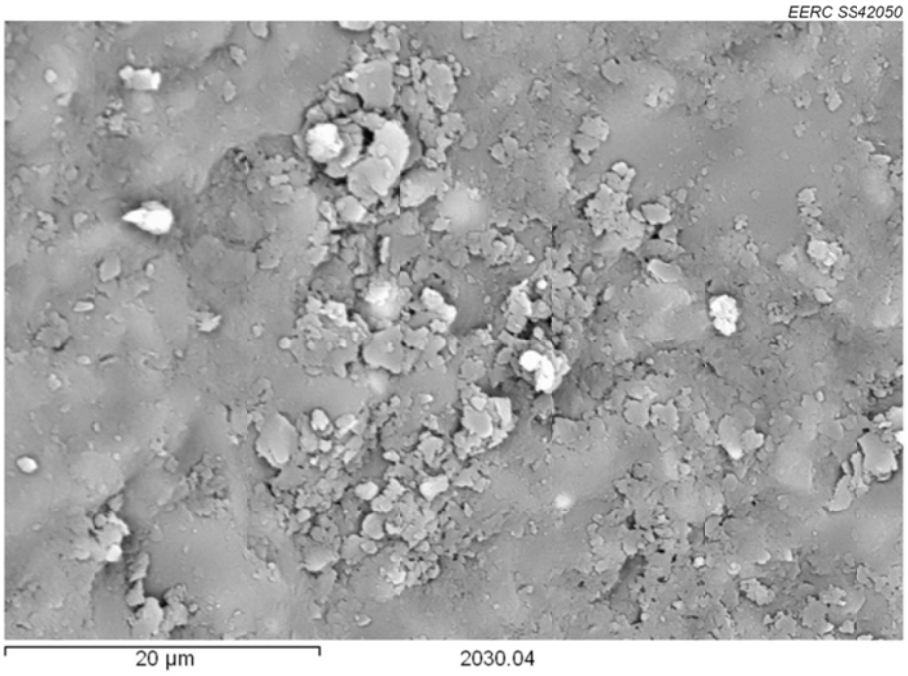

Figure C-5. SEM photomicrograph of TH-1, fractured, 5000× magnification, showing primarily illite clay.

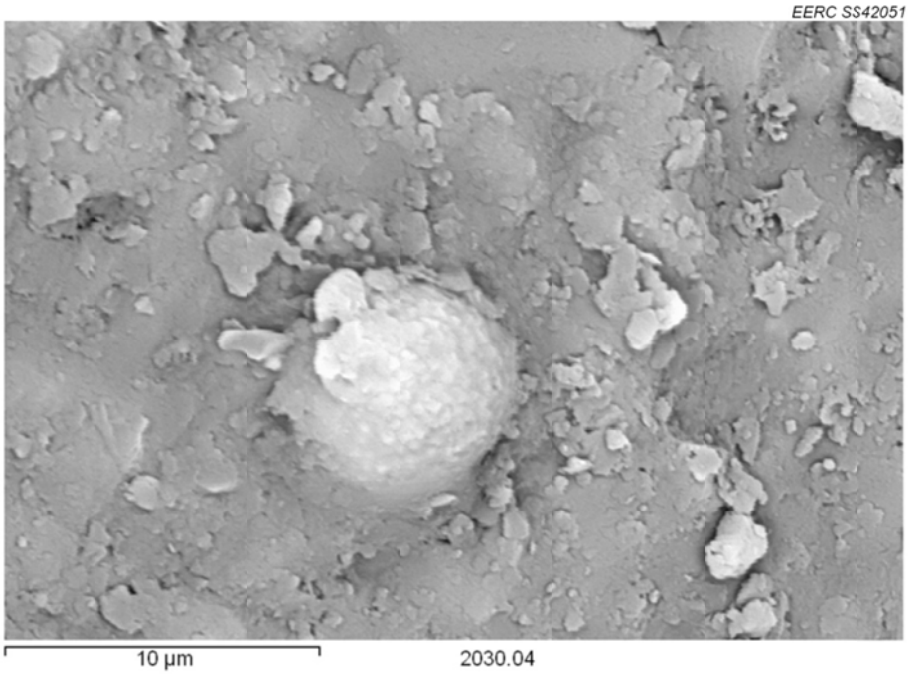

Figure C-6. SEM photomicrograph of TH-1, fractured, 5000× magnification, showing radial pyrite growth in clay.

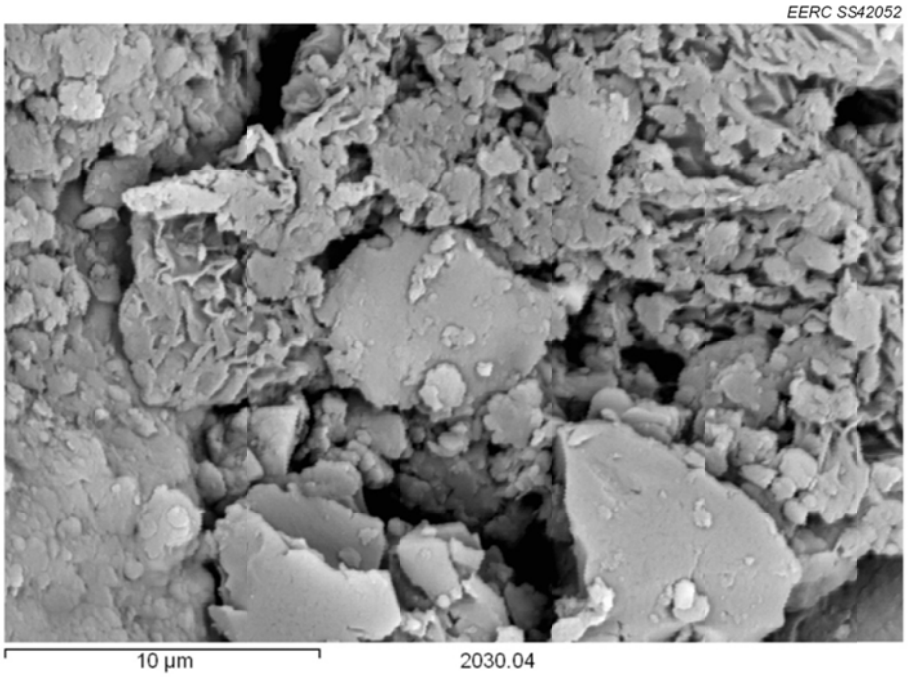

Figure C-7. SEM photomicrograph of TH-1, fractured, 5000× magnification, showing structure of clay matrix.

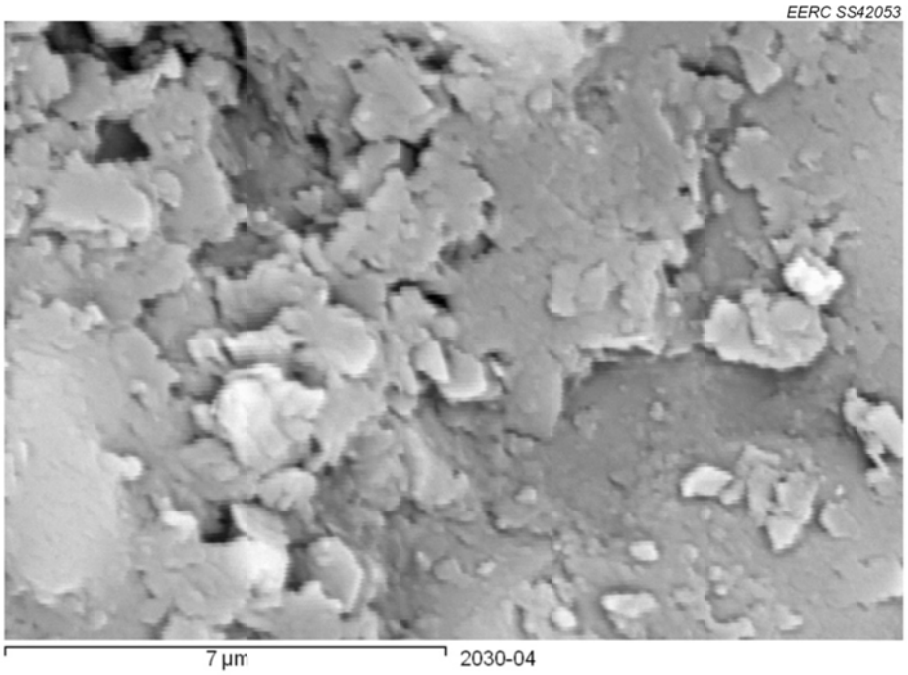

Figure C-8. SEM photomicrograph of TH-1, fractured, 10,000× magnification, showing structure of clay matrix.

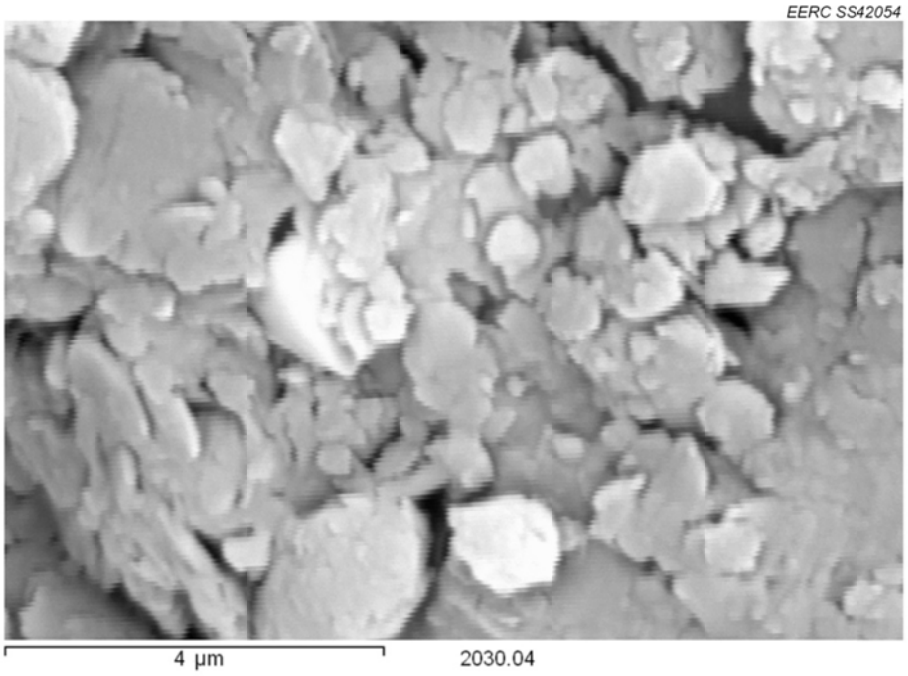

Figure C-9. SEM photomicrograph of TH-1, fractured, 15,000× magnification, showing structure of clay matrix.

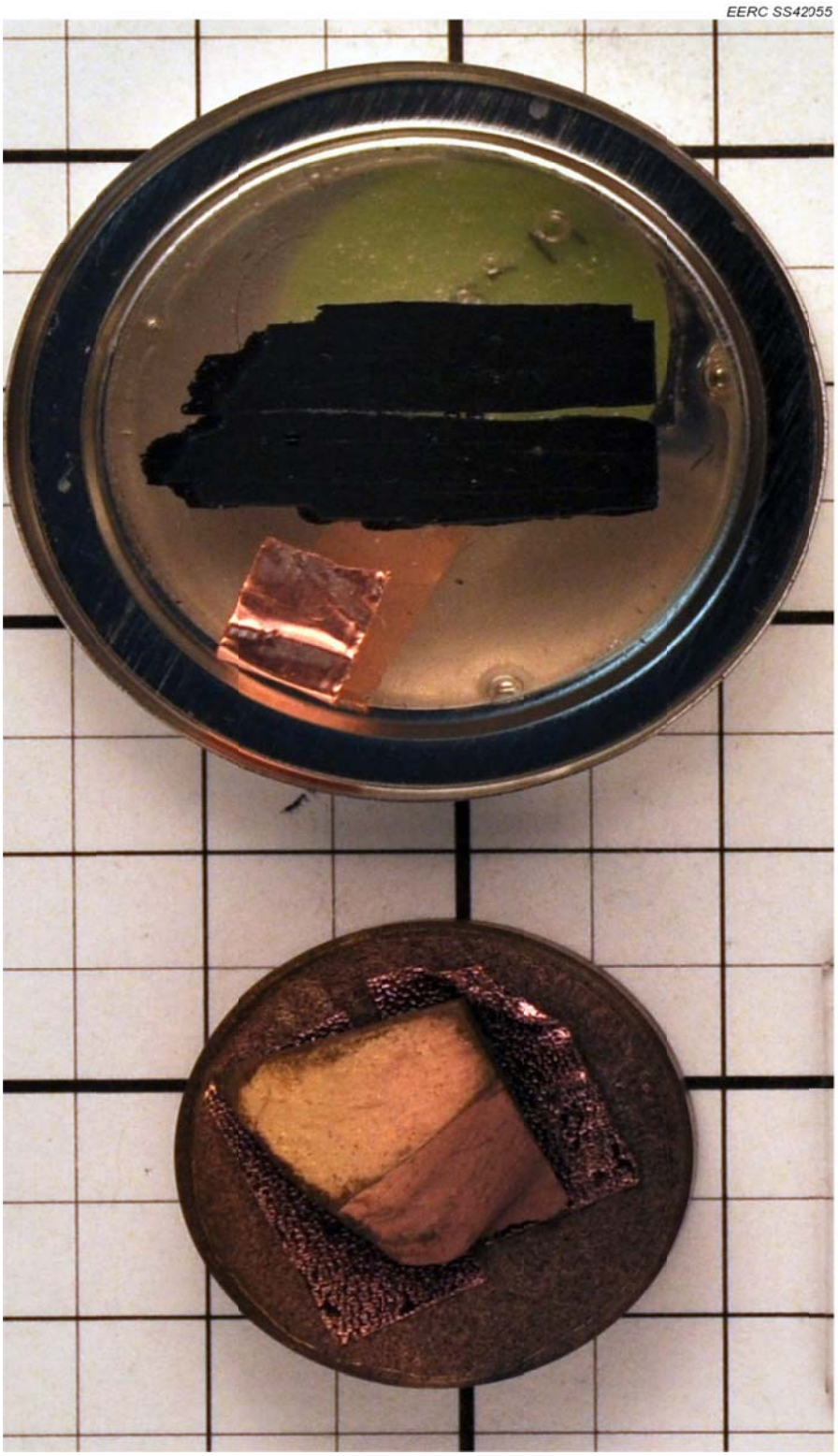

Figure C-10. Photograph of the T-1 specimens after experiment, the polished SEM sample (above) was used for SEM–EDS and QEMSEM measurements, while the fractured, gold-dusted SEM sample (below) was used for imagery.

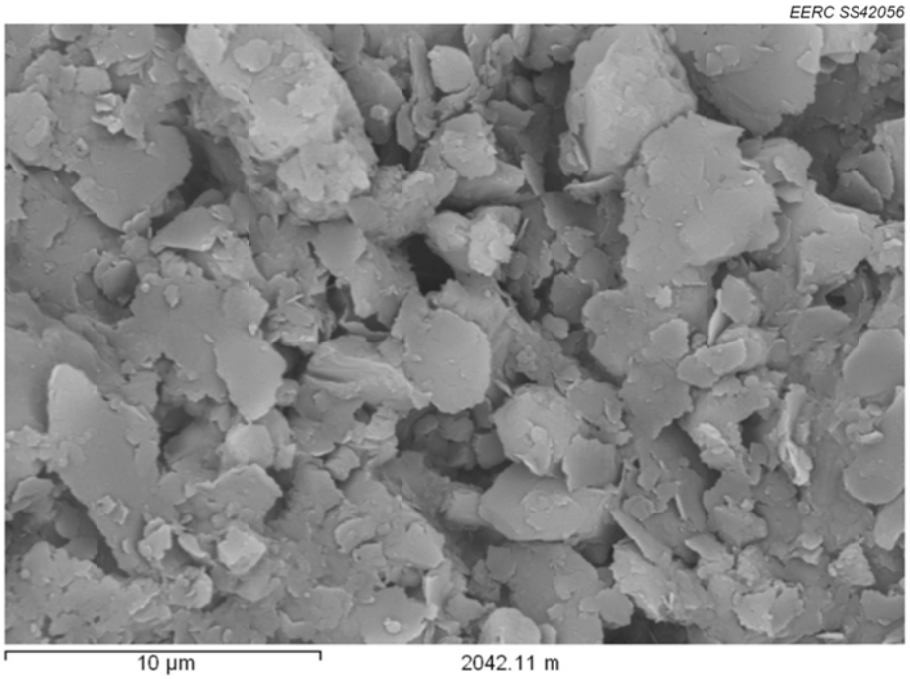

Figure C-11. SEM photomicrograph of T-1, fractured, 5000× magnification, showing structure of clays.

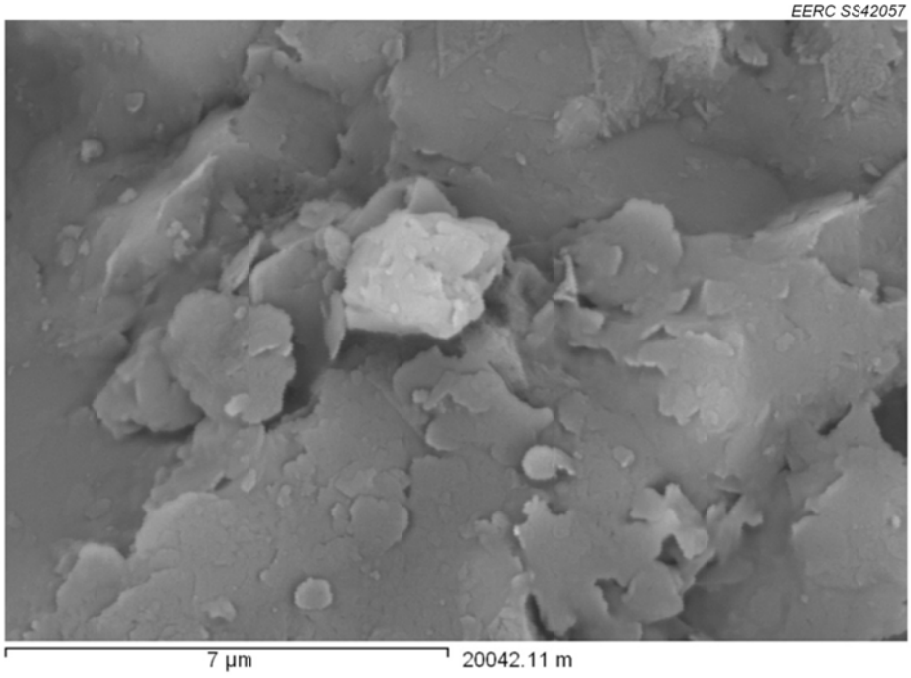

Figure C-12. SEM photomicrograph of T-1, fractured, 10,000× magnification, showing structure of clays.

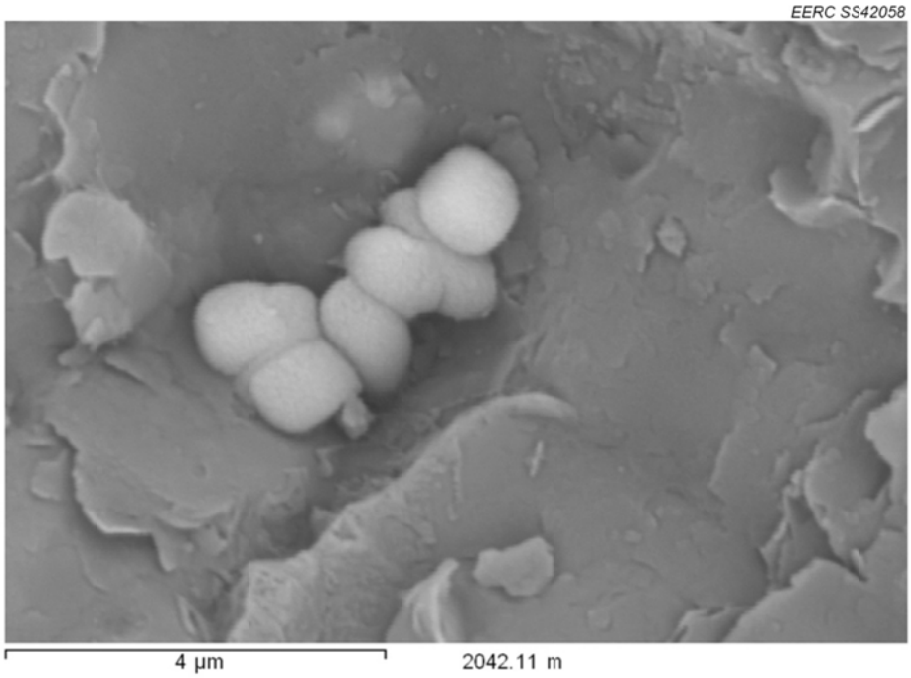

Figure C-13. SEM photomicrograph of T-1, fractured, 15,000× magnification, showing radial pyrite in illite.

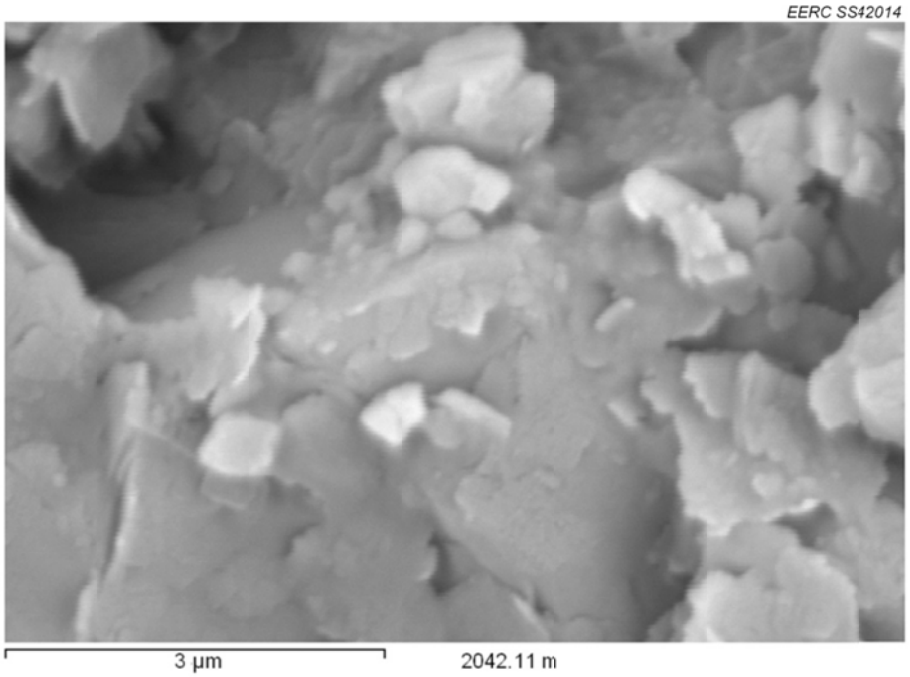

Figure C-14. SEM photomicrograph, of T-1, fractured, 20,000× magnification, showing clay structure.

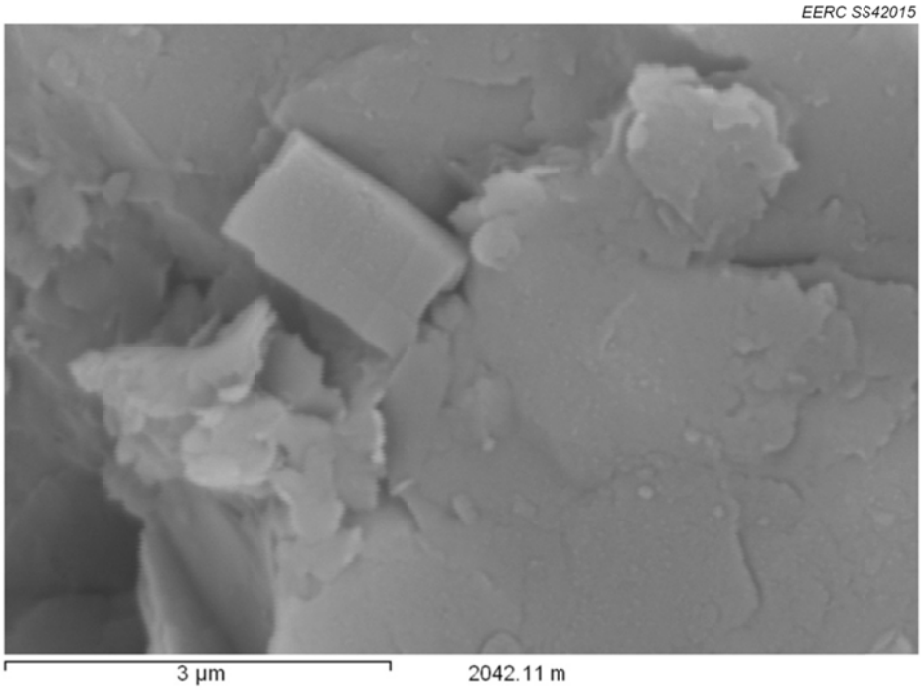

Figure C-15. SEM photomicrograph of T-1, fractured, 20,000× magnification, showing euhedral dolomite in illite.

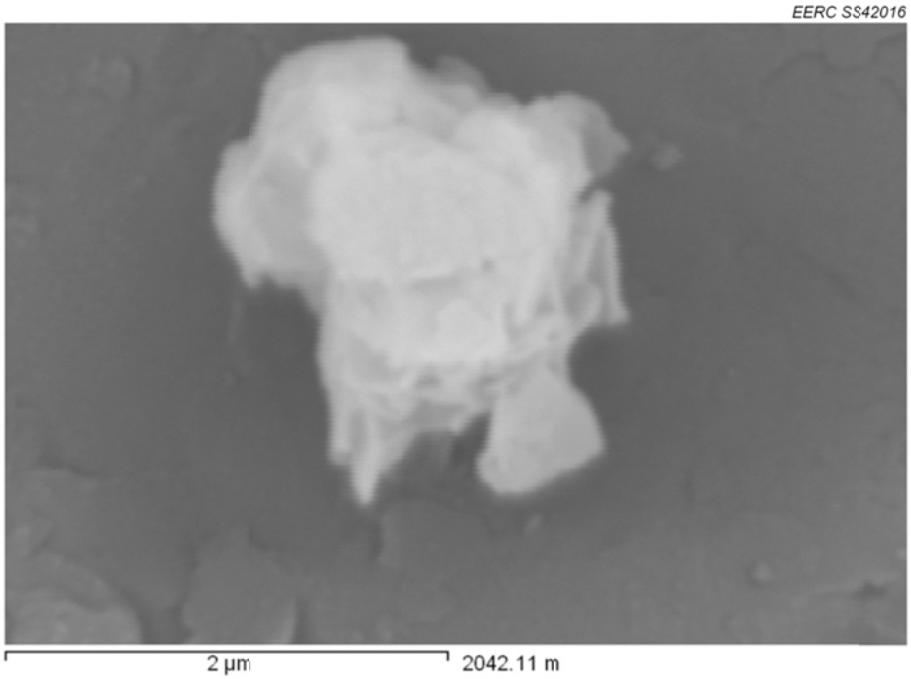

Figure C-16. SEM photomicrograph of T-1, fractured, 35,000× magnification, showing barite in pyrite.

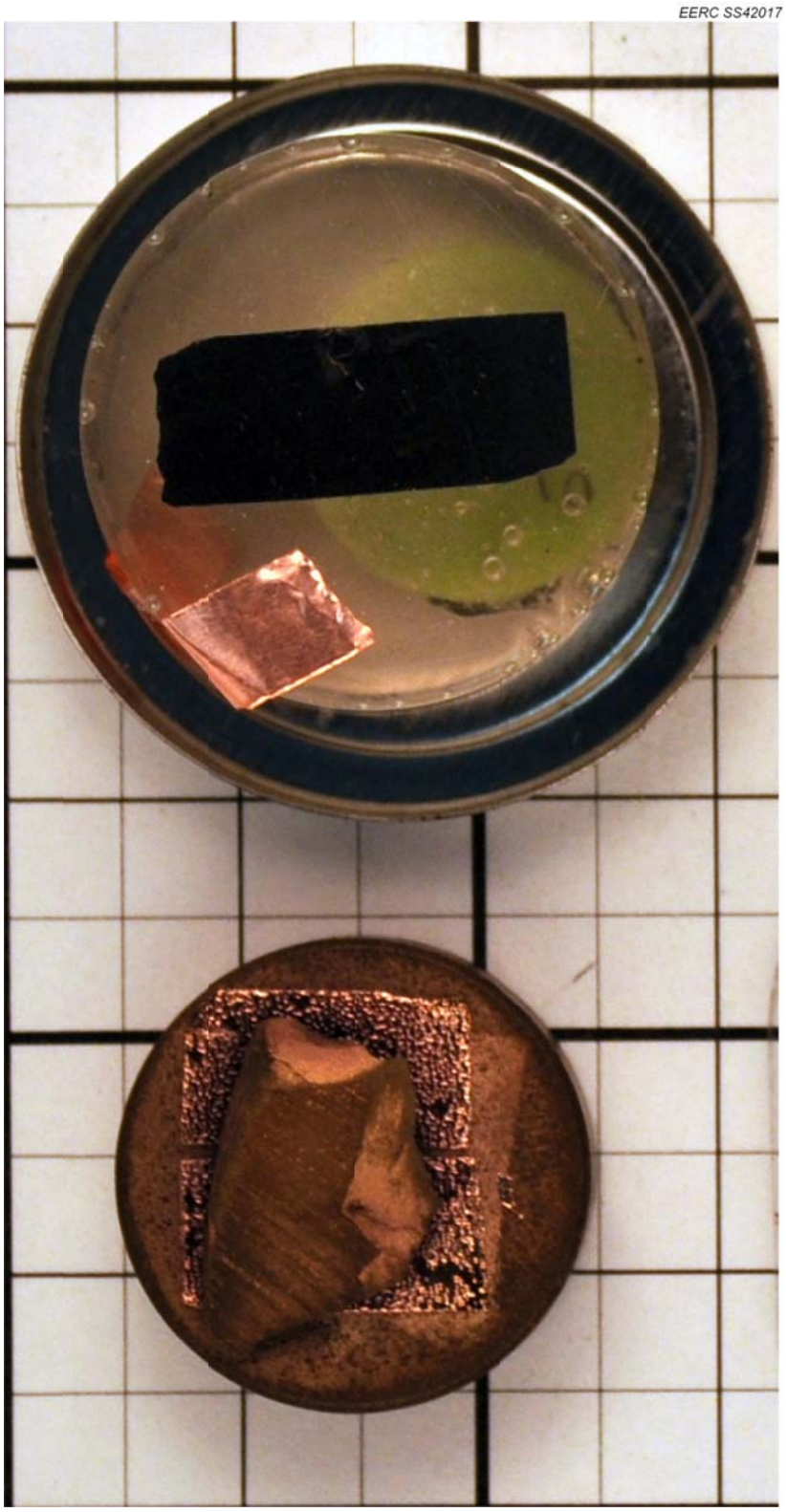

Figure C-17. Photograph of the T-3 specimens after experiment. The polished SEM sample (above) was used for SEM–EDS and QEMSEM measurements and the fractured, gold-dusted SEM sample (below) was used for imagery.

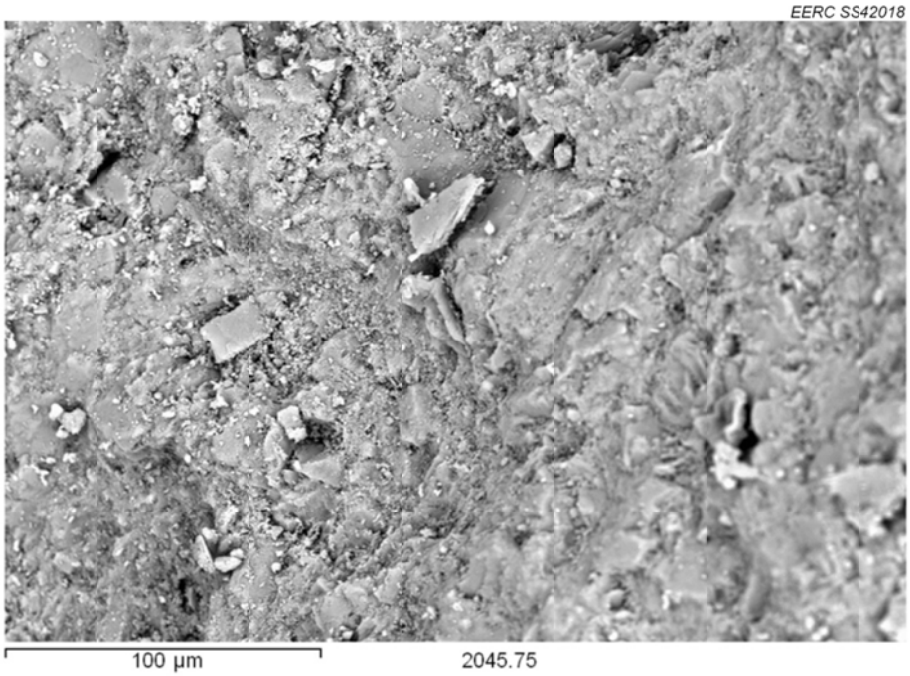

Figure C-18. SEM photomicrograph of T-3, fractured, 500× magnification, showing dolomite and clay structure.

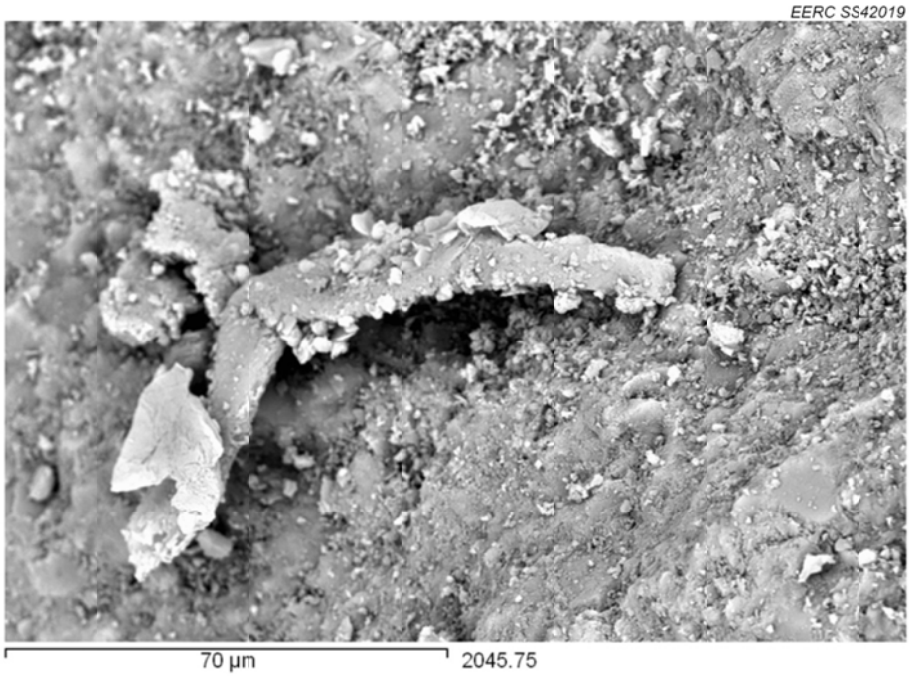

Figure C-19. SEM photomicrograph of T-3, fractured, 1000× magnification, showing intricate structures in the dolomite–clay matrix.

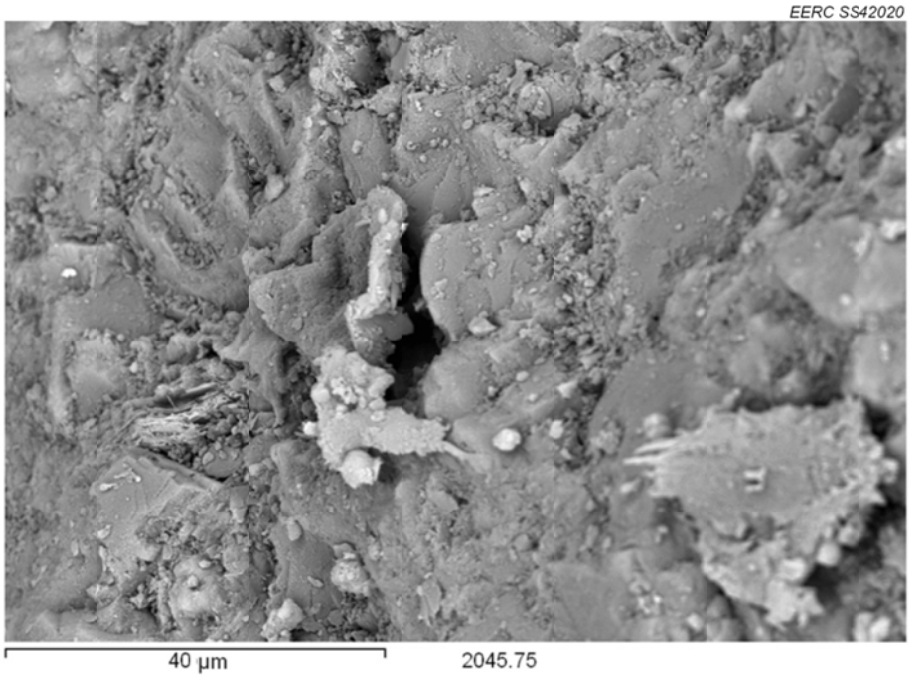

Figure C-20. SEM photomicrograph of T-3, fractured, 1500× magnification, showing mixed dolomite and clay matrix.

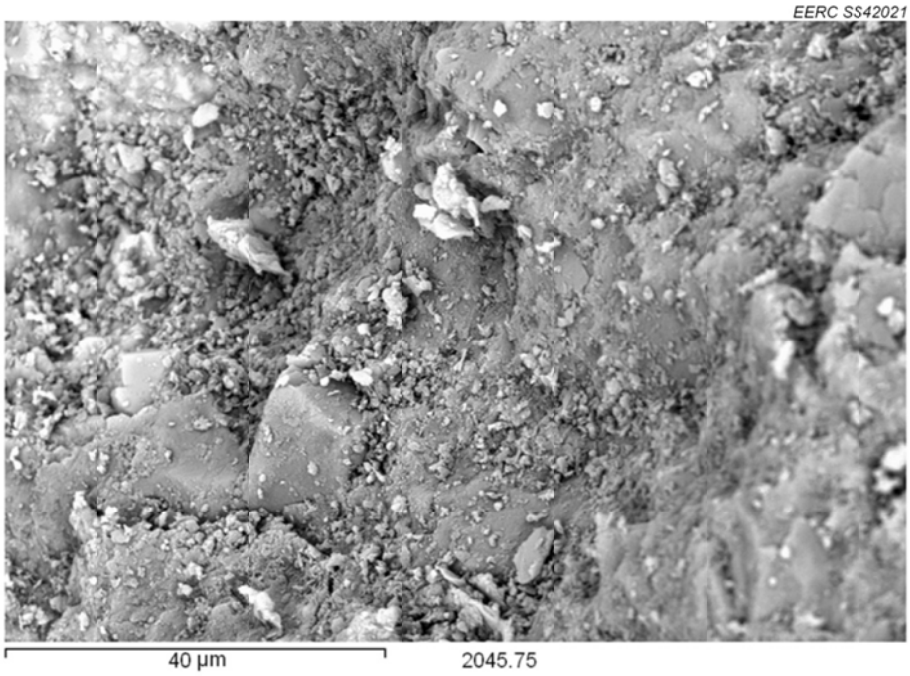

Figure C-21. SEM photomicrograph of T-3, fractured, 1500× magnification, showing dolomite and pyrite in illite clay.

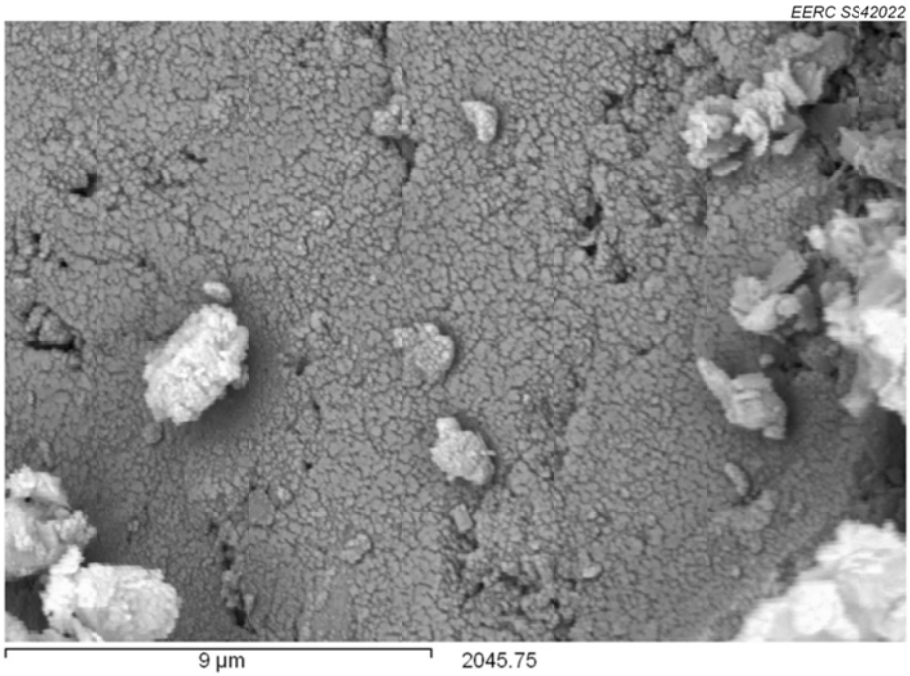

Figure C-22. SEM photomicrograph of T-3, fractured, 1500× magnification, showing pyrite on dolomite.

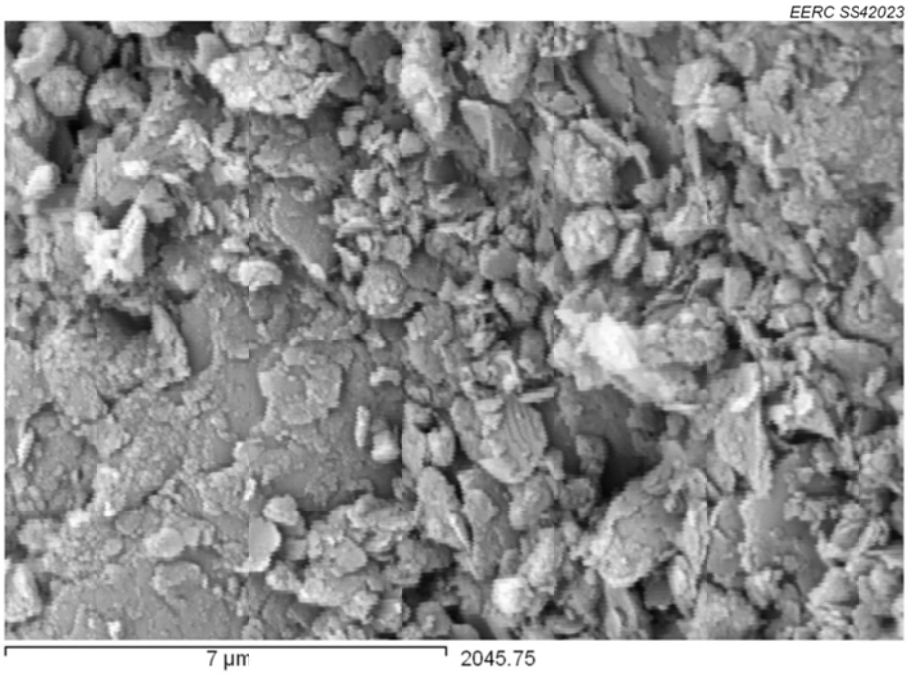

Figure C-23. SEM photomicrograph of T-3, fractured, 10,000× magnification, showing clay and dolomite structures.

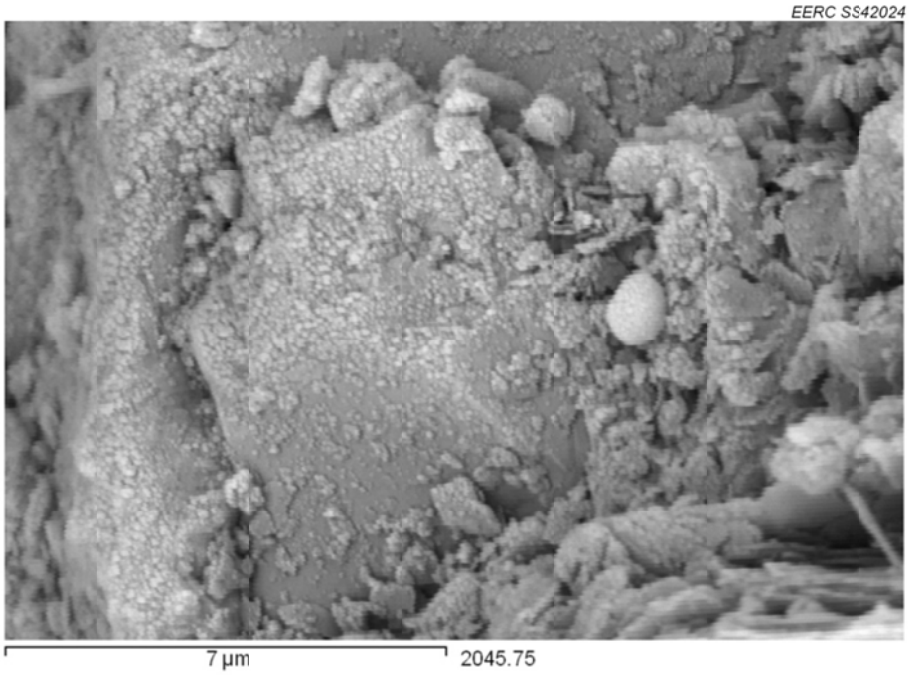

Figure C-24. SEM photomicrograph of T-3, fractured, 10,000× magnification, showing ultrafine pyrite on dolomite.

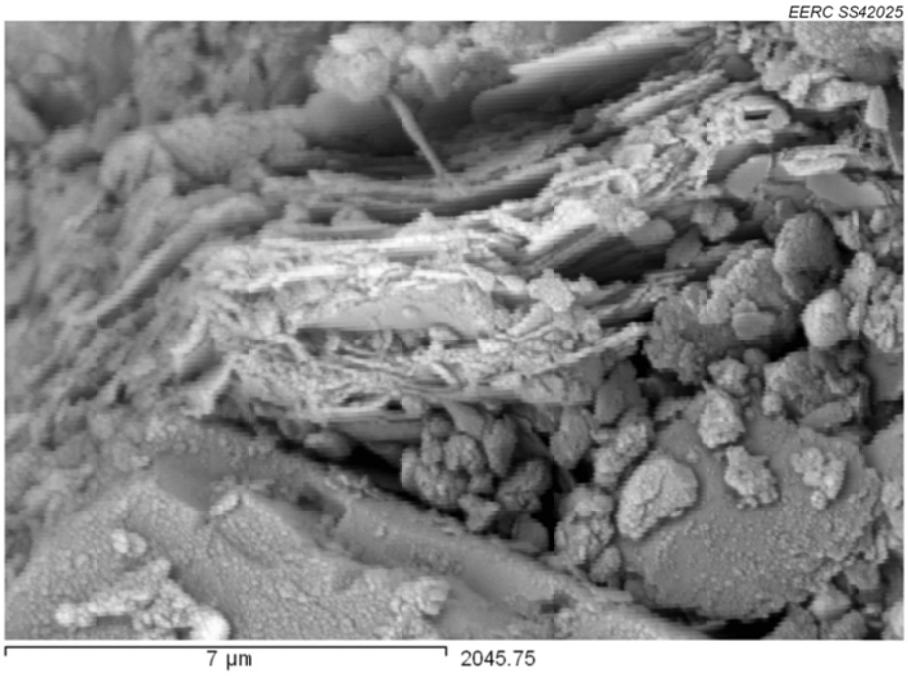

Figure C-25. SEM photomicrograph of T-3, fractured, 10,000× magnification, showing barite around pyrite and ultrafine pyrite on dolomite.

APPENDIX D

SEM–EDS DATA

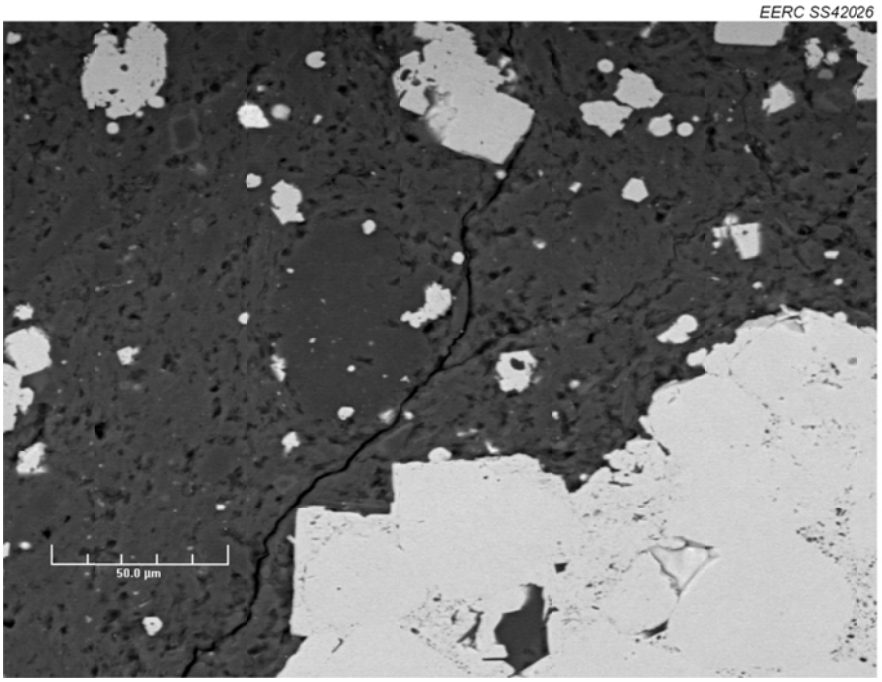

Figure D-1. Field for EDS testing on Sample TH-1 at 500× magnification. Yellow crosshairs indicate the tag number and location.

Table D-1. Results of SEM–EDS Measurements for Points Present in Figure D-1, wt%

Tag	Na	Mg	Al	Si	P	S	Cl	K	Ca	Ti	Fe	Ba	Mineralogy
1	0.00	0.00	1.24	93.07	0.33	1.67	0.00	2.74	0.00	0.01	0.93	0.00	**Clay**
2	0.00	0.00	0.39	95.44	0.00	0.89	0.00	2.66	0.00	0.00	0.62	0.00	**Quartz**
3	0.00	0.00	7.34	84.49	0.00	0.00	0.00	6.95	0.00	0.31	0.91	0.00	**Clay**
4	0.00	29.31	0.78	3.67	0.25	0.13	0.06	0.39	60.09	0.00	5.31	0.00	**Dolomite**
5	0.00	0.56	15.26	70.22	0.00	0.21	0.00	10.81	0.01	1.10	1.83	0.00	**Clay**
6	0.00	0.00	1.94	93.98	0.00	0.00	0.00	3.49	0.00	0.17	0.42	0.00	**Clay**
7	0.00	0.79	16.37	70.11	0.00	0.00	0.00	11.20	0.01	0.37	1.16	0.00	**Clay**
8	0.00	0.84	17.24	66.44	0.00	0.27	0.00	12.81	0.00	0.10	2.30	0.00	**Clay**
9	0.00	0.00	0.00	0.05	0.33	55.57	0.35	0.00	0.04	1.57	42.10	0.00	**Pyrite**
10	0.00	0.00	2.190	2.12	0.11	53.19	0.14	0.25	0.00	1.48	40.53	0.00	**Pyrite**

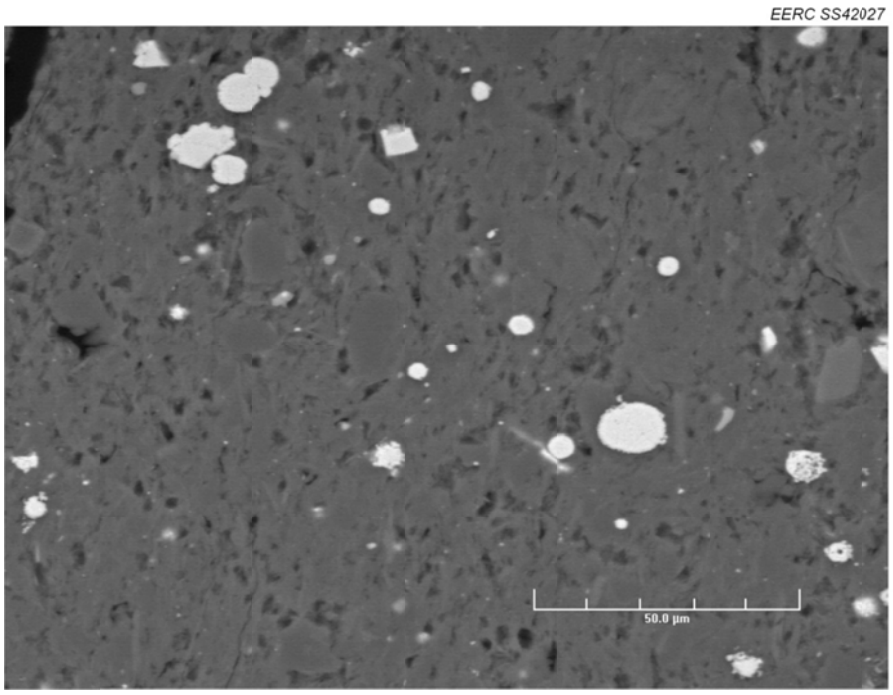

Figure D-2. Field for EDS testing on Sample TH-1 at 750× magnification. Yellow crosshairs indicate the tag number and location.

Table D-2. Results of SEM–EDS Measurements for Points Present in Figure D-2, wt%

Tag	Na	Mg	Al	Si	P	S	Cl	K	Ca	Ti	Fe	Ba	Mineralogy
1	0.00	12.59	7.63	28.23	0.00	0.02	0.00	5.27	33.09	0.23	12.93	0.00	**Dolomite**
2	0.00	0.00	3.74	88.94	0.00	1.18	0.00	4.80	0.00	0.02	1.32	0.00	**Clay**
3	0.00	0.00	4.27	89.67	0.00	0.00	0.00	5.33	0.00	0.06	0.67	0.00	**Clay**
4	0.00	0.00	2.35	92.88	0.00	0.00	0.00	4.06	0.00	0.09	0.61	0.00	**Clay**
5	0.00	0.00	4.16	89.86	0.00	0.00	0.00	5.11	0.00	0.08	0.69	0.09	**Clay**
6	0.00	1.34	22.26	55.58	0.00	0.00	0.00	16.63	0.06	1.01	2.96	0.16	**Clay**
7	0.00	1.57	21.35	50.44	0.00	0.00	0.00	17.48	0.14	0.06	7.82	1.14	**Clay**
8	0.00	0.40	9.63	79.23	0.00	0.00	0.00	9.62	0.00	0.00	1.11	0.00	**Clay**
9	0.00	0.75	15.68	69.92	0.00	0.00	0.00	11.31	0.09	0.37	1.48	0.39	**Clay**
10	0.00	0.35	11.71	76.40	0.00	0.00	0.00	9.64	0.07	0.38	1.18	0.28	**Clay**

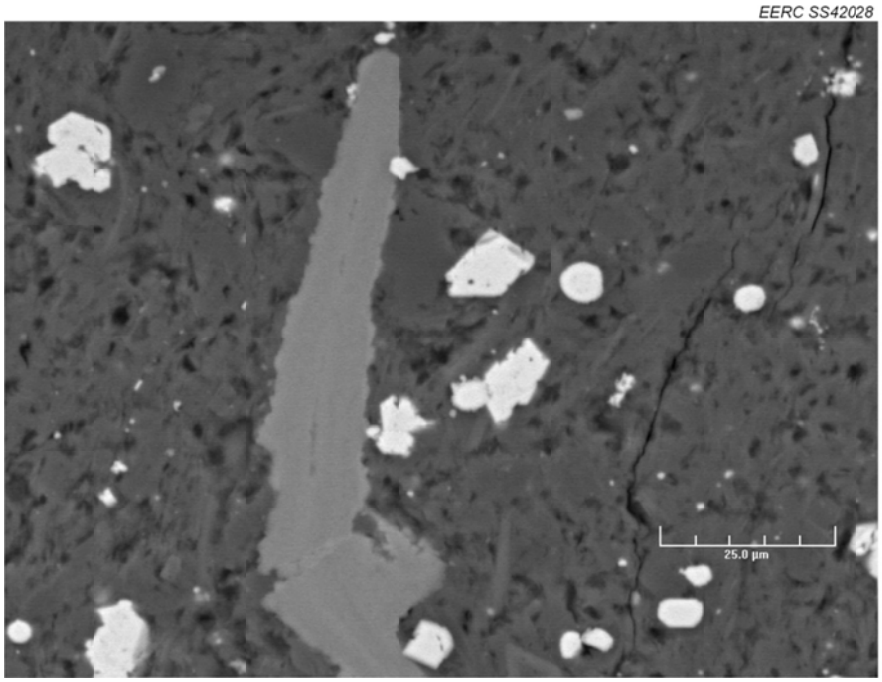

Figure D-3. Field for EDS testing on Sample TH-1 at 1000× magnification. Yellow crosshairs indicate the tag number and location.

Table D-3. Results of SEM–EDS Measurements for Points Present in Figure D-3, wt%

Tag	Na	Mg	Al	Si	P	S	Cl	K	Ca	Ti	Fe	Ba	Mineralogy
1	0.00	0.00	2.99	92.77	0.00	0.00	0.00	3.96	0.00	0.00	0.27	0.00	**Clay**
2	0.00	0.00	1.03	95.11	0.00	0.00	0.00	2.79	0.74	0.00	0.32	0.00	**Quartz**
3	0.00	0.00	0.05	96.95	0.00	0.25	0.00	2.29	0.00	0.00	0.45	0.00	**Quartz**
4	0.00	0.41	13.18	73.80	0.00	0.00	0.00	10.64	0.00	0.71	1.26	0.00	**Clay**
5	0.00	0.84	19.85	55.91	0.58	2.11	0.00	12.62	2.69	1.61	3.79	0.00	**Clay**
6	0.00	0.74	15.83	70.26	0.00	0.08	0.00	11.47	0.00	0.19	1.33	0.10	**Clay**
7	0.00	0.00	0.00	0.51	32.96	0.00	0.00	0.08	66.25	0.00	0.20	0.00	**Apatite**
8	0.00	0.00	0.04	0.51	33.27	0.00	0.00	0.06	65.85	0.00	0.28	0.00	**Apatite**
9	0.00	0.00	0.74	1.62	0.16	54.55	0.04	0.22	0.00	1.34	41.33	0.00	**Pyrite**
10	0.00	0.00	0.05	0.60	0.15	55.53	0.17	0.01	0.00	1.46	42.02	0.00	**Pyrite**

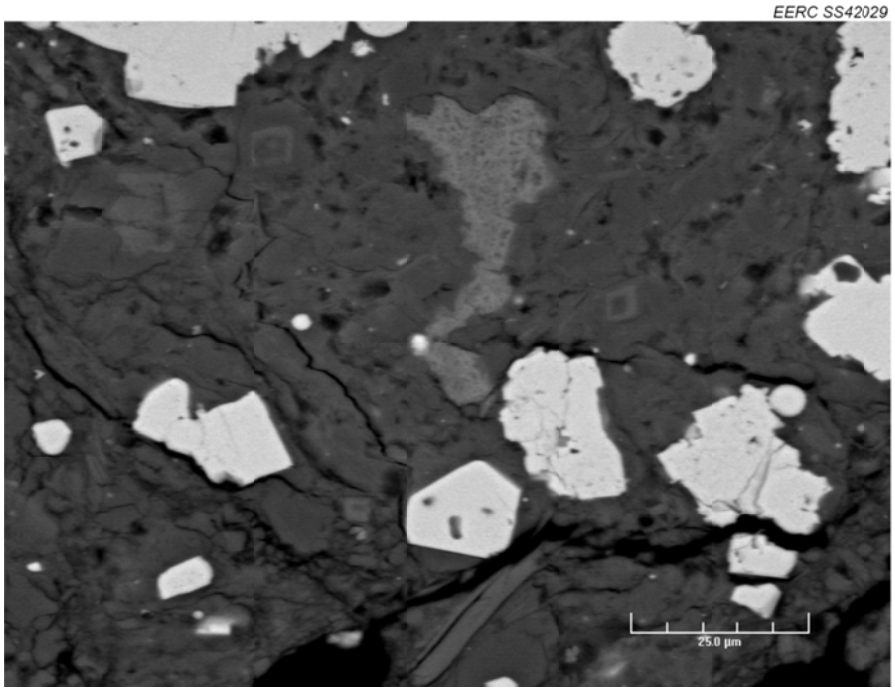

Figure D-4. Field for EDS testing on Sample TH-1 at 1000× magnification. Yellow crosshairs indicate the tag number and location.

Table D-4. Results of SEM–EDS Measurements for Points Present in Figure D-4, wt%

Tag	Na	Mg	Al	Si	P	S	Cl	K	Ca	Ti	Fe	Ba	Mineralogy
1	0.00	30.90	0.55	2.02	0.35	0.51	0.00	0.11	64.61	0.00	0.94	0.00	**Dolomite**
2	0.00	18.14	1.86	5.53	0.25	0.09	0.00	0.95	51.00	0.00	22.19	0.00	**Dolomite**
3	0.00	23.72	0.54	4.00	0.42	0.18	0.07	0.31	59.60	0.45	10.70	0.00	**Dolomite**
4	0.00	25.89	1.44	4.91	0.21	0.01	0.00	0.71	55.01	0.00	11.80	0.00	**Dolomite**
5	0.00	0.00	0.00	0.42	32.71	0.68	0.00	0.00	66.07	0.00	0.13	0.00	**Apatite**
6	0.00	0.00	0.60	3.34	32.10	0.62	0.00	0.36	62.78	0.00	0.19	0.00	**Apatite**
7	0.06	0.73	25.39	50.34	0.00	0.00	0.00	16.93	0.17	0.79	4.76	0.82	**Clay**
8	0.00	0.48	14.56	71.84	0.00	0.00	0.00	11.15	0.00	0.54	1.43	0.00	**Clay**
9	0.00	0.00	0.05	0.04	0.18	55.54	0.15	0.00	0.00	1.42	42.62	0.00	**Pyrite**
10	0.00	0.00	0.16	0.58	0.15	55.37	0.05	0.00	0.00	1.36	42.33	0.00	**Pyrite**

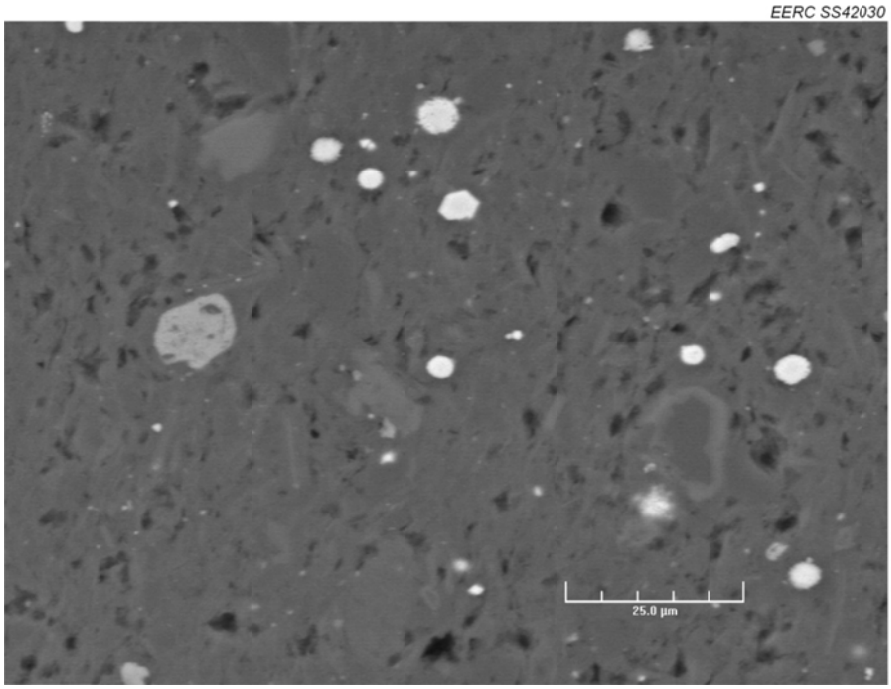

Figure D-5. Field for EDS testing on Sample TH-1 at 1000× magnification. Yellow crosshairs indicate the tag number and location.

Table D-5. Results of SEM–EDS Measurements for Points Present in Figure D-5, wt%

Tag	Na	Mg	Al	Si	P	S	Cl	K	Ca	Ti	Fe	Ba	Mineralogy
1	0.00	12.90	0.31	1.31	0.29	0.07	0.00	0.09	53.60	0.00	31.44	0.00	**Dolomite**
2	0.00	15.28	2.93	12.81	0.43	0.19	0.00	1.88	45.60	0.00	20.89	0.00	**Ankerite**
3	0.00	1.25	22.94	57.21	0.00	0.00	0.00	15.74	0.13	0.36	2.34	0.03	**Clay**
4	0.02	32.86	0.00	0.44	0.50	0.01	0.00	0.00	65.30	0.00	0.87	0.00	**Dolomite**
5	0.00	18.49	1.38	4.55	0.27	0.36	0.00	0.39	50.41	0.00	24.15	0.00	**Ankerite**
6	0.00	0.00	1.33	94.90	0.00	0.00	0.00	3.44	0.00	0.00	0.34	0.00	**Clay**
7*	0.00	0.00	32.53	17.24	33.10	0.29	0.00	3.96	2.45	0.00	0.04	10.39	**Clay**
8	0.00	0.00	1.84	93.86	0.44	0.00	0.00	3.54	0.00	0.00	0.33	0.00	**Clay**
9	0.00	3.89	4.83	60.91	0.00	0.00	0.00	3.18	21.93	0.00	5.27	0.00	**Clay**
10	0.00	0.61	16.99	67.97	0.00	0.00	0.00	12.35	0.00	0.72	1.36	0.00	**Clay**

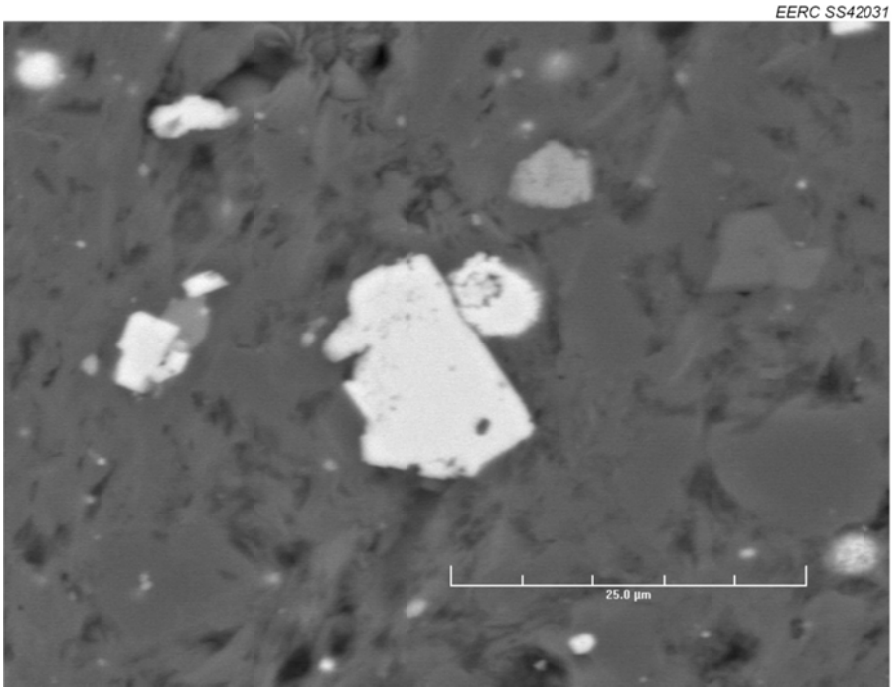

Figure D-6. Field for EDS testing on Sample TH-1 at 2000× magnification. Yellow crosshairs indicate the tag number and location.

Table D-6. Results of SEM–EDS Measurements for Points Present in Figure D-6, wt%

Tag	Na	Mg	Al	Si	P	S	Cl	K	Ca	Ti	Fe	Ba	Mineralogy
1	0.00	0.00	5.36	14.21	21.25	10.98	0.00	2.70	37.87	0.00	7.63	0.00	**Multiple**
2	0.00	0.00	4.51	8.73	0.00	0.46	0.00	1.59	0.01	84.05	0.64	0.00	**High-Ti**
3	0.00	17.76	1.67	6.34	0.08	0.00	0.00	0.68	49.37	0.00	24.10	0.00	**Dolomite**
4	0.00	0.00	2.92	92.11	0.00	0.15	0.00	4.14	0.00	0.00	0.67	0.00	**Clay**
5	0.00	0.07	5.27	86.08	0.00	1.56	0.00	5.74	0.00	0.04	1.25	0.00	**Clay**
6	0.00	0.00	1.44	94.93	0.00	0.00	0.00	3.15	0.00	0.00	0.46	0.02	**Clay**
7	0.00	0.00	0.40	96.40	0.00	0.05	0.15	2.66	0.00	0.00	0.34	0.00	**Quartz**
8	0.00	0.00	0.94	1.72	0.24	54.07	0.24	0.25	0.33	1.34	40.85	0.00	**Pyrite**
9	0.00	0.00	0.00	0.00	0.26	55.47	0.14	0.00	0.11	1.54	42.47	0.00	**Pyrite**
10	0.00	0.00	3.87	91.51	0.00	0.00	0.00	4.30	0.00	0.00	0.32	0.00	**Clay**

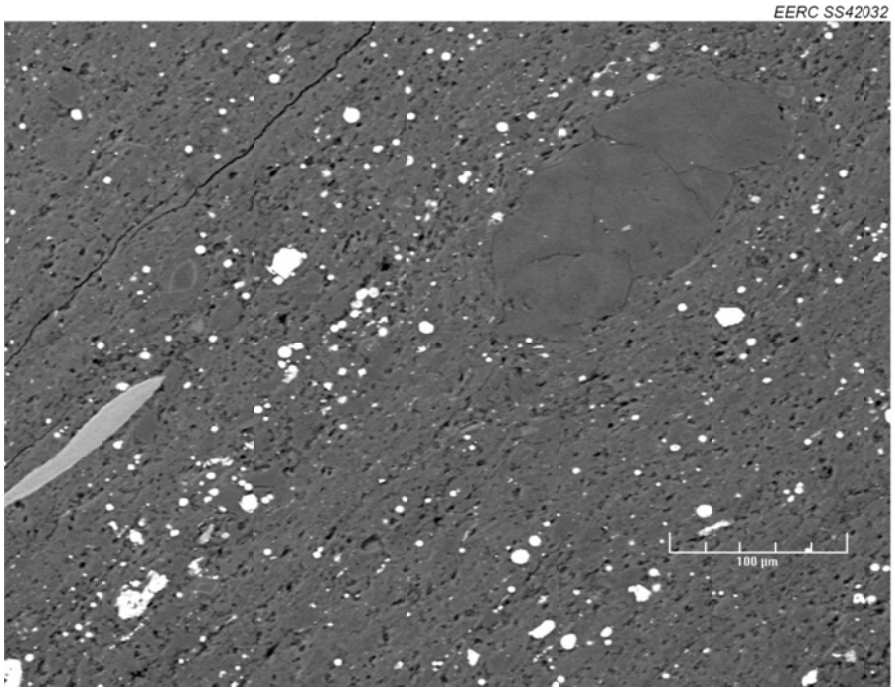

Figure D-7. Field for EDS testing on Sample T-1 at 250× magnification. Yellow crosshairs indicate the tag number and location.

Table D-7. Results of SEM–EDS Measurements for Points Present in Figure D-7, wt%

Tag	Na	Mg	Al	Si	P	S	Cl	K	Ca	Ti	Fe	Ba	Zn	Mineralogy
1	0.00	29.79	0.38	1.12	0.55	0.00	0.00	0.14	67.56	0.00	0.25	0.00	0.20	**Dolomite**
2	0.00	30.29	0.00	0.07	0.70	0.09	0.00	0.00	68.85	0.00	0.00	0.00	0.00	**Dolomite**
3	0.21	31.47	0.03	0.31	0.52	0.05	0.00	0.00	67.41	0.00	0.00	0.00	0.00	**Dolomite**
4	0.00	24.07	0.00	1.09	0.43	0.01	0.15	0.04	64.97	0.00	9.24	0.00	0.00	**Dolomite**
5	0.00	0.00	4.80	88.57	0.00	0.00	0.00	5.73	0.00	0.19	0.57	0.00	0.13	**Clay**
6	0.00	0.00	5.26	11.29	28.19	0.00	0.00	3.07	51.95	0.00	0.24	0.00	0.00	**Clay**
7	0.12	0.00	0.14	1.19	32.00	0.00	0.01	0.20	66.33	0.00	0.00	0.00	0.00	**Apatite**
8	0.00	0.00	3.65	90.60	0.00	0.00	0.00	5.06	0.00	0.13	0.56	0.00	0.00	**Clay**
9	0.00	0.00	0.12	3.35	0.22	51.36	0.22	0.07	0.20	1.05	41.44	0.00	1.98	**Pyrite**
10	0.00	0.00	0.00	0.93	0.24	52.68	0.19	0.00	0.11	1.45	41.93	0.00	2.48	**Pyrite**

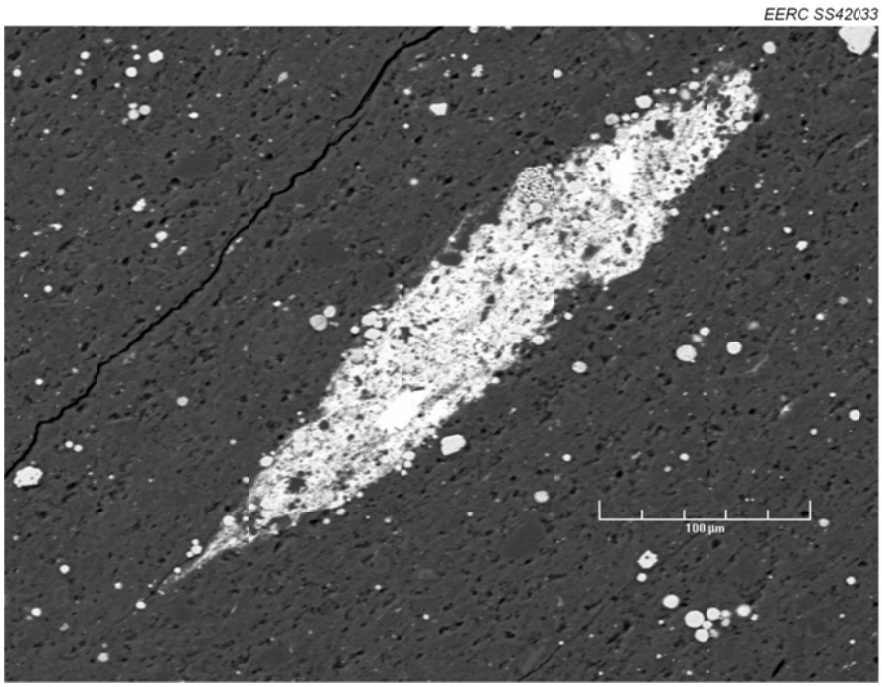

Figure D-8. Field for EDS testing on Sample T-1 at 300× magnification. Yellow crosshairs indicate the tag number and location.

Table D-8. Results of SEM–EDS Measurements for Points Present in Figure D-8, wt%

Tag	Na	Mg	Al	Si	P	S	Cl	K	Ca	Ti	Fe	Ba	Zn	Mineralogy
1	10.01	0.00	5.65	17.38	0.00	25.38	0.09	2.36	0.04	0.11	0.69	0.00	38.28	**Sphalerite**
2	12.40	0.03	1.47	2.99	0.09	31.35	0.00	1.12	0.00	0.15	0.64	0.00	49.75	**Sphalerite**
3	0.00	0.12	1.83	8.51	0.12	44.82	0.46	0.74	0.18	0.69	40.29	0.00	2.25	**Pyrite**
4	15.20	0.00	0.00	0.01	0.11	31.28	0.00	0.66	0.00	0.20	0.44	0.00	52.10	**Sphalerite**
5	14.21	0.00	0.52	0.89	0.00	31.08	0.00	0.82	0.00	0.26	0.52	0.00	51.70	**Sphalerite**
6	0.00	0.00	0.22	96.80	0.00	0.00	0.00	2.68	0.00	0.00	0.15	0.00	0.15	**Quartz**
7	0.00	0.00	0.12	96.37	0.00	0.00	0.00	2.65	0.00	0.00	0.34	0.00	0.51	**Quartz**
8	0.00	0.00	0.22	96.38	0.00	0.13	0.00	2.81	0.00	0.00	0.16	0.17	0.13	**Quartz**
9	0.00	0.09	7.61	81.93	0.08	0.00	0.00	8.85	0.00	0.44	0.88	0.00	0.11	**Clay**
10	0.00	1.13	16.50	67.29	0.00	0.46	0.00	12.61	0.00	0.43	1.56	0.00	0.04	**Clay**

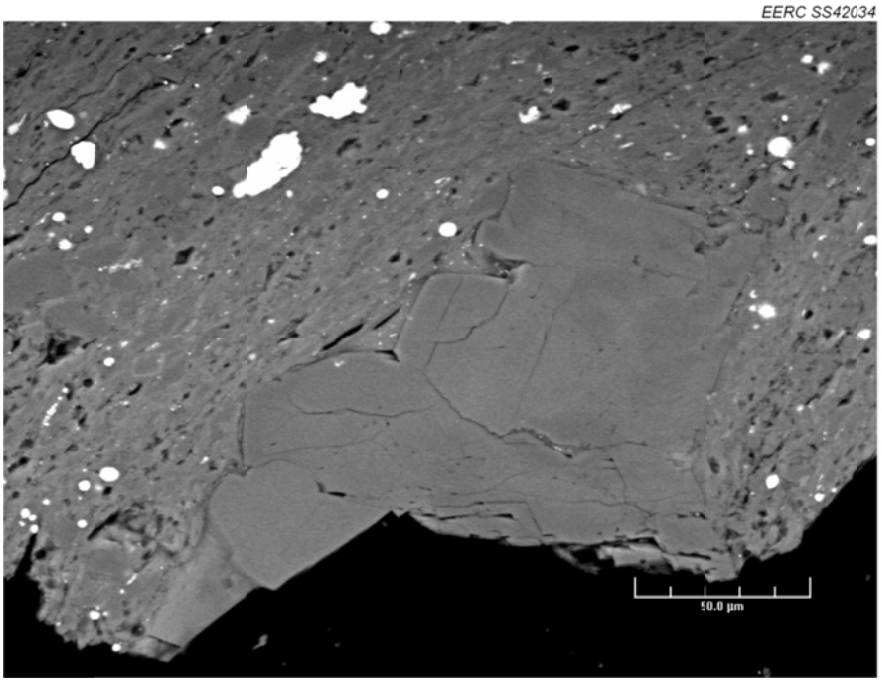

Figure D-9. Field for EDS testing on Sample T-1 at 500× magnification. Yellow crosshairs indicate the tag number and location.

Table D-9. Results of SEM–EDS Measurements for Points Present in Figure D-9, wt%

Tag	Na	Mg	Al	Si	P	S	Cl	K	Ca	Ti	Fe	Ba	Mineralogy
1	0.00	29.53	0.33	1.11	0.58	0.00	0.00	0.00	68.45	0.00	0.00	0.00	**Dolomite**
2	0.00	27.78	0.13	0.22	0.59	0.22	0.00	0.00	71.02	0.00	0.04	0.00	**Dolomite**
3	0.00	30.04	0.00	0.07	0.83	0.07	0.00	0.00	68.90	0.00	0.09	0.00	**Dolomite**
4	0.00	0.08	3.71	89.69	0.02	0.00	0.00	4.90	0.00	0.87	0.73	0.00	**Clay**
5	0.00	26.10	1.06	14.47	0.11	0.00	0.00	0.87	57.10	0.00	0.29	0.00	**Dolomite**
6	0.36	0.83	21.19	60.17	0.00	0.50	0.00	14.23	0.28	0.60	1.84	0.00	**Clay**
7	0.00	1.29	19.72	60.96	0.00	0.00	0.00	14.63	1.17	0.40	1.52	0.30	**Clay**
8	0.00	1.11	19.70	61.24	0.00	0.10	0.00	15.14	0.10	0.65	1.95	0.00	**Clay**
9	0.00	0.01	1.03	1.60	0.17	52.55	0.15	0.38	0.07	1.22	42.82	0.00	**Pyrite**
10	0.00	0.00	0.10	1.12	0.17	54.18	0.08	0.00	0.00	1.19	43.15	0.00	**Pyrite**

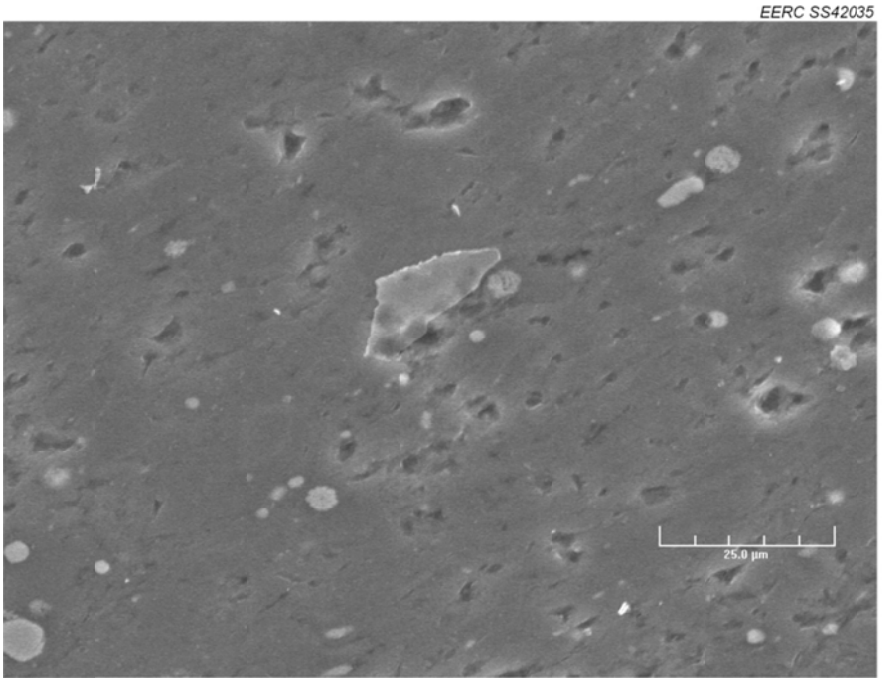

Figure D-10. Field for EDS testing on Sample T-1 at 1000× magnification. Yellow crosshairs indicate the tag number and location.

Table D-10. Results of SEM–EDS Measurements for Points Present in Figure D-10, wt%

Tag	Na	Mg	Al	Si	P	S	Cl	K	Ca	Ti	Fe	Ba	Mineralogy
1	0.00	0.25	8.56	83.61	0.00	0.00	0.00	7.00	0.00	0.00	0.58	0.00	**Clay**
2	0.00	0.23	8.48	81.97	0.00	0.00	0.00	8.29	0.00	0.04	1.00	0.00	**Clay**
3	0.00	0.46	14.94	70.59	0.00	0.00	0.00	12.65	0.00	0.27	1.08	0.00	**Clay**
4	0.00	0.00	2.66	9.92	0.00	47.64	0.00	1.32	0.00	0.08	38.37	0.00	**Pyrite**
5	0.00	0.00	1.56	8.95	0.00	49.76	0.00	0.72	0.00	0.00	39.01	0.00	**Pyrite**
6	0.00	0.00	1.64	6.70	0.00	50.75	0.00	0.56	0.00	0.00	40.35	0.00	**Pyrite**
7	0.00	0.26	13.36	73.86	0.00	0.00	0.00	11.00	0.00	0.00	1.52	0.00	**Clay**
8	0.00	0.29	15.79	71.34	0.00	0.00	0.00	11.22	0.11	0.00	1.26	0.00	**Clay**

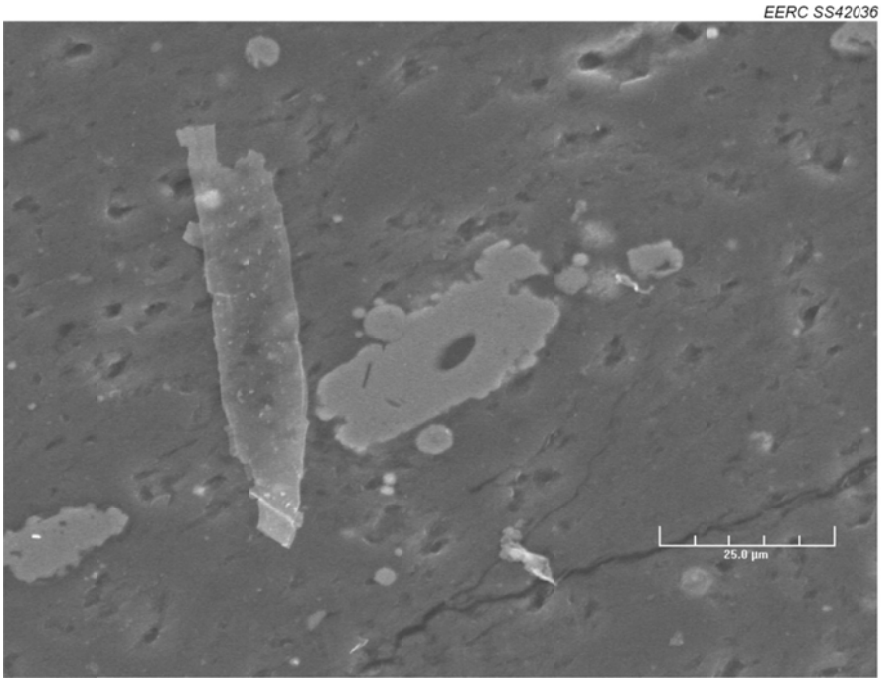

Figure D-11. Field for EDS testing on Sample T-1 at 1000× magnification. Yellow crosshairs indicate the tag number and location.

Table D-11. Results of SEM–EDS Measurements for Points Present in Figure D-11, wt%

Tag	Na	Mg	Al	Si	P	S	Cl	K	Ca	Ti	Fe	Ba	Mineralogy
1	0.00	0.47	14.80	68.06	0.00	0.90	0.01	11.93	2.14	0.00	1.69	0.00	**Clay**
2	0.00	0.00	17.22	67.57	0.00	0.15	0.00	13.46	0.00	0.39	1.20	0.00	**Clay**
3	0.00	0.00	0.40	1.93	0.00	53.98	0.00	0.38	0.06	0.00	43.24	0.00	**Pyrite**
4	0.00	0.00	2.65	10.04	0.00	49.81	0.00	0.94	0.19	0.00	36.36	0.00	**Pyrite**
5	0.00	0.00	0.00	2.28	0.00	52.76	0.00	0.19	0.03	0.31	44.42	0.00	**Pyrite**
6	0.00	0.00	0.23	14.00	0.00	47.69	0.00	0.20	0.00	0.00	37.88	0.00	**Pyrite**
7	0.00	0.00	0.13	99.79	0.00	0.00	0.00	0.08	0.00	0.00	0.00	0.00	**Quartz**
8	0.00	0.71	20.36	60.11	0.00	1.38	0.00	14.27	0.15	0.00	3.04	0.00	**Clay**

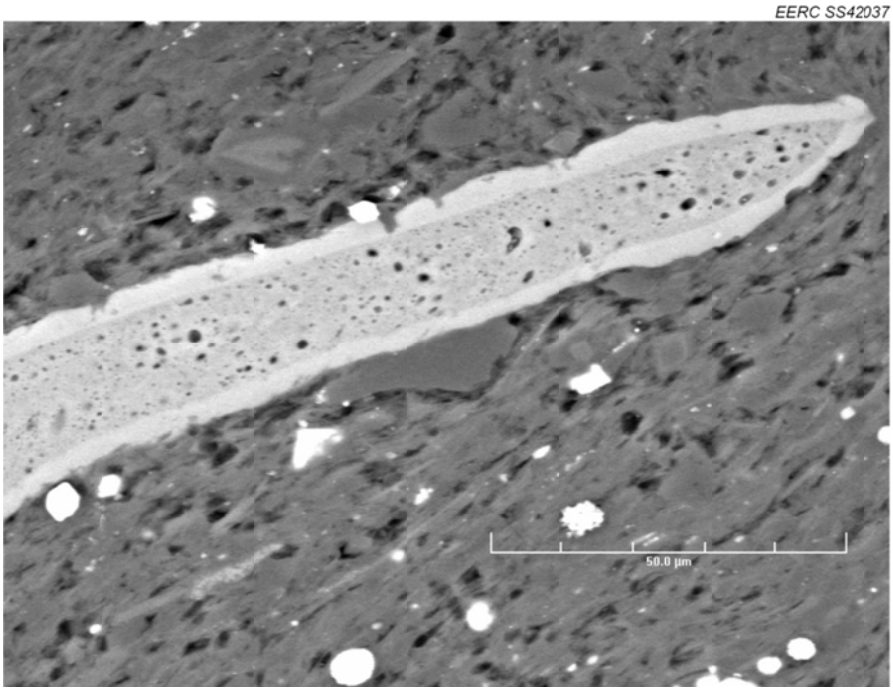

Figure D-12. Field for EDS testing on Sample T-1 at 1000× magnification. Yellow crosshairs indicate the tag number and location.

Table D-12. Results of SEM–EDS Measurements for Points Present in Figure D-12, wt%

Tag	Na	Mg	Al	Si	P	S	Cl	K	Ca	Ti	Fe	Ba	Mineralogy
1	0.00	18.69	0.74	2.74	0.20	0.08	0.00	0.39	58.14	0.00	19.02	0.00	**Ankerite**
2	0.00	0.58	10.15	76.85	0.00	0.50	0.00	9.74	0.88	0.09	1.20	0.00	**Clay**
3	0.00	0.04	5.12	86.45	0.24	0.00	0.00	6.29	1.06	0.00	0.59	0.20	**Clay**
4	0.00	0.00	0.10	0.92	32.81	0.00	0.00	0.12	66.01	0.00	0.03	0.00	**Apatite**
5	0.00	0.00	0.18	1.19	32.04	0.00	0.00	0.14	66.45	0.00	0.00	0.00	**Apatite**
6	0.09	0.00	0.05	0.52	32.61	0.00	0.00	0.12	66.54	0.00	0.07	0.00	**Apatite**
7	0.00	0.00	0.00	0.44	32.80	0.00	0.10	0.06	66.60	0.00	0.00	0.00	**Apatite**
8	0.00	0.00	0.63	95.95	0.39	0.00	0.00	2.70	0.21	0.00	0.11	0.00	**Quartz**
9	0.00	0.00	4.52	88.54	0.00	0.00	0.00	5.39	0.00	0.81	0.74	0.00	**Clay**
10	0.00	0.00	4.71	88.32	0.00	0.00	0.00	5.99	0.00	0.33	0.65	0.00	**Clay**

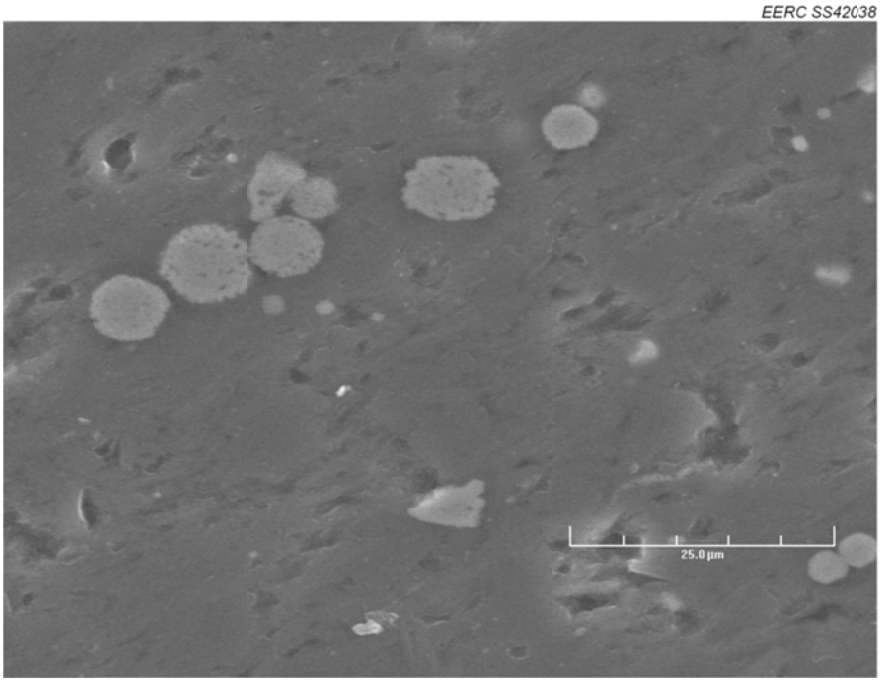

Figure D-13. Field for EDS testing on Sample T-1 at 1500× magnification. Yellow crosshairs indicate the tag number and location.

Table D-13. Results of SEM–EDS Measurements for Points Present in Figure D-13, wt%

Tag	Na	Mg	Al	Si	P	S	Cl	K	Ca	Ti	Fe	Ba	Mineralogy
1	0.00	0.00	0.19	0.56	0.00	54.92	0.00	0.27	0.06	0.00	44.00	0.00	**Pyrite**
2	0.00	0.08	0.16	0.70	0.15	54.70	0.00	0.00	0.00	0.08	44.14	0.00	**Pyrite**
3	0.00	0.00	0.05	0.48	0.00	54.99	0.00	0.32	0.05	0.00	43.46	0.65	**Pyrite**
4	0.00	0.00	0.73	1.97	0.12	53.65	0.00	0.34	0.00	0.40	42.79	0.00	**Pyrite**
5	0.00	0.31	17.06	66.83	0.00	0.00	0.00	13.15	0.33	0.07	2.25	0.00	**Clay**
6	0.05	0.26	3.09	7.10	0.00	49.43	0.03	0.60	0.00	0.00	39.45	0.00	**Pyrite**
7	0.00	0.00	3.98	8.97	0.00	47.86	0.00	1.50	0.00	0.23	37.46	0.00	**Pyrite**
8	0.00	0.39	21.61	59.22	0.00	0.00	0.00	17.17	0.00	0.00	1.61	0.00	**Clay**
9	0.00	0.75	18.14	63.11	0.00	0.00	0.00	15.69	0.22	0.17	1.92	0.00	**Clay**
10	0.00	0.94	17.47	65.51	0.00	0.00	0.00	13.39	0.29	0.84	1.56	0.00	**Clay**

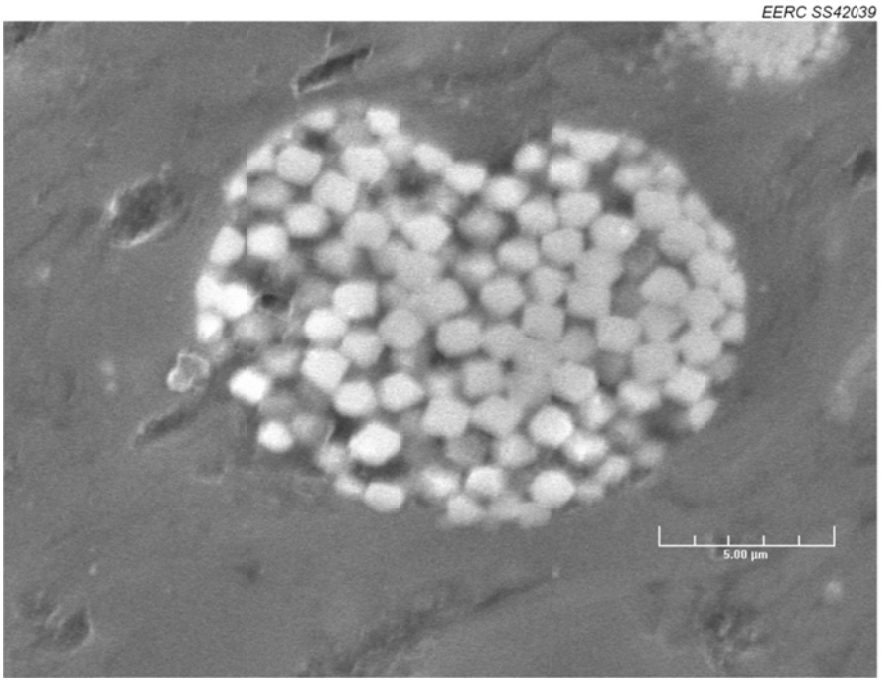

Figure D-14. Field for EDS testing on Sample T-1 at 5000× magnification. Yellow crosshairs indicate the tag number and location.

Table D-14. Results of SEM–EDS Measurements for Points Present in Figure D-14, wt%

Tag	Na	Mg	Al	Si	P	S	Cl	K	Ca	Ti	Fe	Ba	Mineralogy
1	0.00	0.30	15.08	67.07	0.00	2.43	0.00	12.22	0.02	0.91	1.96	0.00	**Clay**
2	0.00	0.00	0.99	3.76	0.00	53.34	0.00	0.47	0.00	0.21	41.24	0.00	**Pyrite**
3	0.00	0.00	0.18	0.30	0.00	56.00	0.00	0.03	0.00	0.07	43.42	0.00	**Pyrite**
4	0.00	0.00	0.00	0.00	0.00	55.54	0.00	0.14	0.00	0.18	44.07	0.07	**Pyrite**
5	0.00	0.00	2.25	5.84	0.00	52.41	0.00	1.14	0.09	0.00	38.28	0.00	**Pyrite**
6	0.00	0.63	16.90	66.77	0.00	0.23	0.00	13.84	0.00	0.49	1.14	0.00	**Clay**

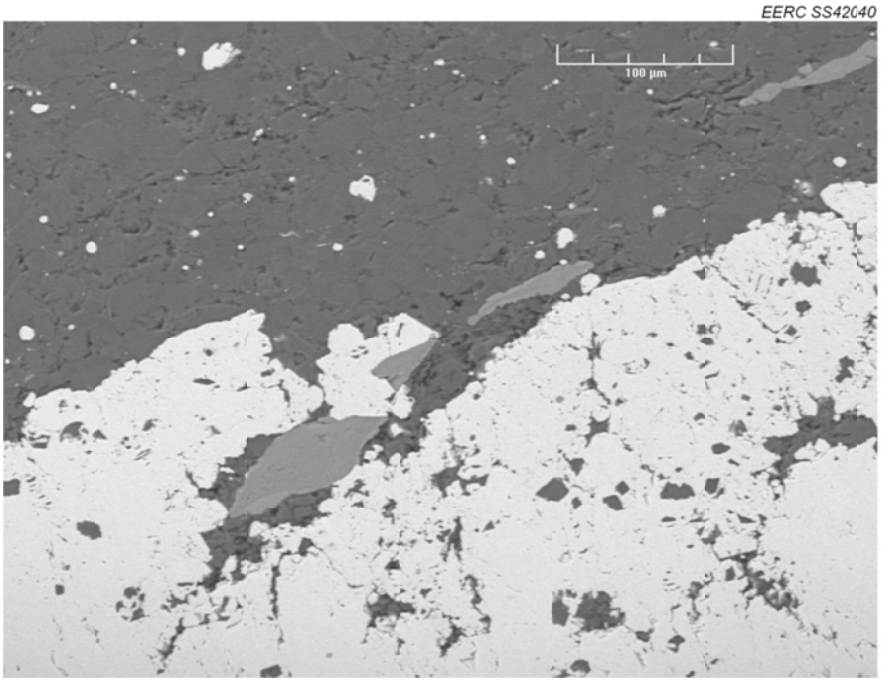

Figure D-15. Field for EDS testing on Sample T-3 at 250× magnification. Yellow crosshairs indicate the tag number and location.

Table D-15. Results of SEM–EDS Measurements for Points Present in Figure D-15, wt%

Tag	Na	Mg	Al	Si	P	S	Cl	K	Ca	Ti	Fe	Ba	Mineralogy
1	0.07	0.00	0.00	0.58	32.02	0.00	0.00	0.02	67.21	0.00	0.11	0.00	**Apatite**
2	0.00	0.00	0.02	0.51	32.41	0.02	0.00	0.00	66.96	0.00	0.07	0.00	**Apatite**
3	0.12	0.02	0.00	0.44	31.68	0.00	0.28	0.18	67.28	0.00	0.00	0.00	**Apatite**
4	0.00	14.63	10.56	20.59	0.00	0.00	0.00	3.38	48.85	0.05	1.94	0.00	**Dolomite**
5	0.00	25.25	0.00	0.88	0.56	0.31	0.00	0.00	72.58	0.00	0.42	0.00	**Dolomite**
6	0.00	24.30	0.14	0.43	0.47	0.06	0.20	0.05	73.37	0.00	0.98	0.00	**Dolomite**
7	0.00	26.46	0.36	0.86	0.50	0.20	0.00	0.19	70.74	0.00	0.70	0.00	**Dolomite**
8	0.00	12.96	0.00	0.45	0.07	30.42	0.00	0.00	30.83	0.00	25.28	0.00	**Pyrite**
9	0.00	23.98	2.14	6.60	0.17	0.73	0.00	2.01	61.34	0.25	2.79	0.00	**Dolomite**
10	0.00	0.00	0.01	0.00	0.10	53.73	0.20	0.00	0.00	1.49	44.48	0.00	**Pyrite**

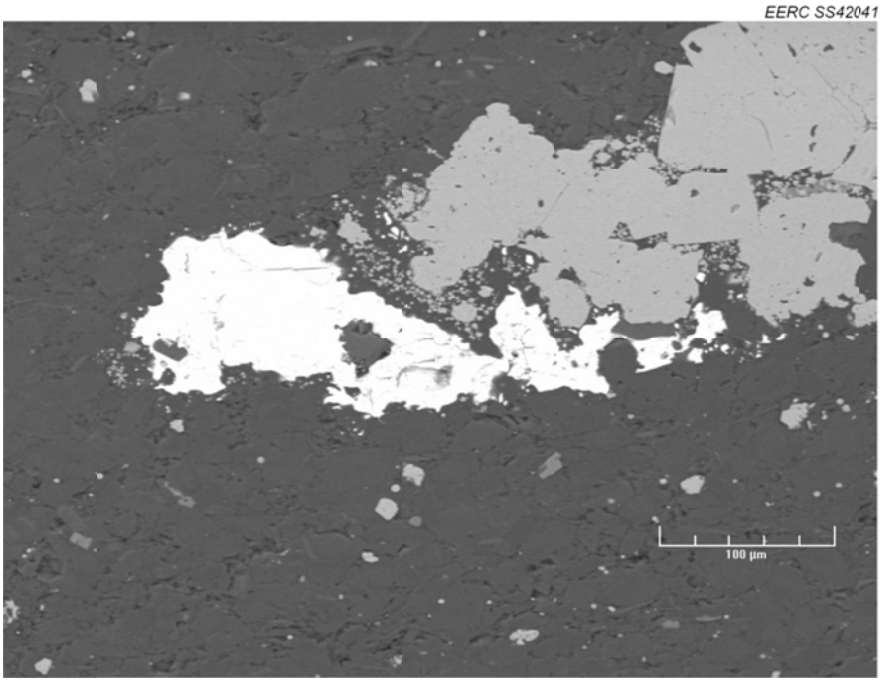

Figure D-16. Field for EDS testing on Sample T-3 at 250× magnification. Yellow crosshairs indicate the tag number and location.

Table D-16. Results of SEM–EDS Measurements for Points Present in Figure D-16, wt%

Tag	Na	Mg	Al	Si	P	S	Cl	K	Ca	Ti	Fe	Ba	Mineralogy
1	0.10	0.00	0.00	0.42	0.02	19.05	0.00	0.00	0.00	9.88	0.00	70.52	**Barite**
2	0.07	0.00	0.00	0.66	0.01	19.48	0.00	0.00	0.00	9.33	0.00	70.45	**Barite**
3	0.00	0.00	0.00	0.03	0.34	53.64	0.24	0.00	0.29	1.38	44.08	0.00	**Pyrite**
4	0.00	0.00	0.00	0.04	0.32	54.00	0.20	0.00	0.06	1.58	43.80	0.00	**Pyrite**
5	0.00	0.03	1.63	4.37	0.14	49.65	0.11	0.44	0.42	1.02	42.20	0.00	**Pyrite**
6	0.00	2.04	1.04	13.78	0.03	0.21	0.00	0.38	2.46	80.01	0.04	0.00	**High-Ti**
7	0.00	0.00	0.00	0.37	0.26	53.79	0.20	0.00	0.44	1.49	43.46	0.00	**Pyrite**
8	0.00	26.24	0.68	2.28	0.42	0.00	0.00	0.29	69.93	0.00	0.17	0.00	**Dolomite**
9	0.00	25.32	1.42	3.14	0.31	0.17	0.35	0.52	68.26	0.00	0.51	0.00	**Dolomite**
10	0.00	26.79	0.04	0.55	0.39	0.30	0.09	0.07	71.46	0.00	0.32	0.00	**Dolomite**

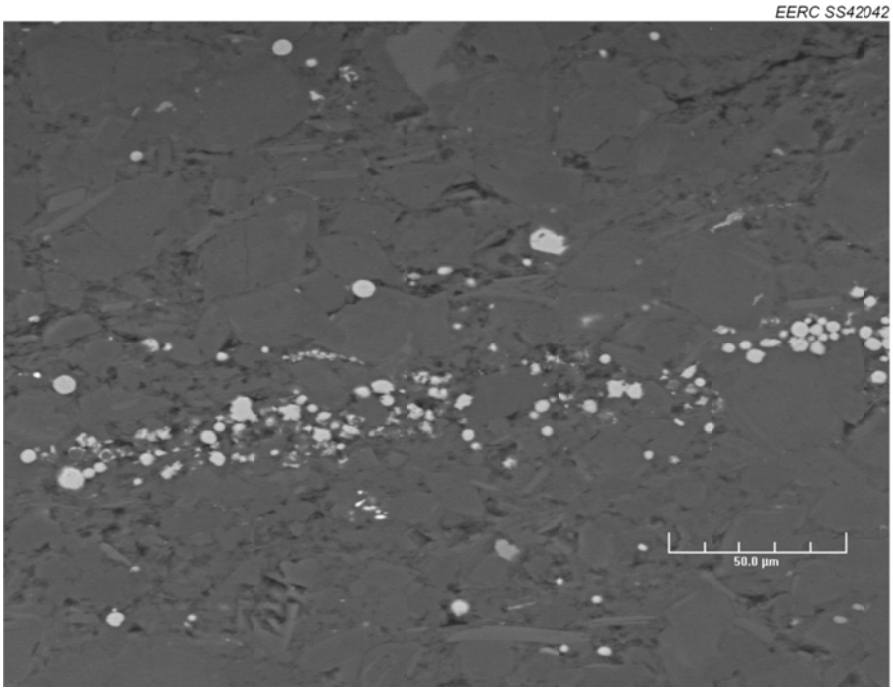

Figure D-17. Field for EDS testing on Sample T-3 at 500× magnification. Yellow crosshairs indicate the tag number and location.

Table D-17. Results of SEM–EDS Measurements for Points Present in Figure D-17, wt%

Tag	Na	Mg	Al	Si	P	S	Cl	K	Ca	Ti	Fe	Ba	Mineralogy
1	0.00	0.30	0.30	0.91	0.64	0.13	0.00	0.08	97.66	0.00	0.00	0.00	**Calcite**
2	0.00	1.44	22.55	50.30	0.00	0.00	0.00	19.11	0.90	0.58	4.68	0.45	**Clay**
3	0.01	26.17	0.23	1.15	0.53	0.35	0.00	0.00	70.64	0.00	0.91	0.00	**Dolomite**
4	0.00	25.72	0.07	0.54	0.53	0.47	0.00	0.02	72.58	0.00	0.06	0.00	**Dolomite**
5	0.00	0.00	0.00	0.08	0.11	54.06	0.04	0.00	0.29	1.51	43.91	0.00	**Pyrite**
6	0.00	24.34	0.07	8.97	0.22	0.23	0.00	0.08	65.29	0.00	0.81	0.00	**Dolomite**
7	0.00	0.00	0.00	1.36	0.38	53.54	0.33	0.01	0.20	1.43	42.75	0.00	**Pyrite**
8	0.00	0.00	0.10	1.88	0.24	53.72	0.12	0.00	0.34	1.38	42.21	0.00	**Pyrite**
9	0.00	1.56	18.50	62.95	0.00	1.39	0.00	13.12	0.63	0.34	1.51	0.00	**Clay**
10	0.00	1.18	24.60	46.85	0.00	0.00	0.00	19.25	0.69	1.43	6.01	0.00	**Clay**
11	0.00	0.00	0.94	1.57	0.13	0.08	0.04	0.20	0.59	96.05	0.39	0.00	**High-Ti**
12	0.00	26.66	0.22	0.45	0.59	0.12	0.00	0.00	71.58	0.00	0.37	0.00	**Dolomite**

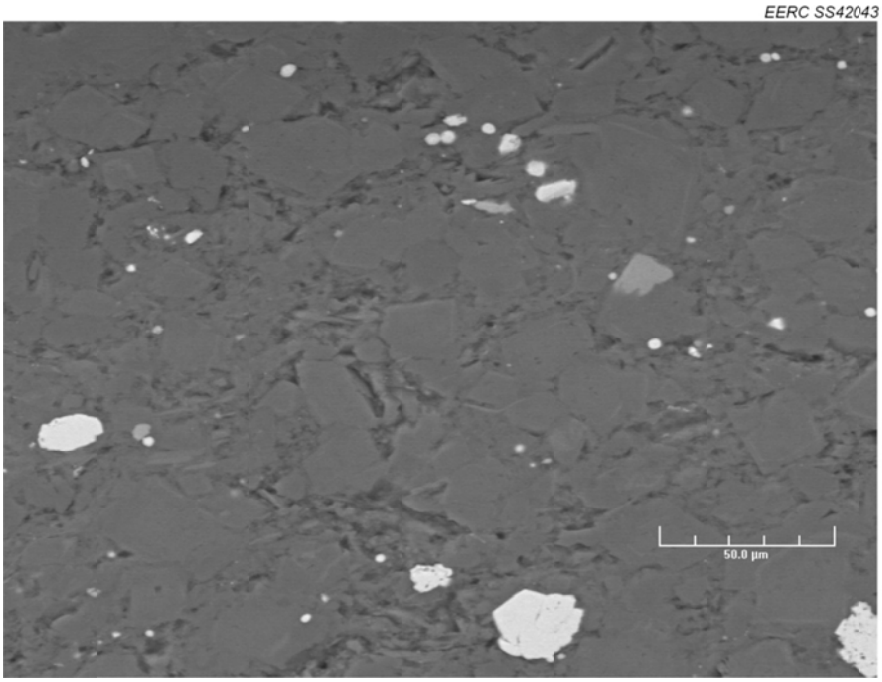

Figure D-18. Field for EDS testing on Sample T-3 at 500× magnification. Yellow crosshairs indicate the tag number and location.

Table D-18. Results of SEM–EDS Measurements for Points Present in Figure D-18, wt%

Tag	Na	Mg	Al	Si	P	S	Cl	K	Ca	Ti	Fe	Ba	Mineralogy
1	0.00	25.71	1.09	3.06	0.15	0.00	0.00	0.66	65.92	0.00	3.40	0.00	**Dolomite**
2	0.00	27.63	0.54	3.34	0.29	0.04	0.29	0.23	67.36	0.00	0.29	0.00	**Dolomite**
3	0.00	26.66	0.03	0.77	0.49	0.13	0.00	0.04	71.79	0.00	0.08	0.00	**Dolomite**
4	0.00	28.22	0.44	1.40	0.39	0.18	0.00	0.33	68.78	0.00	0.27	0.00	**Dolomite**
5	0.00	1.52	6.15	78.75	0.00	1.61	0.00	5.00	6.26	0.00	0.71	0.00	**Clay**
6	0.00	1.11	15.09	65.59	0.00	3.66	0.00	12.12	0.43	0.46	1.53	0.00	**Clay**
7	0.29	0.13	24.18	54.07	0.00	0.00	0.00	16.69	0.31	0.36	3.55	0.40	**Clay**
8	0.00	1.18	18.12	60.40	0.00	0.67	0.00	15.89	1.24	0.38	1.75	0.37	**Clay**
9	0.16	0.17	0.20	0.77	32.23	0.00	0.00	0.23	66.24	0.00	0.00	0.00	**Apatite**
10	0.00	4.34	0.54	1.37	0.08	1.69	0.00	0.12	16.18	74.50	1.19	0.00	**High-Ti**

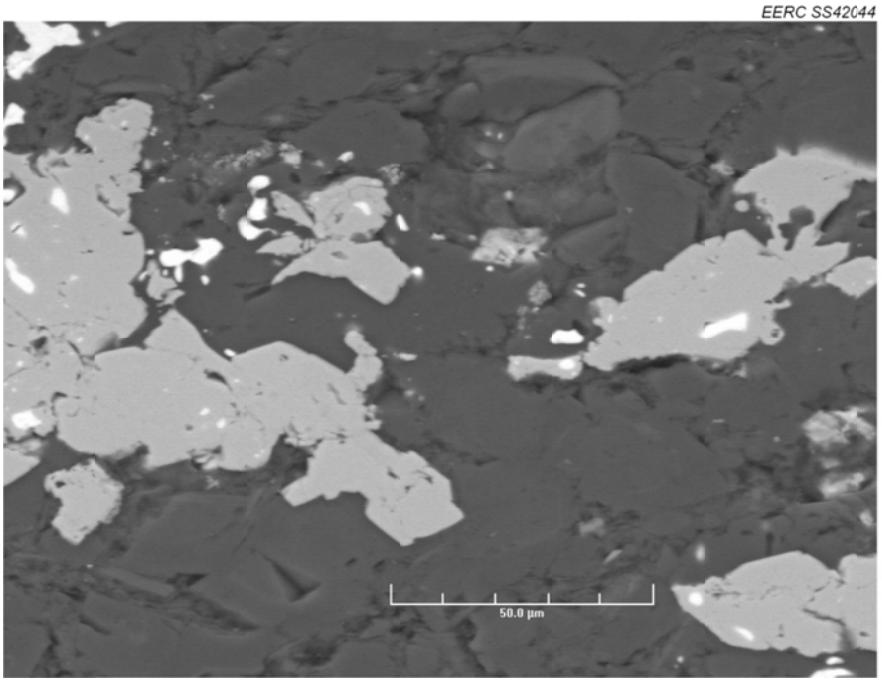

Figure D-19. Field for EDS testing on Sample T-3 at 750× magnification. Yellow crosshairs indicate the tag number and location.

Table D-19. Results of SEM–EDS Measurements for Points Present in Figure D-19, wt%

Tag	Na	Mg	Al	Si	P	S	Cl	K	Ca	Ti	Fe	Ba	Mineralogy
1	0.00	25.08	0.32	1.65	0.29	0.41	0.00	0.14	70.47	0.00	1.65	0.00	**Dolomite**
2	0.00	27.27	0.00	0.58	0.50	0.12	0.00	0.00	70.43	0.00	1.09	0.00	**Dolomite**
3	0.00	30.16	0.13	0.29	0.41	0.15	0.00	0.00	67.63	0.00	1.22	0.00	**Dolomite**
4	0.00	0.00	0.00	0.30	0.24	54.14	0.10	0.00	0.05	1.48	43.69	0.00	**Pyrite**
5	0.00	0.00	0.00	8.89	0.05	16.91	0.00	0.00	0.03	9.17	1.11	63.85	**Barite**
6	0.00	0.00	0.00	0.03	0.33	53.97	0.22	0.00	0.08	1.55	43.80	0.00	**Barite**
7	0.01	0.00	0.00	0.04	0.10	30.05	0.00	0.00	0.00	6.89	14.83	48.08	**Barite**
8	0.00	0.00	0.00	0.59	0.00	28.67	0.00	0.00	0.00	7.46	12.22	51.06	**Barite**
9	0.00	25.68	0.87	3.01	0.68	0.31	0.09	0.42	67.94	0.00	1.00	0.00	**Dolomite**
10	0.00	27.13	0.21	0.62	0.48	0.12	0.00	0.00	69.61	0.00	1.83	0.00	**Dolomite**

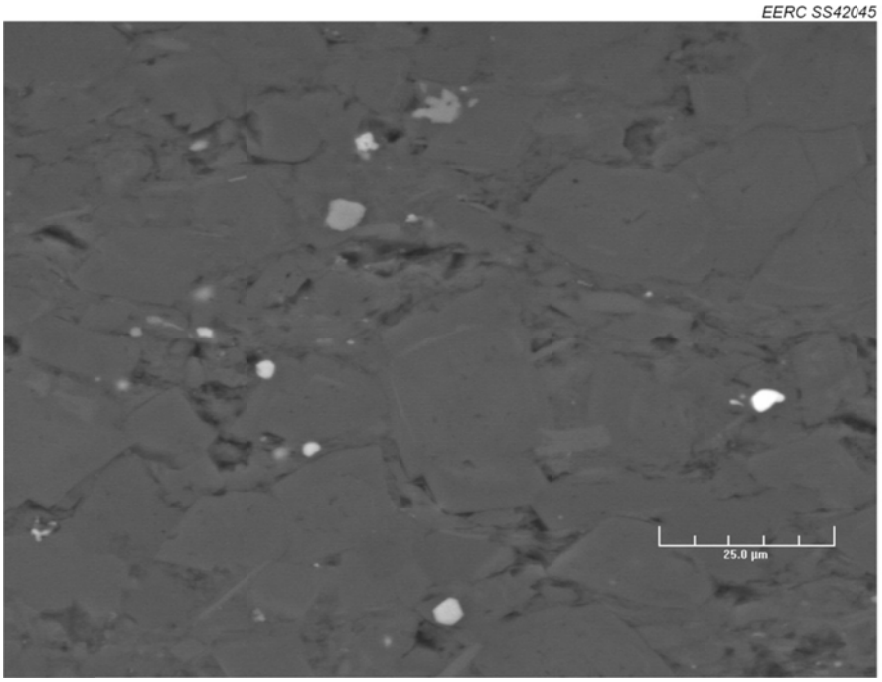

Figure D-20. Field for EDS testing on Sample T-3 at 1000× magnification. Yellow crosshairs indicate the tag number and location.

Table D-20. Results of SEM–EDS Measurements for Points Present in Figure D-20, wt%

Tag	Na	Mg	Al	Si	P	S	Cl	K	Ca	Ti	Fe	Ba	Mineralogy
1	0.00	30.25	0.81	1.86	0.35	0.25	0.10	0.17	65.88	0.00	0.35	0.00	**Dolomite**
2	0.00	25.42	0.82	3.35	0.30	0.06	0.00	0.39	69.23	0.00	0.43	0.00	**Dolomite**
3	0.00	26.96	0.15	0.85	0.46	0.07	0.00	0.05	70.87	0.00	0.53	0.06	**Dolomite**
4	0.00	26.97	0.00	2.34	0.23	0.09	0.00	0.00	70.17	0.00	0.19	0.00	**Dolomite**
5	0.00	1.05	2.74	6.08	0.00	0.02	0.00	1.30	2.48	85.95	0.39	0.00	**High-Ti**
6	0.00	0.41	1.42	4.19	0.10	0.53	0.02	0.47	1.64	89.79	1.42	0.00	**High-Ti**
7	0.00	1.29	22.58	52.68	0.00	0.00	0.00	18.39	0.30	0.81	3.94	0.00	**Clay**
8	0.00	1.56	0.18	0.69	0.21	49.46	0.09	0.01	7.41	0.64	39.73	0.00	**Pyrite**
9	0.00	0.00	0.81	15.18	0.00	17.08	0.00	0.16	0.38	8.33	0.00	58.06	**Barite**
10	0.00	23.02	0.47	1.00	0.47	0.40	0.47	0.21	73.13	0.00	0.83	0.00	**Dolomite**